

# **Processing and interpretation of multichannel seismic data from Van Mijenfjorden, Svalbard**

**Maryam Nasser**



**Master of Science Thesis**

**Department of Earth Science**

**University of Bergen**

**October 2011**

## **Abstract**

This work was done based on 19 seismic lines from Van Mijenfjorden, collected during Svalex in 2007 and 2008. In the first part of the thesis the seismic data, with particular emphasis on removal of seabed multiples have been described. In the second part of the thesis the profiles are broadly interpreted. The interpretation part emphasized on identifying large-scale structures and to interpret the different seismic units on the basis of a pre-defined seismic stratigraphic framework of western Spitsbergen.

The challenging part of data processing was to remove the strong, dominant seabed multiples in shallow water. These are generated as a result of abnormally high velocities in the seabed, estimated at up to 4.5 km/s from the seabed refractions on the shot collections. Most of the actual arrivals are masked by multiples as relatively shallow water depths (100-200 m) leads to short distances between multiples. Multiple removal was performed by applying a variety of different data processing steps. CDP positions, shot and receiver collections were calculated, and velocity filtering was performed on data sorted according to each of these positions.

By sorting the receiver collection, one can simulate collections that are shot in the opposite direction. Estimation of the velocity filter on this sorting will be somewhat different from the estimated filter of the shot collection, as apparent velocities are different when one shoots "up-dip" or "down-dip". The result appears to be considerably better than the velocity filtering performed only on CDP-collections. Then deconvolution was applied on the seismic data, a process that estimated filters for both the shot position, receiver position and offset values to remove what is left of multiples in the water layer (pre-critical reflections and small angles-of-incidence) before FK and Radon filtering. This processing sequence worked well where there was high velocity in the seabed and shallow water. In addition, a number of processes were applied, among other things, to improve the signal/noise ratio. Velocity analysis, pre-stack migration and a final frequency filtration of the data were also performed.

The data were interpreted with the support of former on- and offshore surveys from western parts of central Spitsbergen. A series of continuous reflectors under Van Mijenfjorden depicts a broad, asymmetric syncline, the central Spitsbergen basin, with deposits of Tertiary age.

Furthermore, units from Cretaceous to Permian were identified. Jurassic and Lower Cretaceous layers have a clear thickening to the east. This is interpreted as compacting of faulted material and further amplified by reverse faulting and formation of duplexes related to a detachment in the Lower Jurassic. The unit of Permian age has a similar thickening to the west. The study area is increasingly deformed towards the west, where eight large reverse faults with increasing dip towards the west, with some uncertainty, is interpreted through all the profiles.

The study area is divided into two tectonic zones, based on correlation with previous studies in the area: the west is characterized by the foreland oriented zone of the western Spitsbergen fold and fault belt, defined by thin skin folding and faulting structures. A foreland province dominated by the Spitsbergen Central Basin characterizes the eastern part of the study area.

## **Acknowledgments**

I am very grateful for having been given the opportunity to participate in the master program at the University of Bergen. I would like to acknowledge my supervisor, Professor Rolf Mjelde for his guidance, encouragement and support. I would also like to thank my co-supervisor Bent Ole for his immense help during data processing.

My deep notes of appreciation are directed towards my parents, Mahvash Shahali and Hatam Nasserri who followed me up all the time during this work and encouraged me all the time to fulfil it for second time.

Finally and most importantly, I must express my profound gratitude to my husband, Hamidreza Nasiri who gave me motivation during this work. Without his help and encouragement it was really difficult to finalize this study.

Bergen, October 2011

Maryam Nasserri



# Table of Contents

<b>Abstract</b> .....	II
<b>Acknowledgments</b> .....	IV
<b>1 Introduction</b> .....	1
<b>2 Fold- and-Thrust-Belts</b> .....	3
<b>3 Geological Background</b> .....	8
3.1 Svalbard tectonic setting .....	9
3.2 Svalbard's geological development .....	11
3.2.1 Precambrian- Paleozoic .....	11
3.2.2 Mesozoic .....	12
3.2.3 Tertiary.....	12
3.2.4 Central Spitsbergen Basin (CSB).....	13
3.2.5 West Spitsbergen fold and thrust belt (WSFTB) .....	14
3.3 <b>Stratigraphy</b> .....	15
3.3.1 Heckla Hoek.....	17
3.3.2 Devonian .....	17
3.3.3 Billefjord Group.....	17
3.3.4 Gipsdalen and Tempelfjorden Group.....	17
3.3.5 Sassendalen and Kapp Toscana Group .....	17
3.3.6 Adventdalen group.....	18
3.3.7 Van Mijenfjorden group .....	18
<b>4 Data and Method</b> .....	20
4.1 Background .....	20
4.2 General acquisition method.....	20
4.2.1 Source .....	22
4.2.2 Receiver .....	23
4.2.3 Acquisition parameters for the multichannel seismic profiles.....	23
4.3 General processing method .....	26
4.3.1 Fourier analysis.....	28
4.3.2 Operation steps of seismic data processing .....	31
4.3.3 Seismic resolution.....	41
4.4 Principles of seismic interpretation .....	44

4.4.1	Impedance .....	47
<b>5</b>	<b>Acquisition and Processing of Geophysical Data</b> .....	<b>49</b>
5.1	Acquisition data.....	49
5.1.1	Svalex 2007.....	49
5.1.2	Svalex 2008.....	50
5.2	Seismic data Processing .....	51
5.2.1	Editing.....	51
5.2.2	Filter and Deconvolution .....	52
5.2.3	Velocity analysis.....	59
5.2.4	Stacking and Migration.....	61
<b>6</b>	<b>Seismic Interpretation</b> .....	<b>64</b>
6.1	Interpretation frame work.....	64
6.2	Interpretation tool.....	67
6.3	Data quality .....	68
6.4	Estimation of the thickness, dip, and seabed.....	69
6.5	Interpretation of seismic lines .....	70
6.5.1	Unit 1: Tertiary .....	72
6.5.2	Unit 2 - Cretaceous .....	72
6.5.3	Unit 3 - Jurassic .....	73
6.5.4	Unit 4 - Triassic .....	74
6.5.5	Unit 5 – Permian .....	75
6.5.6	Unit 6: Carboniferous and older .....	76
<b>7</b>	<b>Discussion</b> .....	<b>78</b>
7.1	Sedimentary units.....	79
7.1.1	Tertiary unit .....	79
7.1.2	Cretaceous unit.....	79
7.1.3	Jurassic unit.....	80
7.1.4	Triassic unit.....	81
7.1.5	Permian unit .....	82
7.1.6	Carboniferous and older units.....	83
7.2	Interpretation of faults.....	84
<b>8</b>	<b>Concluding Remarks</b> .....	<b>90</b>
	<b>References</b> .....	<b>92</b>

<b>Appendix 1</b> .....	95
<b>Appendix 2</b> .....	103

# 1 Introduction

The study area in this work includes the outer part of Van Mijenfjorden on the west coast of Spitsbergen, the largest island that make up Svalbard. This Arctic Archipelago is located between  $74^{\circ}$  -  $81^{\circ}$  N and  $10^{\circ}$  -  $35^{\circ}$  E. The geology of the study area is dominated by a large-scale syncline (see Figure 1.1); the main basin to the east and the eastern zone of the west Spitsbergen fold and fault belt in the west.

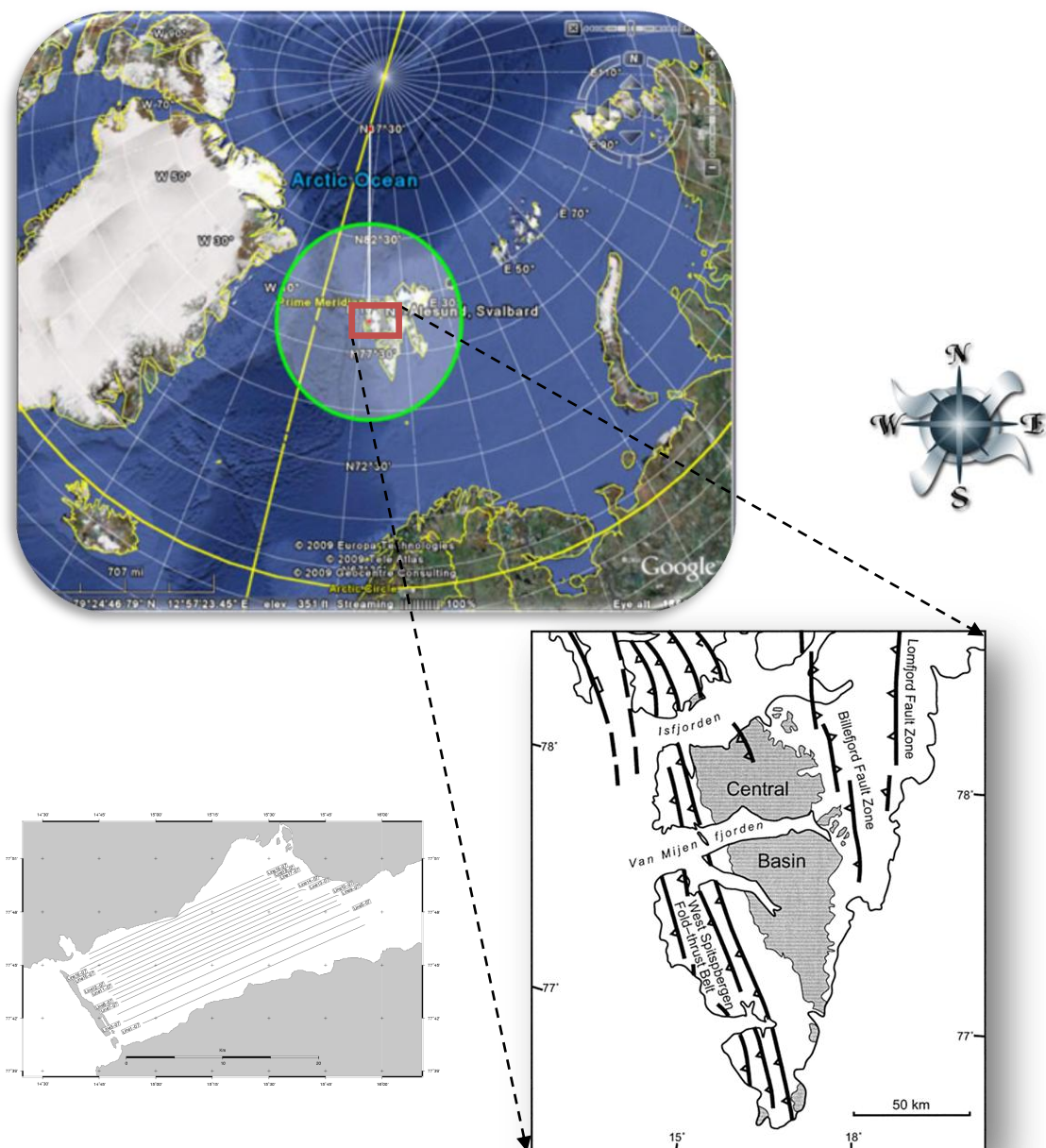


Figure 1.1: Svalbard. This Arctic Archipelago is located between  $74^{\circ}$  -  $81^{\circ}$  N and  $10^{\circ}$  -  $35^{\circ}$  E. The study area is in Van Mijenfjorden.

The thesis is based on multichannel seismic data, collected along 19 lines during Svalex 2007 and 2008 (Cruise report 2007 and 2008). The lines cover an approximately 30 x 7 km wide area in the western part of Van Mijenfjorden, and belong to two different grids, oriented SSW-NNE and WSW-ENE (Figure.1.1).

The study presented in this work addresses processing of seismic data in a way that the best possible imaging of sub-surface geological structures can be achieved. Firstly, in chapters 2 and 3 the fundamental geology of the study area will be reviewed. Chapter 4 gives a review about the fundamentals of geophysics including data acquisition, processing and interpretation. In Chapter 5 and 6 result of the processing and interpretation of the seismic data from the Svalbard area will be given. In the processing part there is particular emphasis on removal of strong seabed multiples which are very dominant in the seismic raw data collected. In the interpretation chapter, the aim is to present a rough interpretation of the data, where the main emphasis will be on correlation of seismic units and to identify the dominant deformation structures in the area. Chapter 7 and 8 gives the discussion and concluding remarks of this study.

## **2 Fold- and-Thrust-Belts**

This part is an introduction of general aspects to fold-thrust belts. Geologic terranes, in which regional horizontal tectonic shortening of the upper-crust yields a distinctive development of thrust faults, and related folds, are called fold-thrust belts or fold-and-thrust belts (Pluijm and Marshak, 2004).

Fold-thrust belts are developed due to contraction faults, which are faults that cause shortening of the crust. Contraction fault with dip greater than  $30-45^\circ$  are usually called reverse faults and low to medium angled contraction faults ( $30-45^\circ$ ) are usually referred to as thrust faults. A thrust fault should have dominant dip-slip movement, and in principle, emplace older rocks above younger rocks so that the stratigraphy in vertical direction is duplicated (Fossen and Gabrielsen, 2005). Thrusts require high pore pressures beneath the thrust plane to develop. The body of rock above the fault plane that has been transported due to thrusting is called a thrust sheet. Horizontal beds of sediment may become tilted or folded because of thrusting.

Contraction faults are formed mainly at convergent plate boundaries and collision zones (Figure 2.1), whereas thrust faults will always choose the lightest transport direction (Pluijm and Marshak, 2004).

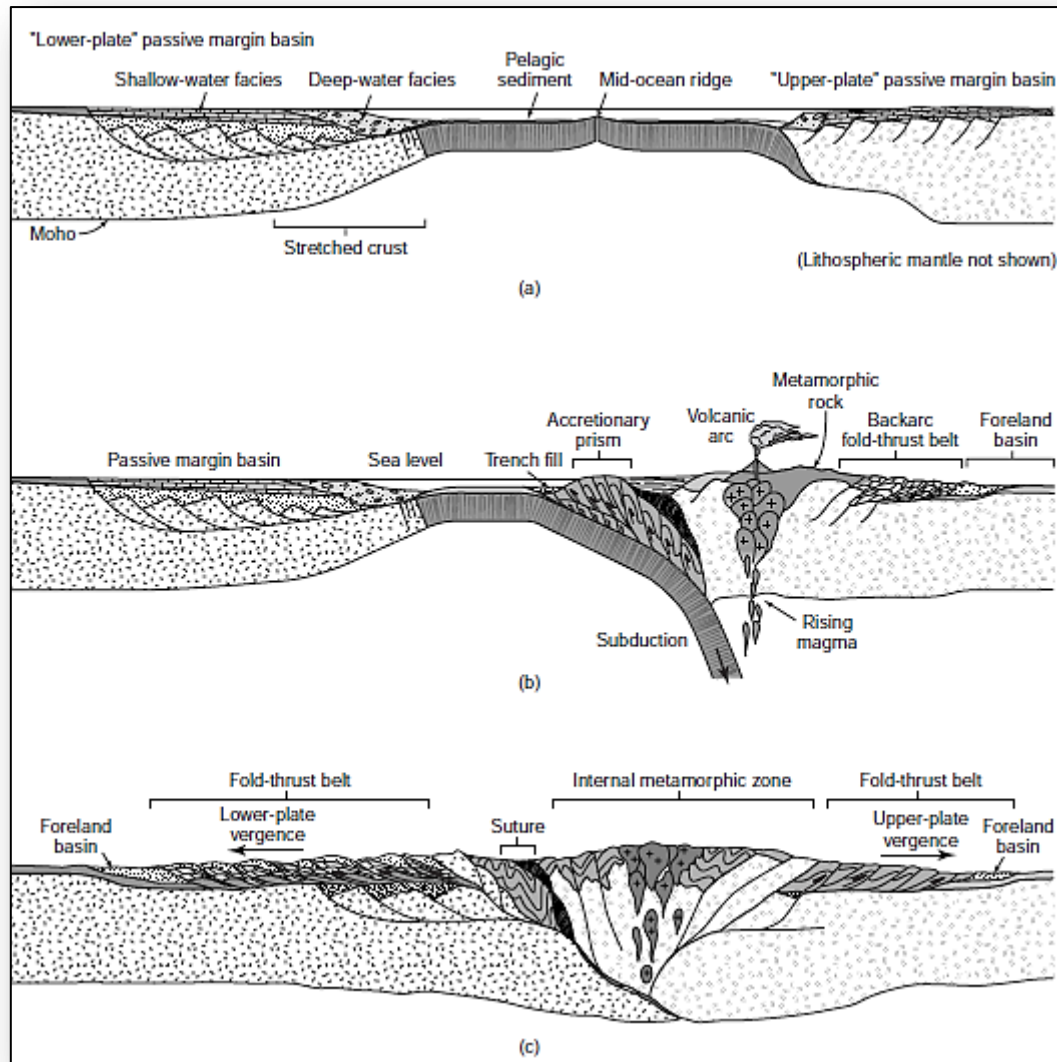
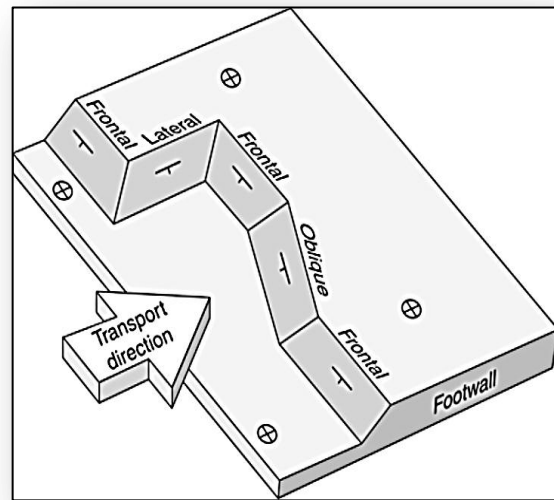


**Figure 2.1:** Regional cross sections depicting stages of fold-thrust belt development, first during convergent-margin tectonism and then during continent-continent collision. (a) Passive margin strata are deposited on thinned continental crust. In this sketch, basins on opposite sides of the margin do not have the same shape, because the basement beneath underwent different amounts of stretching. The so-called lower-plate margin underwent more stretching, whereas the so-called upper-plate margin underwent less stretching. (b) With the onset of convergence, an accretionary prism develops that verges towards the trench, and a backarc fold-thrust belt forms cratonward of the volcanic arc and verges towards the upper-plate craton. (c) Eventually the two continents collide. A fold-thrust belt forms in the foreland of the orogen on both sides of the orogen. Slivers of obducted ocean crust may separate lower-plate rocks from the metamorphic hinterland of the orogen and define the suture between the two plates (Pluijm and Marshak, 2004).

Typically, ramps curve and change strike along their length. A frontal ramp is a ramp segment that strikes approximately perpendicular to the direction in which the thrust sheet moves (Figure 2.2), a lateral ramp is a ramp segment that cuts upsection laterally and strikes

approximately parallel to the direction in which the thrust sheet moves, and an oblique ramp is a ramp segment that strikes at an acute angle to the transport direction. Note that dip-slip movement dominates on frontal ramps, oblique-slip movement dominates on oblique ramps, and strike-slip movement dominates on lateral ramps. Lateral or oblique ramps that break a thrust sheet into segments that move by different amounts into the foreland are tear faults.

**Figure 2.2:** Three-dimensional block diagram illustrating different types of fault ramps (hanging wall removed). Tear faults are vertically dipping oblique ramps or lateral ramps (Pluijm and Marshak, 2004).



A fold-thrust belt's geometric characteristics depend on the ductility of the rock sequence and the ductility contrast between the layers in the sequence. All the faults related to the same detachment fault or decollement is referred to as a thrust system (Jackson, 1997).

Duplexs and imbricate fans are the two end member types of thrust systems. Imbricate zones have a fault geometry that propagates from a basal detachment surface and either breaks the surface, or die out in an upper zone (Pluijm and Marshak, 2004). In a duplex a series of thrusts with approximately the same orientation branches upwards from a lower decollement, also called a floor thrust, and merges with a higher decollement also called roof thrust (Figure 2.3). Duplex faults (Figure 2.3) can be defined as the discarded shells ("horses") that are bounded by the ceiling and sole faults (Pluijm and Marshak, 2004).

The faults that comprise duplexs and imbricate fans, do not all initiate at the same time but usually forms in a break-forward sequence (Figure 2.4). It means that one fault forms first and the next fault forms to the foreland side of the previous one and so forth.



**Figure 2.3:** Idealized flat-roofed duplex that develops by progressive break-forward faulting. Note that the roof thrust undergoes a sequence of folding and unfolding, and that formation of the duplex results in significant shortening (Pluijm and Marshak, 2004).

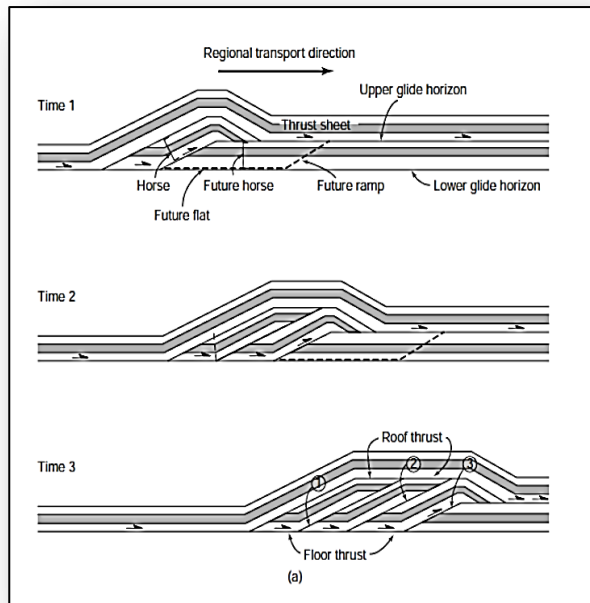
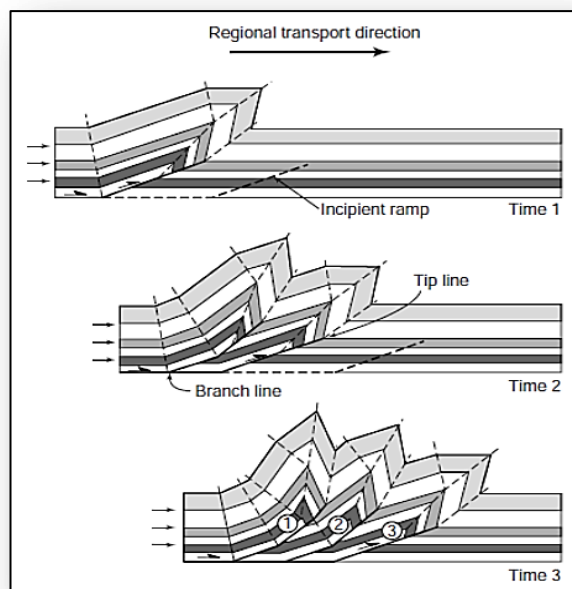
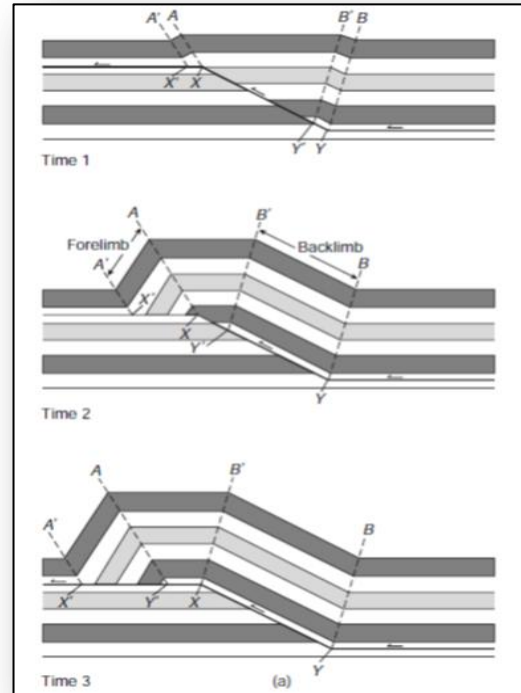


**Figure 2.4:** An idealized imbricate fan that develops by progressive break-forward thrusting. Note that successively younger thrusts cut into the footwall, and older faults and folds become deformed by younger structures. The dashed lines are the traces of fold axial surfaces. In the cross section showing “Time 3,” the sequence of thrusts is labeled. Fault 1 is the oldest and Fault 3 is the youngest. On this cross section, tip lines and branch lines are points; in three dimensions, they go into and out of the page (Pluijm and Marshak, 2004).



Fold structures that commonly develop in foreland fold-thrust belts include fault-propagation folds, fault-bend folds and detachment folds. When hanging-wall strata move up over a thrust ramp or a bend in an underlying fault, a fold form because the sheet can not rise into the air at the top of the ramp due to pull of gravity. The hanging-wall strata instead bend to form an anticline, which is called a fault-bend fold (Figure 2.5) (Pluijm and Marshak, 2004).

**Figure 2.5:** (a) Cross-sectional model showing the progressive stages during the development of a fault-bend fold. The dashed lines are the traces of axial surfaces. (b) Photo of a fault-bend fold above the McConnell Thrust, near See bed, Alberta (Canada). These Paleozoic strata have been displaced over 5 km vertically and 40 km horizontally, and now lie above Cretaceous foreland basin deposits. The foreland basin deposits have preferentially eroded and are now forested (Pluijm and Marshak, 2004).



Folding developing just in advance of the tip of a ramp as the ramp propagate updip is called fault-propagation folding. Detachment fold develop without the presence of the ramp. They are instead related to distributed deformation above a decollement or bedding-parallel thrust that typically propagate within thick shale or salt layers.

### 3 Geological Background

In this chapter the structural and sedimentary development in the study area will be discussed. The aim is to provide an overview of the major lithostratigraphic units and structures. In the last century several different names and definitions have been given to the stratigraphic units in the Svalbard area, which is a result of extensive research activities in this area.

The study area is located in the Barents Sea between 74° and 81° N and 10° and 35° E. The Cenozoic uplift has been more extensive in the northern and western parts and it shows progressively younger rocks towards southeast and south. Svalbard has an extensive post-Caledonian geological record including rocks ranging from the Devonian to the paleogene period. During this time period Svalbard has also moved northwards from a position near the equator to its current position (see Figure 3.1).

The post-Devonian depositional and tectonic evolution of Spitsbergen has also been greatly influenced by N-S and NNW-SSE structure lineaments. The most important lineaments are Billefjorden and Lomfjorden Fault Zones. As Figure 3.1 shows the geology of Spitsbergen may be divided into five units, metamorphic basement (Heckla Hoek), late Silurian-Devon, Carboniferous-Permian, Mesozoic, and Tertiary, respectively (Steel & Worsley, 1984; Eiken, 1985).

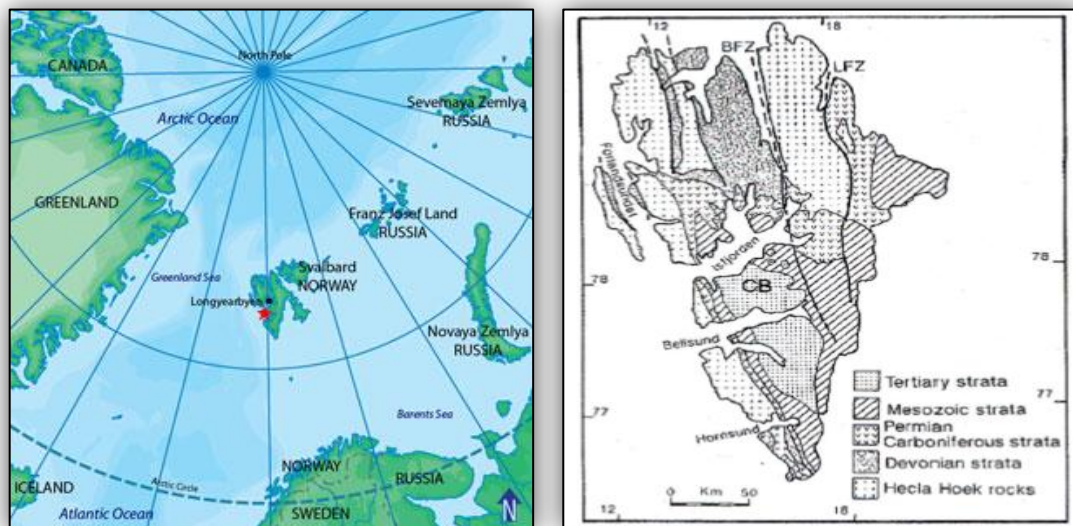


**Figure 3.1:** Left: Location of Svalbard. Right: Geology of Spitsbergen. **HFZ** = Hornsund fracture zone, in green line, **SFZ** = Senja fracture zone in yellow line, **LFZ** = Lomfjorden fracture zone, in blue line, **BFZ** = Billefjorden fracture zone, in red line ((Steel & Worsley, 1984).

### 3.1 Svalbard tectonic setting

The Svalbard archipelago represents the northwestern uplifted portion of the submarine Barents shelf (Nøttvedt et al., 1993b; Dallmann, 1999) characterized by a complex mosaic of basins and platforms (Worsley, 2008; Nøttvedt et al., 1993a). Svalbard can be used as an onshore analogue of the Barents shelf region, as it shows great similarity in the Devonian stratigraphy (Nøttvedt et al., 1993b).

The Western Svalbard continental margin is primarily a sheared margin with transtensional and transpressional components. In this area from west to east there are the Knipovich Ridge, oceanic crust, continental-ocean transition (sheared margin), continental shelf and Spitsbergen, respectively (see Figure 3.4 ) (Faleide et al., 2008). Knipovich Ridge is an ultraslow spreading ridge. Between 50 and 100 km north of the coast of Svalbard is a steep continental slope boundary with the Eurasian Basin in the Arctic Ocean (Figure 3.2). The northwest corner of the shelf borders the Yermak Plateau (Figure 3.2), the northern part of which may be the remainder of an early Tertiary hot spot (Dallmann, 1999). On the northwestern Spitsbergen, there has been volcanic activity in both the Tertiary and Quaternary (Eiken, 1985).

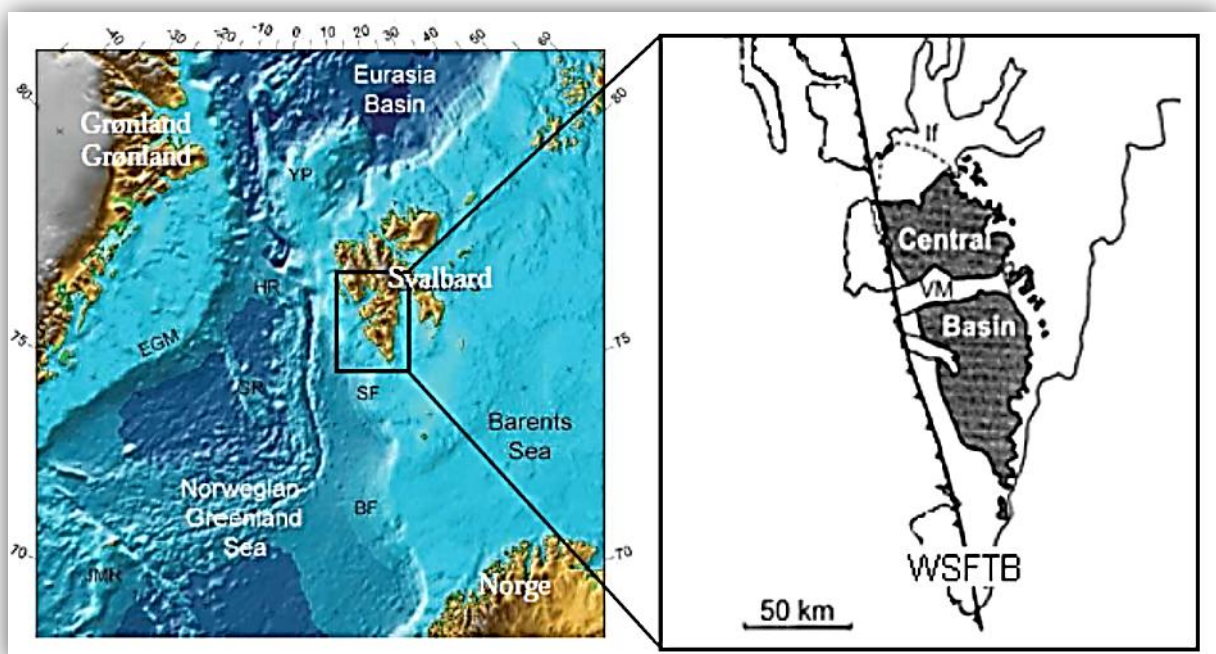


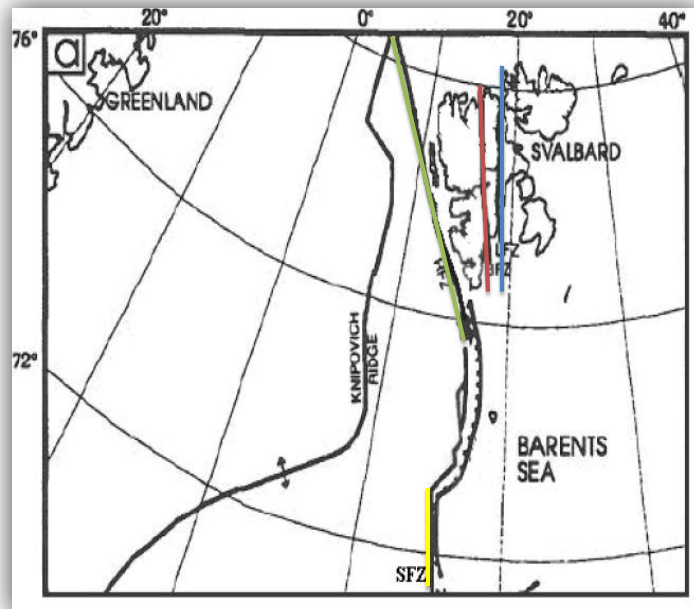
**Figure 3.2:** Regional setting, with a view of western Spitsbergen. EGM = East Greenland margin, YP = Yermak Plateau, SF and BF = Storfjord and Bear Island -fan. In view image defined western Spitsbergen fold and fault belt of the line marked WSFTB, and dark area marks the Spitsbergen Central Basin. IF = Isfjorden, VM = Van Mijenfjorden (Faleide et al., 2008 and Blinov et al., 2009).

Two major tectonic episodes, extension-related shear movements in the late Devonian and folding in the early Tertiary, can be characterized as the most important episodes in the development of the Svalbard archipelago as it stands today (Steel & Worsley, 1984). Varying tectonic regimes are reflected in the stratigraphic formations by changing patterns in sediment thickness and the origin and transport direction (Steel & Worsley, 1984).

The tectonic framework of Spitsbergen is dominated by a series of NNW to SSE-oriented lineaments, formed by several tectonic episodes of approximately similar orientation on deformation direction. The clearest lineaments are Lomfjorden fault zone (LFZ), Billefjorden fault zone (BFZ), inner Hornsund and Paleo-Hornsund fault zones (Figure 3.3) (Steel & Worsley, 1984; Eiken, 1985).

**Figure 3.3:** Image of major fault zones. Slightly modified from Braathen & Bergh (1995).

- HFZ** = Hornsund fracture zone, in green line
- SFZ** = Senja fracture zone in yellow line
- LFZ** = Lomfjorden fracture zone, in blue line
- BFZ** = Billefjorden fracture zone, in red line



Lineaments restrict a number of sedimentary basins. Among them is the Spitsbergen central basin (CSB), an asymmetric syncline that dominates large areas in central parts of Spitsbergen (Figure 3.2). Tectonic activity along the lineaments has taken place in most geological periods, but was most pronounced in the earliest and latest phases of sediment deposition period, in the Devonian, Carboniferous and early Tertiary (Steel & Worsley, 1984; Eiken, 1985).



### 3.2 Svalbard's geological development

Figure 3.4 shows a geological map of Spitebergen and a cross-section of different zones of West Spitsbergen Fold and Thrust Belt (WSFTB), characterized by western hinterland, basement involved fold-thrust complex, central zone with thick skin folding and faulting and eastern foreland province from west to east, respectively (Blinova et al., 2009).

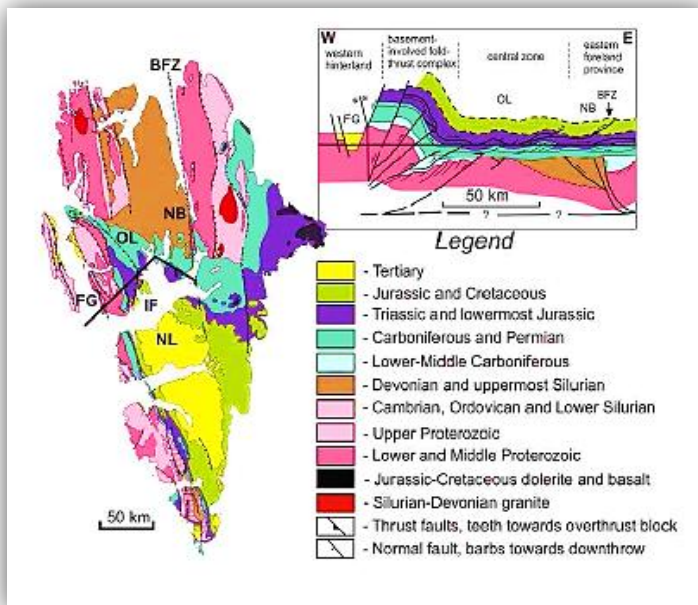


**Figure 3.4:** Geological map of Spitsbergen (Hjelle, 1993) and cross-section of a profile through the fjord.

**BFZ** = Billefjorden fault zone,  
**FG** = Forlandsundet graben,  
**OL** = Oscar II Land,  
**IF** = Isfjorden,  
**NB** = North block area,  
**NL** = Nordenskiöld Land.

#### 3.2.1 Precambrian- Paleozoic

Heckla Hoek constitutes the bedrock of Spitsbergen. This unit consists of metamorphic sedimentary and igneous rocks of Precambrian to middle Ordovician age, and is defined as the rocks that were present during the Caledonian mountain chain folding in the middle Silurian (Dallmann, 1999). Mountain chain folding, which is called "New Friesland-orogeny" on Spitsbergen, was a result of closure of the Iapetus Ocean and subsequent collision between the Fennoscandian plate and the Greenland-Canada-plate (Laurentia). The rocks that make up the "Heckla Hoek" is folded and faulted, shows large local variations in the degree of metamorphism especially in the older parts, and is exposed in the western and northeastern parts of Spitsbergen and North Eastern (Birkenmajer, 81; Nøttvedt et al. 1993a; Dallmann, 1999). In recent years, U-Pb zirkon isotopic age determination has shown several Precambrian tectonic events which indicate that the unit has a poly-orogenic origin (Ohta, 1994).

During the Devonian period, the young Caledonian mountain range eroded down, and large amounts of sediments were deposited in fault grabens in the northern parts of Svalbard (Dallmann, 1999). Through the Carboniferous period Svalbard went from being dominated by sedimentation controlled by fault blocks to become a stable area that experienced overall subsidence with the exception of the southern part of Spitsbergen (Dallmann, 1999). In the middle Carboniferous tectonic movements along the existing tectonic lines resulted in a new constellation of troughs, mainly half-grabens, with a syntectonic sedimentary record (Dallmann, 1999). Reduction in the tectonic movement until the early Permian led to the development of a carbonate platform with evaporite formation, while the later part of the Permian experienced renewed clastic influx, and a subsequent hiatus at the era boundary (Steel & Worsley, 1984).

### **3.2.2 Mesozoic**

Mesozoic sequences were deposited in a tectonically stable platform environment. These consist of delta-related coastal and shallow shelf sediments (Triassic-early Jurassic), deeper shelf sediments (Middle Jurassic to earliest Cretaceous), and then again shallow shelf-delta deposits (Later part of early Cretaceous) (Dallmann, 1999). Intrusion of dolerites from the latest Jurassic through the early Cretaceous boundary is the first sign of break-up between Greenland and the Europe (Steel & Worsley, 1984; Dallmann, 1999). These intrusions act as sills in Carboniferous through to Jurassic strata, and are progressively younger towards the east.

### **3.2.3 Tertiary**

In early Tertiary (Paleogene) the development of the region is characterized by tectonic activity along the western Svalbard continental margin, ahead of the opening of the Arctic Ocean and the Norwegian and Greenland Sea (Worsley, 2008). A Transform fault system led to the formation of the west Spitsbergen orogenic belt (WSOB), and involved significant crustal shortening, estimated to approximately 30 km (Bergh et al. 1997; Worsley, 2008).

### 3.2.4 Central Spitsbergen Basin (CSB)

The central Basin is located on the eastern side of the west Spitsbergen Orogen and formed simultaneously with the orogenic belt and also acted as a foreland basin (e.g. Steel et al., 1985; Helland-Hensen, 1990; Plink-Bjørklund et al., 2001; Mellere et al., 2002; Bruhn and steel, 2003). Bruhn and steel (2003) suggested that the basin first formed as a flexural depression in front of the thrust wedge in late Cretaceous or early Paleocene time but, similar to the events concerning the development related to the opening of the Atlantic Ocean, the exact timing of events is not known. The majority of the Paleogene deposits on Svalbard are confined to the Central Basin.

Central Spitsbergen Basin is characterized by shifting sedimentation and various tectonic settings through the Tertiary. In the early to middle Paleocene the basin has been characterized by tensional stress (phase I, Figure 3.5), with the greatest sedimentation from the east and northeast (Steel et al., 1985). A general transpressive package, from the coal-bearing sandstone to marine shale and sandstone, characterizes this transition phase (Kellogg, 1975; Steel et al., 1985). From the late Paleocene to early Eocene, there was a significant change in tectonic setting, probably due to uplift of the western margin of the CSB, associated with the formation of WSOB (Steel et al., 1985). The basin was in this period characterized by transpressional stress (phase II, Figure 5). Shifting in the tectonic regime is reflected in a change of direction of sediment transport from the east and northeast to the west, presumably in response to increasing compression in WSOB (Steel et al. 1985; Nøttvedt et al., 1993a). The asymmetry of the basin is developed primarily after middle Paleocene (Steel et al., 1985). A large-scale regressive package from marine shale to continental sandstones and shales characterize the shift to a transpressional regime (Kellogg, 1975, Steel et al., 1985). The Central Basin can be considered as a foreland basin from late Paleozoic time, with the cyclic infill of mixed continental and marine clastic deposits (Steel et al. 1985; Nøttvedt et al., 1993a). Through the Tertiary deep basins formed outside the western coast of Spitsbergen, with the change from sheared to rifted margins around 37 Ma when the Svalbard platform was separated from Greenland in the early Oligocene (Steel & Worsley, 1984).



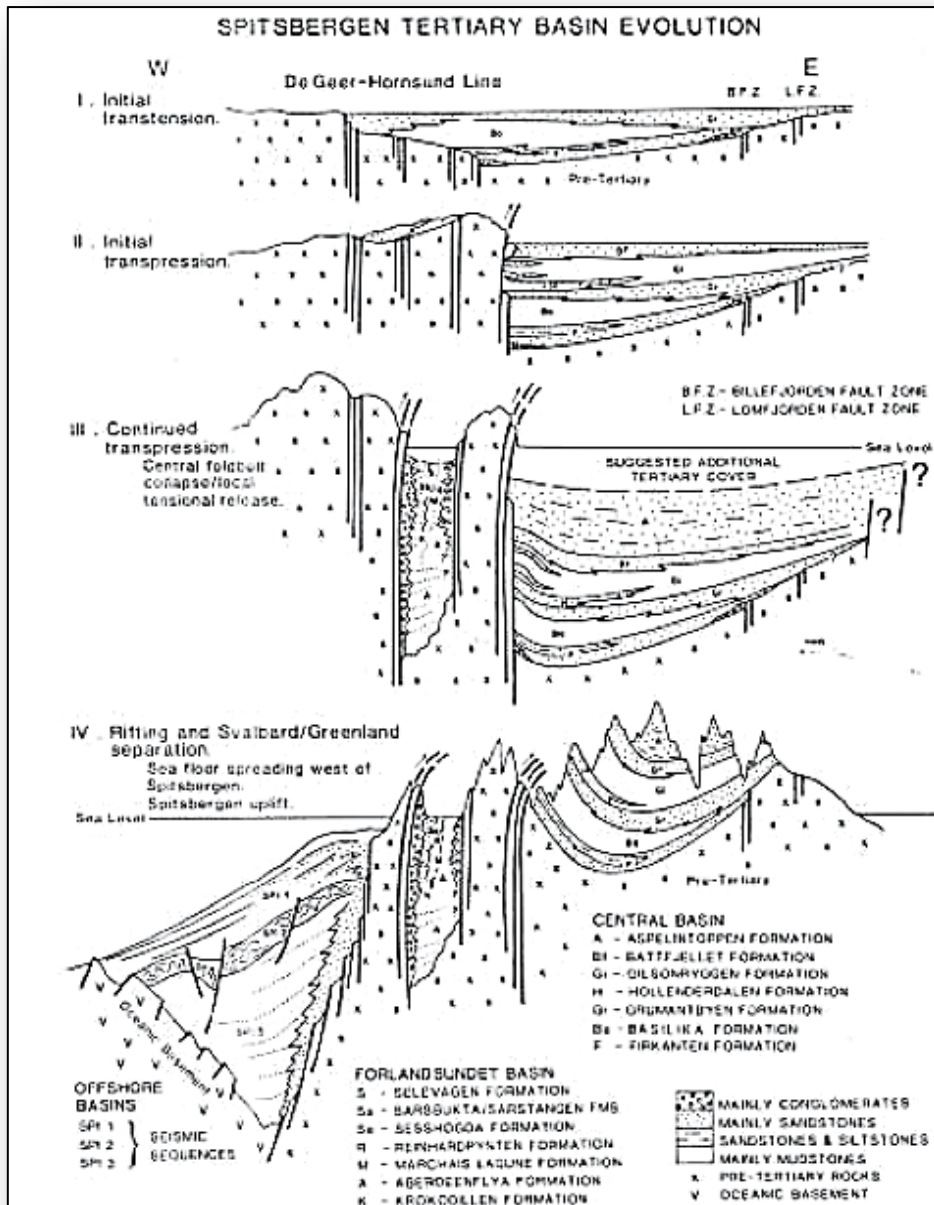


**Figure 3.5:** Schematic summary of CSB developments regarding the Svalbard margin tectonic development through the Tertiary period (Steel et al., 1985).

### 3.2.5 West Spitsbergen fold and thrust belt (WSFTB)

The compressional regime in the Paleocene or early Eocene which formed CSB also caused an approximately 50 km wide and 300 km long fold- and fault belt along the west coast of Spitsbergen (Eiken, 1985, Steel et al., 1985). The west Spitsbergen orogenic belt is defined as the part of the fold- and fault belt that has been exposed for the first time during Tertiary deformation, or Tertiary deformation of previously deformed rocks (Dallmann et al., 1993). WSTFB represents a classic foreland fold- and fault belt along the Paleo-plate boundary (De

Geer-fault) (Nøttvedt et al., 1993a). The formation of the fold- and fault belt is related to right-lateral movements along the transformed plate boundary "De Geer-Zone", and is interpreted to be a folding- and thrust fault belt formed by right-lateral transpression (Kellogg, 1975; Steel et al., 1985).

Deformation in the Tertiary was dominated by compression in the ENE-WSW direction and is transferred eastward past the fold- and fault belt along glide planes ("decollement") in Paleozoic and Mesozoic strata such as shales and evaporites deposits (Dallmann, 1999). The regional southern slope of the post-Caledonian strata leads to deeper decollement southeast of Spitsbergen (Bergh & Andresen, 1990). Although the belt has occurred in a plate tectonic dextral setting between Greenland and the Barents shelf, structures in the belt are associated with converging movements. This indicates a decoupling model (Bergh & Andresen, 1990), where both the strike-slip and convergent movements can be located in different deformation zones. The WSFTB can be divided into different zones with different tectonic nature (e.g. Braathen et al., 1995; Bergh et al. 1997; Blinov et al., 2009), with a western basement involved folding- and faulting stack, and a central to the eastern foreland folding and faulting belt. Later stage in the development of the fold belt in the Eocene to the Oligocene include the formation of small sedimentary basins with a more complex structural registry in areas further west (Dallmann, 1999). A passive post-Eocene continental margin west of Svalbard was formed when it was separated from the Greenland continental plate (Steel & Worsley, 1984). East-west oriented extension movements related to the separation led to the formation of both new- and reactivation of existing faults along the fold belt (Dallmann, 1999).

### **3.3 Stratigraphy**

Large amounts of sediments were deposited on Svalbard between the late Devonian "Svalbardian" deformation and the tertiary orogeny. Different tectonic regimes along both the eastern, western and northern margin of the continental shelf have influenced sedimentation patterns, and also short- and long-term variations in local and regional sea level had an impact on the deposition history of the area (Worsley, 2008). Climate change, which is primarily attributable to paleo-continental drift to the north, has also had a significant impact on the variation in the stratigraphy and development of sedimentary facies (Steel & Worsley,

1984). The sequences can be divided into seven different units; Figure 3.6 shows the name, age and lithology of each.

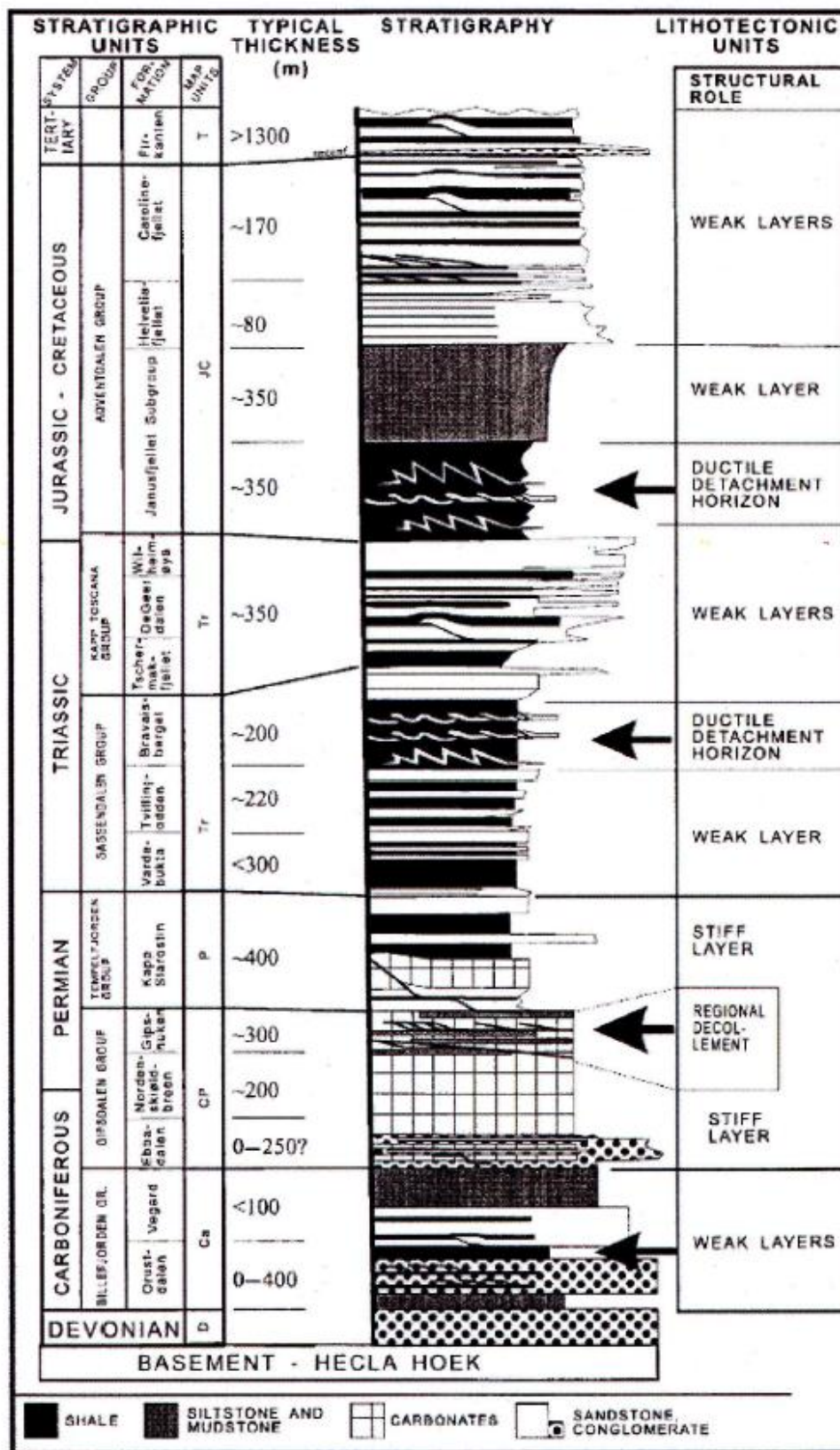


Figure 3.6: Stratigraphy of Svalbard (from Brathen et al., 1999)

### **3.3.1 Heckla Hoek**

The bedrock of Spitsbergen is defined by a deformed, metamorphic sequence called Heckla Hoek. An unconformity separates it from overlying Paleozoic, Mesozoic and Tertiary sequences (Steel & Worsley, 1984).

### **3.3.2 Devonian**

"Old Red" molasse sediments, mostly deposited in grabens. In central Spitsbergen the thickest sequences are located from the Devonian of the Nordfjord-block (Steel & Worsley, 1984).

### **3.3.3 Billefjord Group**

Terrestrial rocks such as conglomerate, sandstone and shale are deposited from the late Devonian to late Carboniferous, and is an unconformity on Heckla Hoek (Dallmann, 1999). Through Carboniferous sediments were deposited in alluvial fans, braided rivers and on flood plains, with thicknesses of up to 2 km (Steel & Worsley, 1984).

### **3.3.4 Gipsdalen and Tempelfjorden Group**

Gipsdalen group consisting of carbonates and evaporites deposited from the late Carboniferous to middle Permian. A sharp, locally erosive contact separates it from the overlying Tempelfjorden group, a formation with mainly carbonates and siltstone deposited from the middle to late Permian (Steel & Worsley, 1984).

### **3.3.5 Sassendalen and Kapp Toscana Group**

Rocks from the Triassic are divided into two groups; Sassendalen and Kapp Toscana. Sassendalen Group is deposited from the early to middle Triassic and consists mainly of marine shales with layers of silt and sandstone. The group is characterized by coastal and delta depositional environment in the west and mudstones with a high content of organic matter further east of Svalbard, as well as south of the Barents Sea shelf (Steel & Worsley, 1984; 18 Dallmann, 1999). Kapp Toscana group is deposited from the middle Triassic to middle Jurassic, and consists of sands and shales deposited in shallow marine environment (Dallmann, 1999).

### 3.3.6 Adventdalen group

Over Kapp Toscana is the Adventdalen group, with rocks from the Jurassic and Cretaceous. The group can be divided into three subgroups: Janusfjellet subgroup, consisting of shales deposited in open marine environment, Helvetiafjellet formation, which mainly consists of sandstones deposited in the delta environment and Carolinefjellet formation, with alternating layers of marine deposits of shale, silt and sandstone (Steel & Worsley, 1984; Eiken, 1985; Dallmann, 1999).

### 3.3.7 Van Mijenfjorden group

Van Mijenfjorden group, constitute deposits from Tertiary on the central parts of Spitsbergen, and consists mainly of sandstone, siltstone and shales deposited in the CSB (Steel & Worsley, 1984; Dallmann, 1999). The Paleogene Central Basin in Spitsbergen is filled with up to 2.4 km thick successions of siliclastic sediments that belong to the Van Mijenfjorden Group (Figure 3.7).

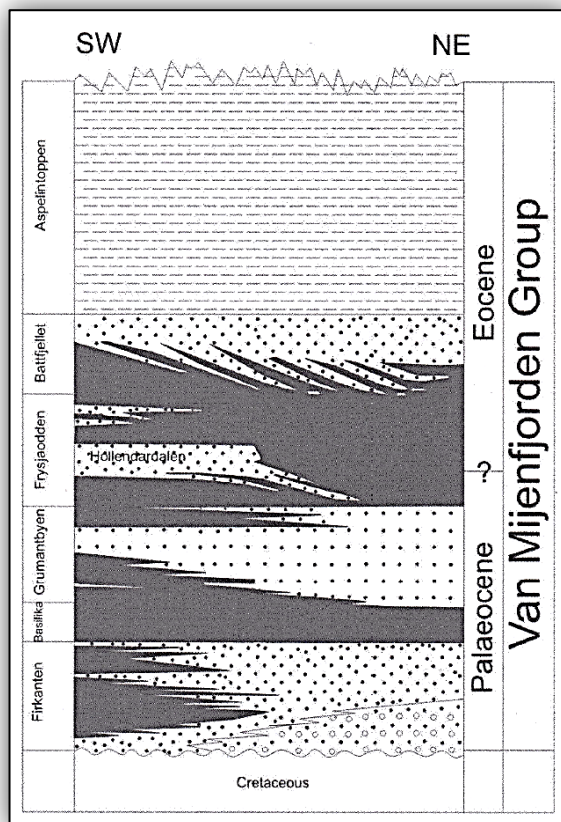


Figure 3.7: Stratigraphy of the Van Mijenfjorden Group (Steel et al, 1985).

The deposits in the Van Mijenfjorden Group reflect the alternating transtensional and transpressional conditions that occurred along the fold- and thrust- belt (Steel et al, 1985).

The most recent stratigraphic scheme divides the succession into seven different formations (Dallmann, 1999), which represents the scheme used in this study.



## 4 Data and Method

### 4.1 Background

Seismic exploration consists of three main steps (Figure 4.1). Acquisition of measurement data (raw data) is the first step which in most cases is carried out from the surface. These raw data, in second step, are then processed employing advanced methods within signal processing and wave-theory to give images of the subsurface. The seismic images or sections represent vertical slices through the geological model, which can be input to advanced workstations where the actual interpretation (third step) can take place. Based on the seismic interpretations one will decide if an area is a possible prospect for oil or gas. An initial drilling program will be performed thereafter if the answer would be positive. Finally, if the target area is a commercial reservoir, it will be replaced by a production phase.

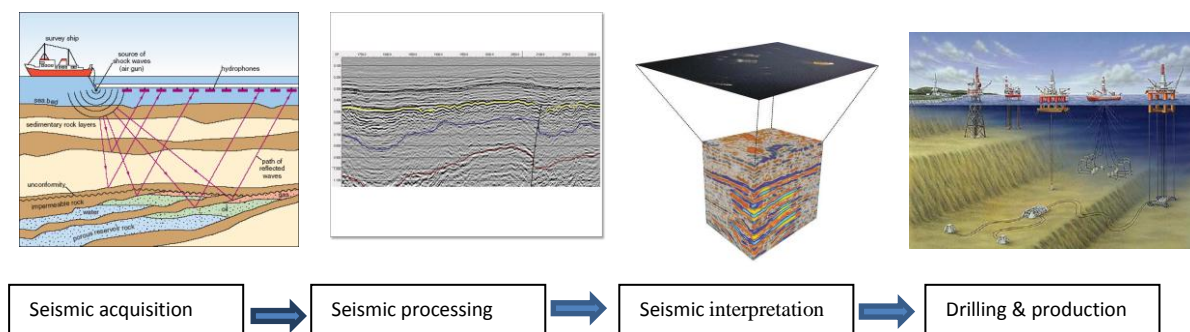


**Figure 4.1:** Seismic exploration steps.

The following chapter explains the basic principles for collecting, processing and interpreting seismic data, as well as a brief theoretical description of seismic resolution.

### 4.2 General acquisition method

Offshore (marine) seismic surveying represents the most important geophysical exploration method on the Norwegian continental shelf, and is generally accomplished using large ships with one or multiple air gun arrays for sources (see Figure 4.2). Air guns are deployed behind the seismic vessel and generate a seismic signal by forcing highly pressurized air into the water. Receivers are towed behind the ship in one or several long streamers that could be

several kilometers in length. Marine receivers are composed of piezoelectric hydrophones, which respond to changes in water pressure.

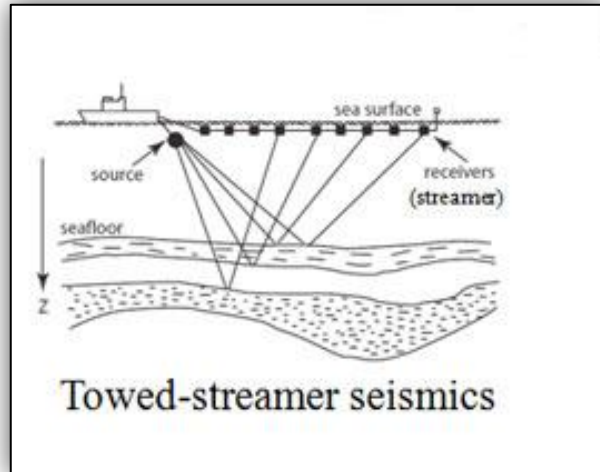


**Figure 4.2:** Towed-streamer seismic methods.

Marine seismic navigation involves two aspects: (a) placing the ship at a desired position and (b) determination of the actual location afterwards so that the data can be mapped properly. The ships used for marine seismic acquisition are usually large, 30 to 95 m in length and 5 to 20 m in beam. The acquisition method uses the principle of the ray and wave front including amplitude decay, reflection coefficient, Snell's law, direct wave, reflected, refracted and diffracted waves, multiples and noise (Sheriff & Geldart, 1995). Figure 4.3 shows the basic principles of reflection seismology.

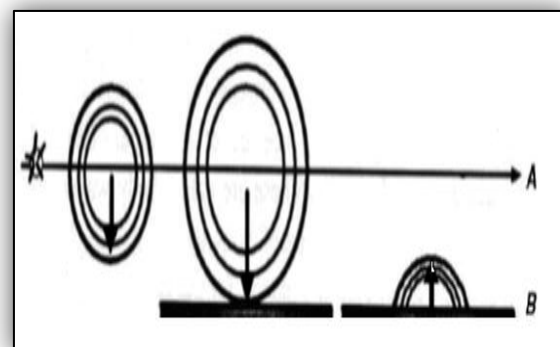


**Figure 4.3:** The basic principal of reflection seismology. An acoustic pulse generates a spherical expanding wave front. At any point, it is conceivable a ray path perpendicular to the wave front. When the wave front hitting a layer boundary (marked B in the figure), some of the energy reflected back is recorded by seismic receivers and provide information on two-way travel time and amplitude of the reflected energy (Hart, 2000).

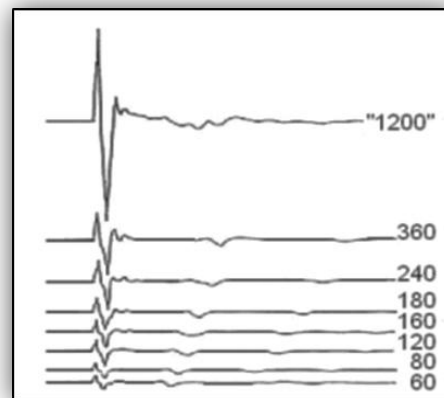


### 4.2.1 Source

The most widely used marine energy source is air guns, a device that discharges air under very high pressure (up to 10 000 psi) into the water. In marine multichannel seismic acquisitions one or more sources are used to generate the acoustic pulse. The high-pressured air released by the air gun will generate a seismic pulse that is transmitted through the water. The bubbles of the air subsequently collapse due to the hydrostatic pressure, and then expand as they rise to the surface. The energy reflected from the ground is registered by hydrophones in the streamer (Sheriff & Geldart, 1995).

Directivity is a measure of how much of the energy emitted from the source that propagates in a given direction. With various locations of the sources, one can sum up the energy in a particular direction (see Figure 4.4). Directivity applies to both sources and receivers, and is subject to a number of factors such as the number of air guns and hydrophones, the distance between them and their size and sensitivity (Sheriff & Geldart, 1995).

**Figure 4.4:** Using a collection of air guns provides increased amplitude of the generated pulse, reduced bubble pulse and increased directivity.

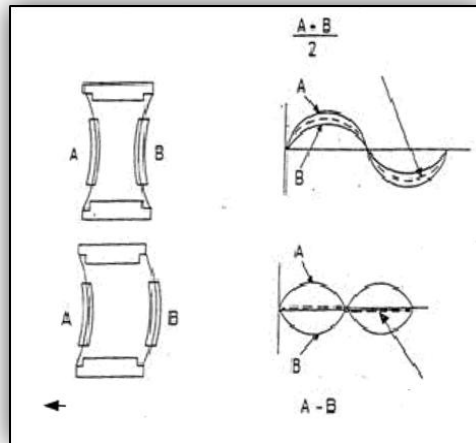


One of the main problems in marine seismic acquisitions is ghost-multiple. Ghost-multiple is the upward energy from the source that is reflected from the surface. The same principle applies to the receiver, which also will record the energy reflected from the surface. The depth of the source and receivers can be selected with emphasis on creating positive interference between the direct downward and the ghost for vertical wave propagation, thus strengthening the signal (Sheriff & Geldart, 1995).

#### 4.2.2 Receiver

Hydrophones are used to detect seismic signals in marine seismic. A hydrophone consists of two circular piezoelectric plates with opposite polarity, located opposite each other in a copper cylinder (Sheriff & Geldart, 1995). Pressure fluctuations from seismic waves will thus be summed and converted into an electrical signal, while acceleration related movements will be cancelled (see Figure 4.5).

**Figure 4.5:** Circular piezoelectric plates with opposite polarity.



The hydrophones are mounted in the active portion of a streamer, and connected in series with 6.25, 12.5, 25 or 50 m group length (Sheriff & Geldart, 1995). The streamer also consists of a "lead in" cable and stretch sections in order to reduce the strain both in front of and behind the active part of the streamer, as well as cables that transmit data from the hydrophones to the digitizing units and registration on board the vessel. The streamer is filled with oil to provide neutral buoyancy at a collection speed of 5 knots, and its depth can be adjusted using lead weight and "birds". Digitization of the data is done as a rule already in the streamer.

The recorded data are monitored during the raw data collection, and stored on magnetic tapes for further processing.

#### 4.2.3 Acquisition parameters for the multichannel seismic profiles

The typical scenario for seismic surveys is 3D data acquired by a commercial contractor. In this study, however, a single streamer is being used for 2D marine data acquisition.

The following information is acquired from the cruise report made from the MCS survey, in Van Mijenfjorden and inner Isfjorden between 23 to 31 August 2007 by participants from the University of Bergen, institute of marine research, Statoil, and institute for petroleum technology NTNU (Trondheim). This survey was originally an extension of the Svalex 2007 MCS survey (Cruise report, 2007).

The survey was performed as four legs, in order to assure that as many student as possible could join the seismic acquisition part for Svalex. Leg I and II were performed in Van Mijenfjorden. 16 profiles with total length of 376.7 km were acquired there. The other legs were acquired in Isfjorden.

The streamer was slightly heavy in Van Mijenfjorden, most likely due to fresh water blockage by Akseløya. Part of the streamer was thus too deep for profile 1,3,5,7 and 8. A part of profile 19 was up to 270 m offline (south) due to shallow bathymetry close to land (Mjelde, 2007).

The streamer was well balanced in Isfjorden. Some parity errors, probably related to electrical leakage in the streamer, were observed on the streamer control.

All lines running West to East (line 1,3,7,8,11,12,15, and 16) and the lines running East to West (line 5,9,10,13,14,17,18 and 19) were acquired in 2007 (see Figure 4.6). The remaining lines (line 2,4 and 6) were acquired in 2008.

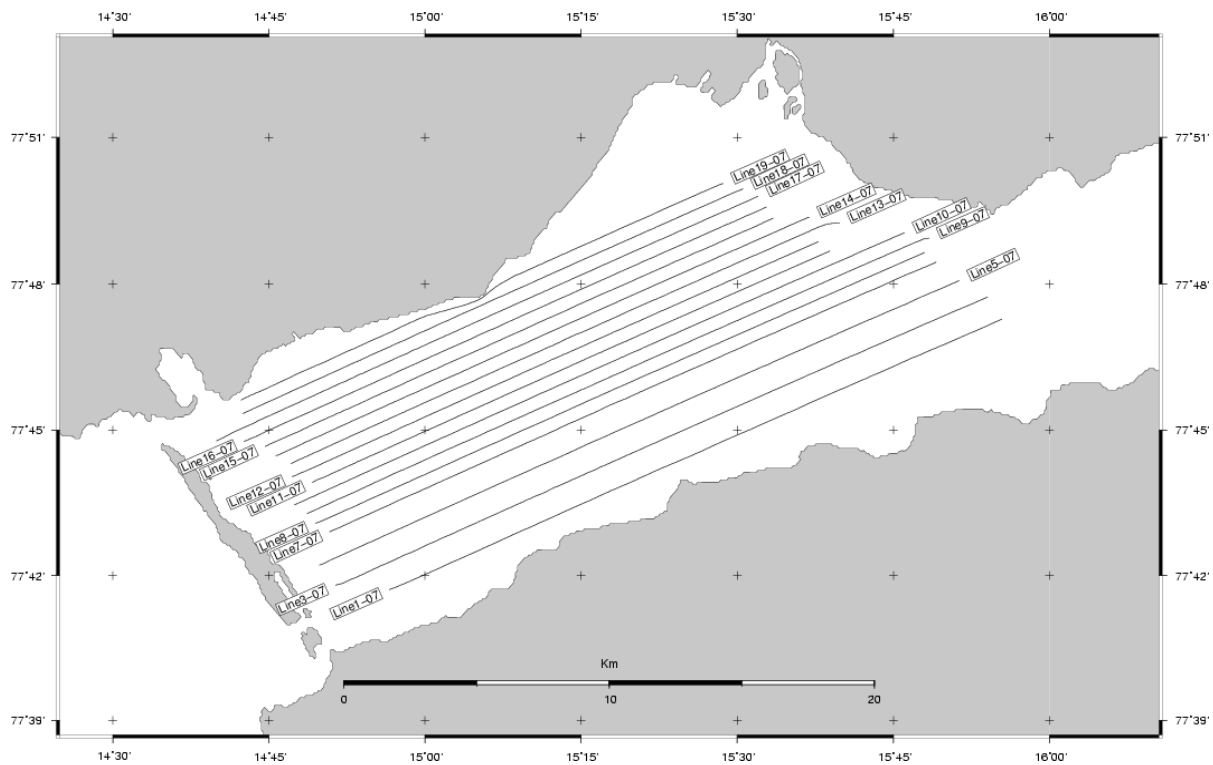


**Figure 4.6:** Seismic lines in this study

#### 4.2.3.1 Geophysical equipment

Multichannel seismic:

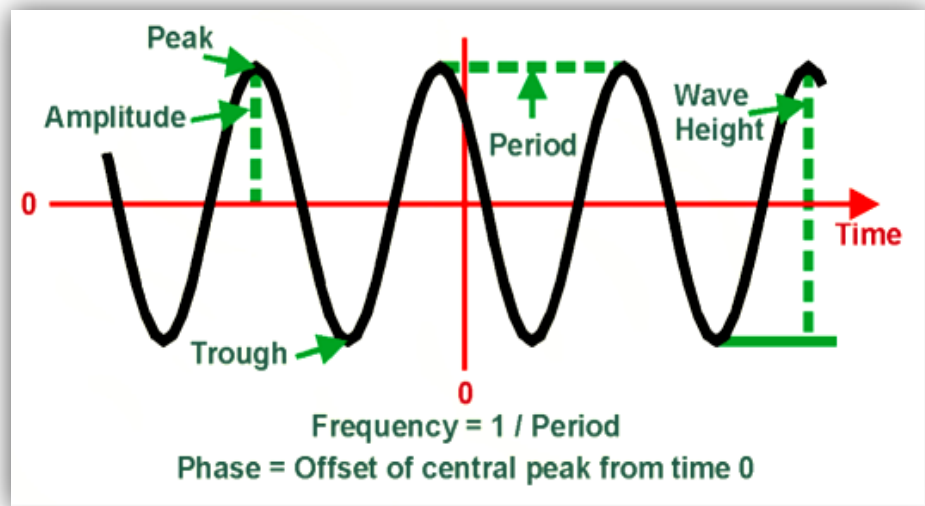
- 3.0 km digital streamer (WesternGeco nessie 3)
- triac recording (WesternGeco)
- Tuned air-gun array (6 Bolt air-guns). Total volume: 976 cu. inch
- 50 m shot-point interval
- 5.0 kn
- 12 s recording length
- 6m air-gun depth (pressure detector on one gun)
- 8 m streamer depth
- 12.5 m group length
- Distance from GPS antenna to center of source: 58 m
- Distance from GPS antenna to first active channel : 100 m leg I-III, 149 m leg IV
- Recording filter: 3 Hz (18 dB/octave), 180 Hz (72dB/octave)

Lacoste-romberg gravity meter

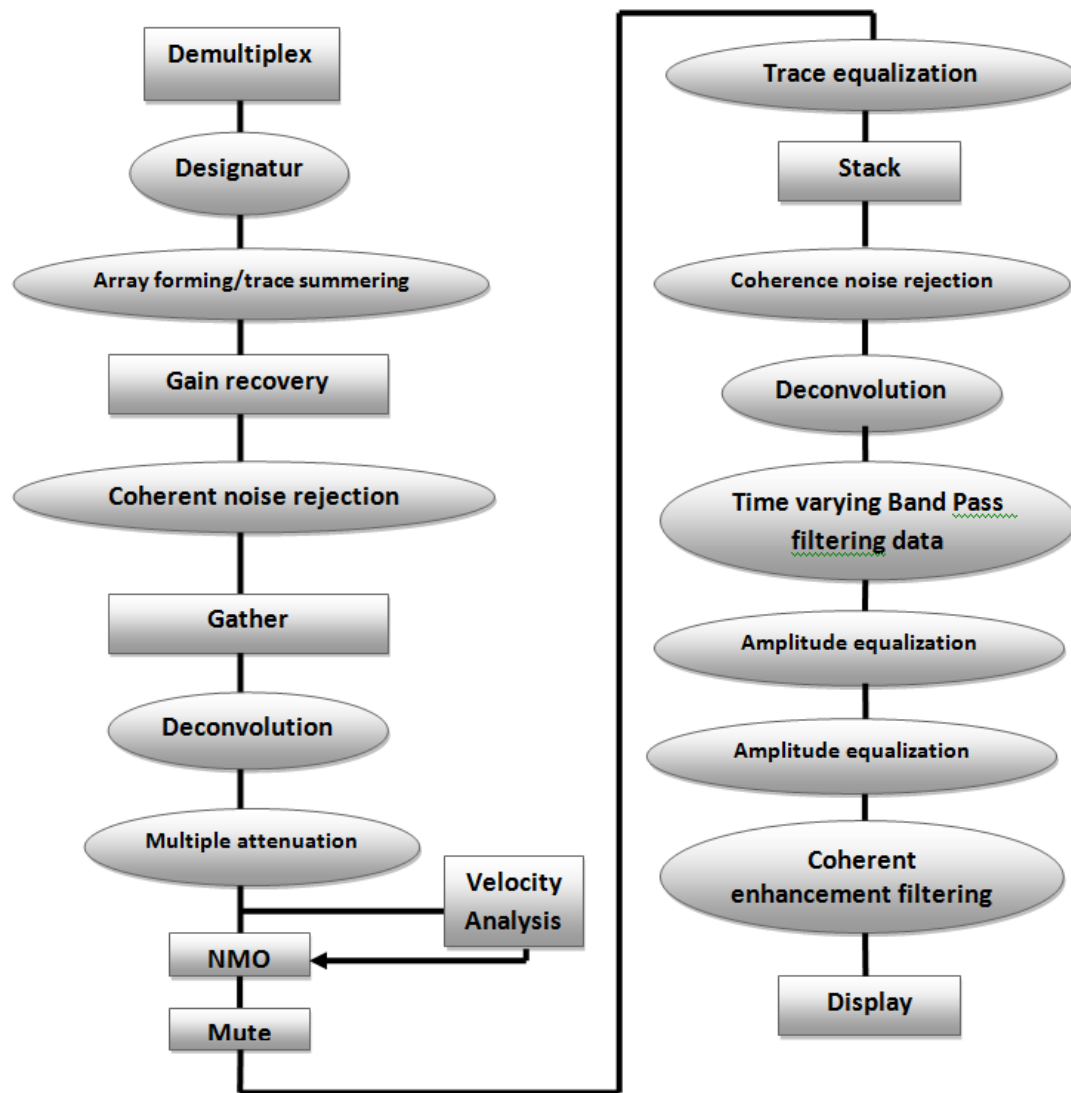
Marine proton magnetometer

### 4.3 General processing method

In this section, an overview of seismic processing will be discussed. Figure 4.7 shows some basic definitions in seismic processing such as peak, trough, frequency and phase and also a typical processing scheme for marine seismic data. Multichannel reflection data are acquired by shooting frequently along profiles, and detecting the reflected wave field by a large number of receivers on the surface.



(a)



(b)

**Figure 4.7:** (a) Basic definition in seismic processing. (b) Typical processing scheme for marine seismic data

In order to read or interpret the data in terms of geological boundaries, the data must first be corrected for the different source-receiver distance involved, noise must be reduced etc. This treatment or analysis of data is called processing. Good processing requires understanding of the concepts of data acquisition and interpretation as well as mathematical analysis behind the process. In this regard Fourier analysis, which is the most important mathematic analysis with respect to seismic processing, has been reviewed below. The steps of seismic processing will be discussed afterward.

### 4.3.1 Fourier analysis

#### 4.3.1.1 Theory

The Fourier-function transforms a function of the time,  $t$ , to a function of frequency  $\omega=2\pi f$ , where  $\omega$  is the angular frequency. There is also an inverse transform, which functions backwards i.e. from the frequency domain to the time domain. The Fourier-transform, or the Fourier integral, and the inverse transform are defined as follows:

$$F(t) = \frac{1}{2\pi} \int_{-\infty}^{\infty} F(\omega) e^{+i\omega t} d\omega =$$

$$\frac{1}{2\pi} \int_{-\infty}^{\infty} |F(\omega)| e^{+i[\omega t + \varphi(\omega)]} d\omega = \frac{1}{\pi} \int_0^{\infty} |F(\omega)| \cos[\omega t + \varphi(\omega)] d\omega$$

$$F(\omega) = \frac{1}{2\pi} \int_{-\infty}^{\infty} f(t) e^{-i\omega t} dt$$

Where  $F(\omega)$  is the Fourier-spectrum of  $f(t)$  and in signal analysis, the length,  $|F(\omega)|$ , is denoted the amplitude (see Figure 4.8) and the phase,  $\varphi(\omega)$  (see Figure 4.9).

**Figure 4.8:** A plot of amplitude  $|F(\omega)|$  as a function of frequency which is denoted the amplitude spectrum.

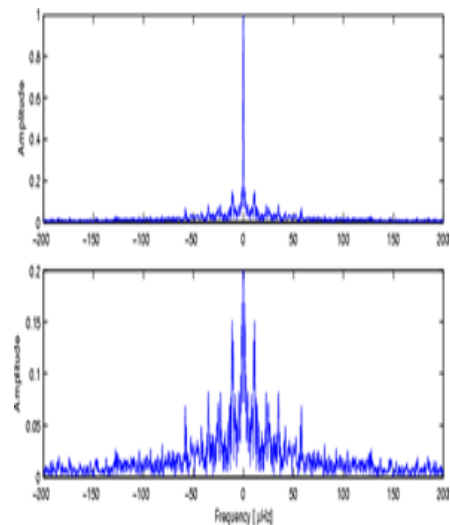
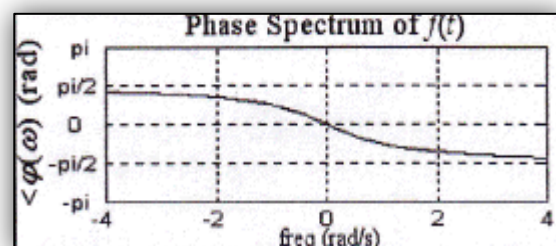


**Figure 4.9:** A plot of the phase  $\varphi(\omega)$  as a function of frequency which is denoted the phase spectrum.



#### 4.3.1.2 Spectra, pulse synthesizing revisited

The Fourier integral can be written as follow:

$$F(\omega) = \int_{-\infty}^{\infty} f(t) \cos(\omega t) dt - i \int_{-\infty}^{\infty} f(t) \sin(\omega t) dt$$

An integral is a sum with a summation step approaching zero. Figure 4.10 and Figure 4.11(a) show the visualization of the Fourier integral and attributed seismic signal. The signal, which is a function of time, can be considered as the sum of various Cos and Sin with different frequency, amplitude and phase. Each of those functions is infinite in time, but their sum, through constructive and destructive interferences, gives the seismic signal at the bottom of the Figure 4.11 (a).

The minimum phase wavelet has a short time duration and a concentration of energy at the start of the wavelet. It is zero before time zero (causal). An ideal seismic source would be a spike (maximum amplitude at every frequency), but the best practical one would be minimum phase. It is quite common to convert a given wavelet source wavelet into it's minimum phase equivalent since several processing stages (e.g. predictive deconvolution) work best by assuming that the input data is minimum phase (Figure 4.12).

The zero-phase wavelet is of shorter duration than the minimum phase equivalent. The wavelet is symmetrical with a maximum at time zero (non-causal). The fact that energy arrives before time zero is not physically realisable but the wavelet is useful for increased resolving power and ease of picking reflection events (peak or trough: Figure 4.7-a). The convolution of a zero-phase and minimum phase wavelet is mixed phase (because the phase spectrum of the original minimum phase wavelet is not the unique minimum phase spectrum for the new modified wavelet) and should be avoided (Figure 4.12 ).

By changing the phase spectrum various pulses (or signals) can be synthesized all having the same amplitude spectrum. Figure 4.11 (a) shows a casual pulse which corresponds to a so-called minimum-phase spectrum. The phase-spectrum in the figure express how the different components are shifted relative to each other along the time-axis. Figure 4.11(b) shows the zero-phase signal, where all components have their maximum at zero time.



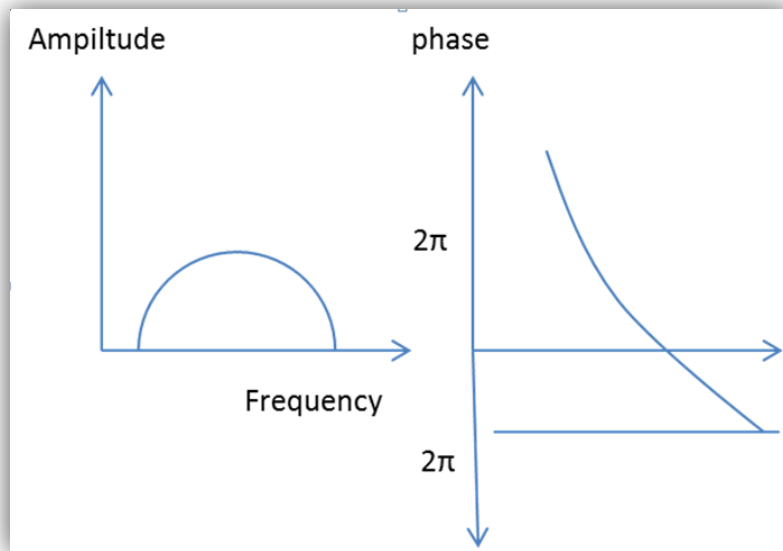


**Figure 4.10:** the Fourier integral

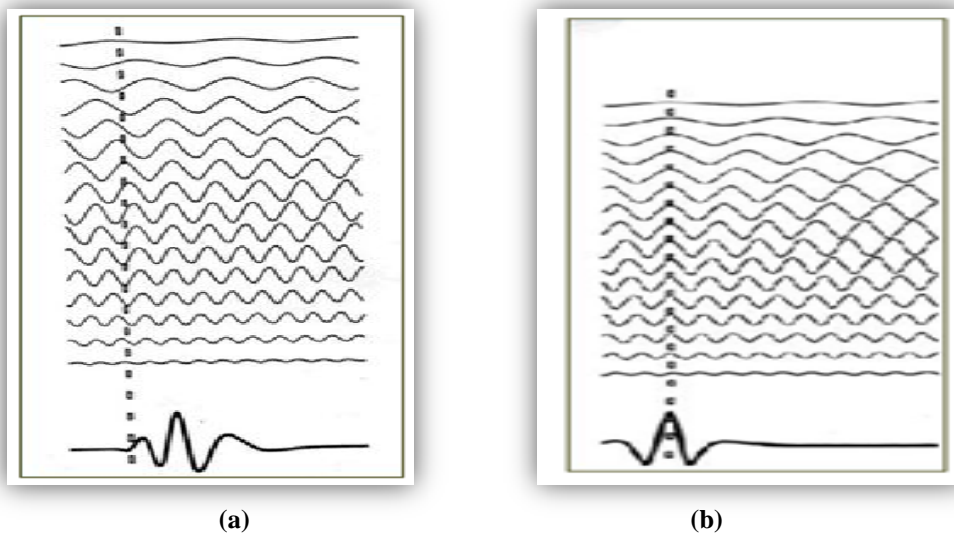


**Figure 4.11:** (a) Attributed seismic signal, (b) Zero-phase spectrum gives a time-symmetric pulse. It presents a non-physical or non-causal pulse.

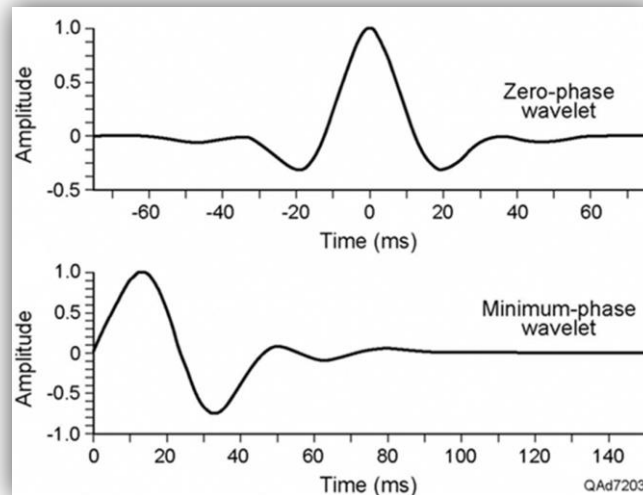


**Figure 4.12:** Zero\_phase and Minimum\_phase

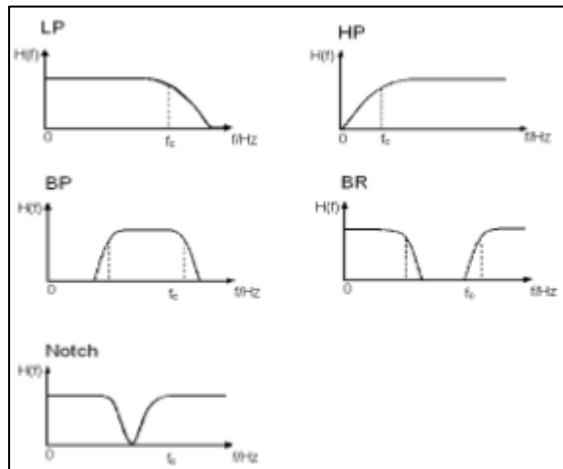
### 4.3.2 Operation steps of seismic data processing

Editing of the seismic traces involves the removal of traces that are either dead or contains much noise. The noise can be due to technical problems in a hydrophone, which will affect the signal to noise ratio negatively when stacking the data. Poor traces are removed as early as possible in the processing and replaced with interpolated traces or are set to zero. Editing in this part also means to reverse the polarity if necessary. The aim of the seismic processing is editing the result by applying different steps described below:

#### 4.3.2.1 Frequency Filtration

In this part, any rounded upper and lower cut off will be filtered to avoid "ringing" (Gibbs phenomenon) in the data (Kearey et al., 2006). Low-pass (LP) filter removes high-frequency noise such as electronic noise, and high pass filter (HP) removes low-frequency noise such as noise from ocean waves. Band pass (BP), band-reject (BR) and notch filters, respectively, retain and suppress frequencies within a specified frequency bands like 55 Hz electronic noise (see Figure 4.13). To perform frequency filtering, the data are converted from the time domain (amplitude as a function of time) to the frequency domain (amplitude and phase as a function of frequency) through a Fourier transform. After filtering, the data is converted back to the time domain through an inverse Fourier transform (Sheriff & Geldart, 1995).

**Figure 4.13:** Frequency response  $H(f)$  plotted as a function of frequency (in Hz) for different filter types. LP = low Pass, HP = high-pass, BP = band pass, notch and BR = band-reject filters. Outlined by Hatton et al. 1986; Kearey et al. 2006; Sheriff & Geldart, 1995.

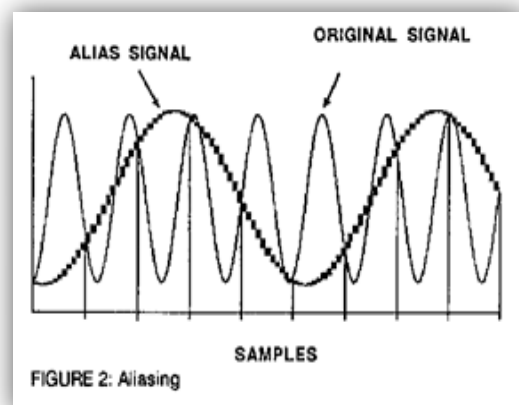


Another filter which must be used is the Anti-Alias filter (see Figure 4.14). The seismic measurement is stored as sequences of real numbers (digital data). If  $\Delta t$  is the time interval between each sample point, we can define the Nyquist frequency as:

$$f_N = \frac{1}{2\Delta t}$$

This frequency can be recovered from a sampled signal that gives the highest (theoretical) frequency. If the seismic measurement contains frequency above the Nyquist frequency, the sampled data will be aliased. Aliasing in time is avoided by using an anti-Alias filter before digitizing the data. An anti-alias filter is a low-pass filter with a steep slope (70 dB/octave), i.e. frequencies above the  $f_N$  are attenuated more than 70 dB compared to the maximum (flat) amplitude level of the filter (Keary et al., 2002).

**Figure 4.14:** Aliasing is a frequency ambiguity caused by under sampling of the continuous signal. Occurs for frequencies above the Nyquist value and results in high frequencies appearing as low frequencies after the sampling



FK-filtering is another filtering used. A two-dimensional Fourier transform over time and space is called an F-K transform where F is the frequency and K refers to wave-number. The space dimension is controlled by the trace spacing and must be sampled according to the Nyquist criterion to avoid spatial aliasing. Temporal Aliasing was previously discussed. In the F-K domain there is a two-dimensional amplitude and phase spectrum but usually only the former is displayed for clarity with colour intensity used to show the amplitudes of the data at different frequency and wave-number components.

In FK-filtering, the seismic data is plotted with frequency against apparent wavenumber  $k_a$ , where the relation between frequency and apparent wavenumber is given by this equation:

$$\omega = v_a * k_a$$

Where  $\omega$  is frequency,  $k_a$  is the apparent wavenumber and  $v_a$  is the apparent velocity of arrivals along the streamer. This means that arrivals can be filtered out on basis of their apparent velocity along the streamer. Deeper arrivals will have very high apparent velocities, since the angle between the wave-front and the streamer will be small. Disturbance propagation along the streamer will have low apparent velocities, because their wave-fronts will be almost perpendicular to the streamer (keary et al., 2002).

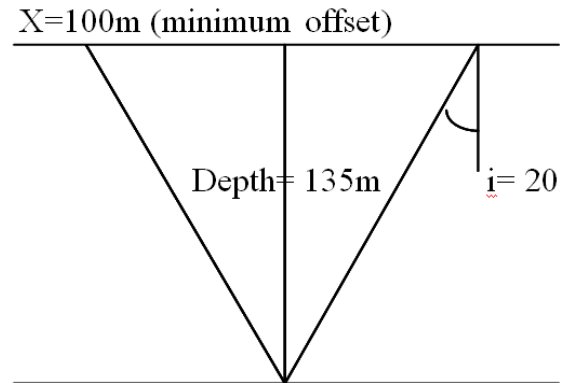
#### 4.3.2.2 Filtration Rate (dip-filtering)

As also noted above, Fourier transform can be used to convert data to the frequency-wave number (FK) domain. In this domain, different velocities have different slope, and one can thus perform filtering velocities by using a dip-filter. This is particularly effective in filtering out ocean bottom multiples, which has a lower velocity (thus varying dip) deeper than the real reflections. An inverse filtering transforms the data back in the time domain.

We can also use a hyperbolic or linear Radon transformation to discriminate between real arrivals and multiples. The data is transformed to the  $\tau$ -p domain, where one can separate the arrivals after the reflection, and thus the basis of velocity. The angle in Figure 4.15 is used in the calculation of a beam parameter (p):

$$P = \frac{\sin i}{v}$$

**Figure 4.15:** Trigonometric calculation of the minimum angle of seabed and minimum offset value of 100 meters.



#### 4.3.2.3 Deconvolution

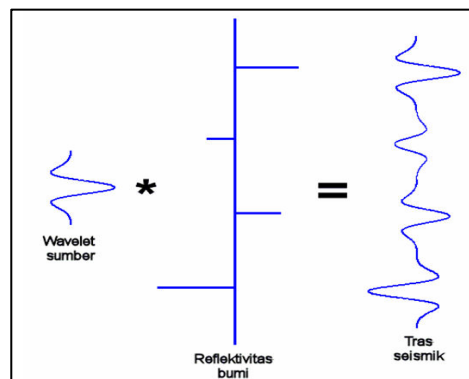
The simplest version of this model is based on the following assumptions:

- Horizontally layered earth model
- Normal incident plane waves
- Stationary source pulse
- Noise contribution to be neglected

By this condition convolution means: the seismic trace  $x(t)$  that can be described as a linear convolution between the source pulse  $s(t)$  and the earth's reflectivity  $r(t)$  (see Figure 4.16).

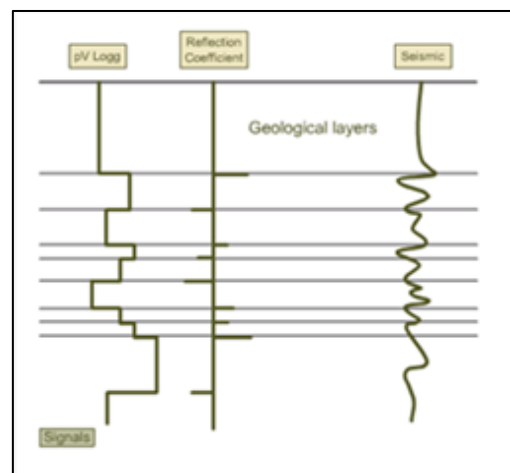
**Figure 4.16:** Convolution; if  $s(t)$  is the wavelet and  $r(t)$  is the reflection series, then  $x(t)$  is the seismic trace:

$$s(t) * r(t) = x(t)$$



Convolution with an inverse filter is a mathematical operation that separates the different signals. Generally, a process that used to improve seismic records by counteracting the effect of previous filtering processes is defined as deconvolution or inverse filtering. A deconvolution filter can remove the effect of e.g. multiples, and is one of the important operations in seismic data processing (Sheriff & Geldart, 1995). If the information about the signal and filter would be sufficient, deconvolution can be used to find the reflectivity range of the seismic traces. Spiking deconvolution compresses the signal and reduces the bubble pulse. Predictive deconvolution applied to mitigate the seabed multiples based on the assumption that these are periodic, while real reflections (prime honors) will arrive randomly (see Figure 4.17). Deconvolution can be performed either before or after stacking or both.

**Figure 4.17:** The left of the figure shows a simplified earth model with some horizontal layers. We can see these layers seismically if they have contrast in the physical parameter  $\rho v$  (acoustic impedance). Mathematically, the seismic trace is obtained by convoluting the transmitted signal with the reflection coefficient log. We make most practical use of this by doing the inverse; unwanted pulses in our data which can be attenuated by deconvolution.



The deconvolution model can be described as:

$$s = c * r + n$$

Where  $s$  is the recorded seismic signal,  $c$  is the effective seismic pulse,  $r$  is the earth's reflection number and  $n$  is noise. The aim of the Wiener-Levinson deconvolution is to find the inverse of  $c$  from the seismic data, and use this to remove the effect of  $c$  in the end to get the reflection line (Bed Bush & Hu, 1986). The algorithm requires minimum phase data.

#### 4.3.2.4 Sort of a common midpoint (CMP) and common shot point (CSG)

If the vessel moves along the line and air guns shoot at regular intervals, the same reflection points will be detected by different channels along the streamer (CSG-gather). In CMP-gathers the data is rearranged in order to contain traces representing the mid-point between

source and receiver (assuming the horizontal layer). CMP is shown schematically in Figure 4.18.

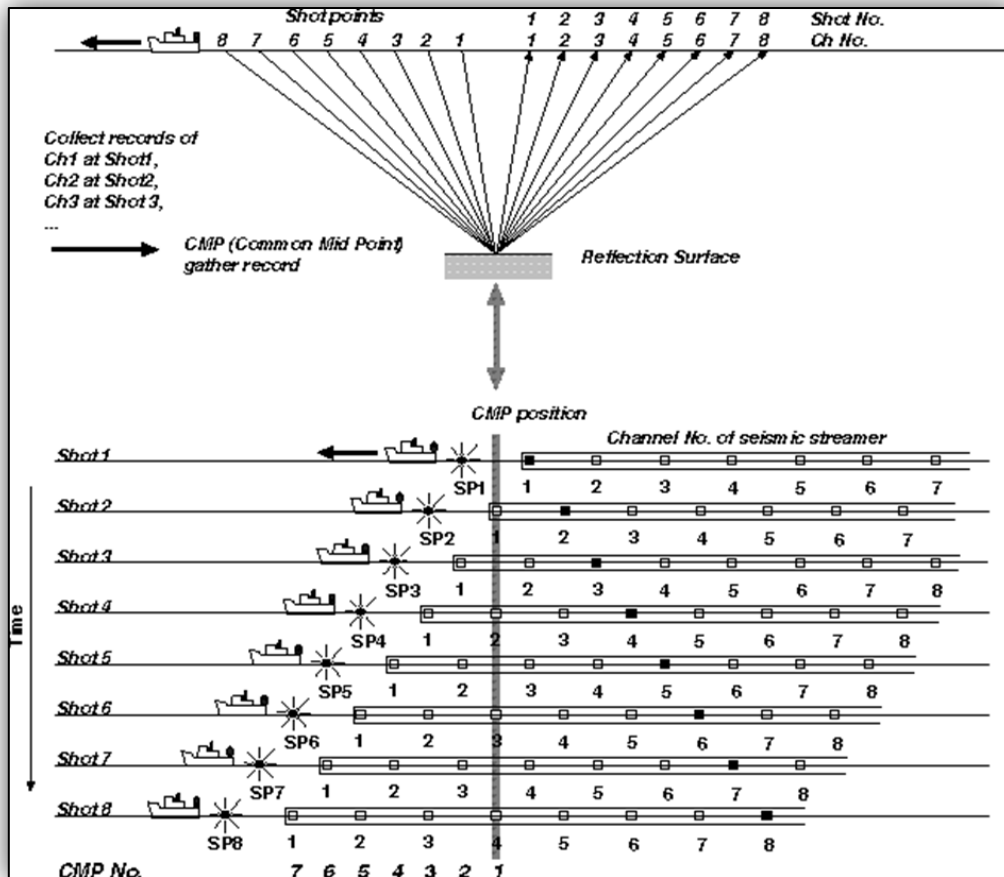
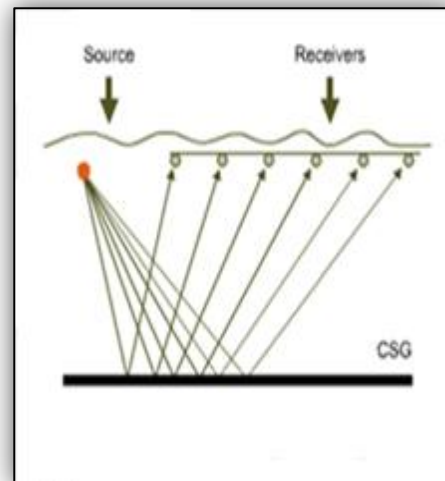


**Figure 4.18:** The raw data files are traces usually sorted by common shot number. Assuming that the collection vessel has constant speed and the shooting interval is regular for the whole line, the reflections of various shots depict the same point in the subsurface, but detected by different channels from shot to shot. Before stacking the data is sorted by common midpoint (CMP).

In multichannel streamer a single shot from a source will be detected by several groups of hydrophones or channels, distributed along the entire length of the streamer. Typically, each shot will be detected by 96 channels depending on the group length and 96 seismic traces will be recorded. When these traces are displayed next to each other, the display is called a common shot gather (CSG) (see Figure 4.19).

**Figure 4.19:** Example of CSG where one shot is recorded by 6 channels, note that the reflection point is different from each recording, meaning that a different part of the reflector is imaged by different recording channels.



#### 4.3.2.5 Adjustment of the amplification factor ("Gain recovery")

The gain recovery function is a procedure performed on the data to compensate for losses in amplitude due to geometrical spreading, absorption and wave conversions with depth. When the shot is fired, a pressure wave is generated. At the firing time the energy is collected at a point, and it expands spherically as a function of time in a homogeneous medium such as water. If  $r$  is the wave front's radius, the energy is given by  $\frac{E}{4\pi r^2}$ . Due to geometric spreading when distance increases along a beam path of the wave, energy will decrease with  $r^{-2}$ . The wave's amplitude is proportional to the square root of energy, and thus decreases with  $r^{-1}$ . (Sheriff & Geldart, 1995).

#### 4.3.2.6 Velocity Analysis

An accurate interpretation of the reflections requires knowledge of velocities of all points along the paths of reflection. Even if detailed information about the velocities would be available, calculations become infinitely long. Therefore, one can interpret based on a simplified velocity model that is detailed enough to provide a usable result, for example by assuming a constant velocity between the surface and the reflective layer boundary (Yilmaz, 2001).

Velocity analysis is to estimate a velocity that best matches observed move out, and is carried out by using a coherence plot: the highest amplitude is assumed to be the best stacking velocity (Yilmaz, 2001).



#### 4.3.2.7 NMO Correction

In a seismic survey, there is always a certain offset distance between the source and each of the receivers. This offset distance results in differential arrival times of an event recorded from the subsurface. The effect of this would be visible as a hyperbolic curve on the seismogram, where arrivals with a large offset will have a longer running time than the traces that are recorded by the receivers closer to the source (Yilmaz, 2001). Such a systematic difference in running time, called "moveout", is corrected for by use of the NMO correction, where the reflectors are horizontalized. Stacking velocities from the velocity analysis is used in the NMO-correction, so that the amplitude reflected from the reflectors is equal to two-way travel time, allowing constructive stack of primary reflections (see Figure 4.20)

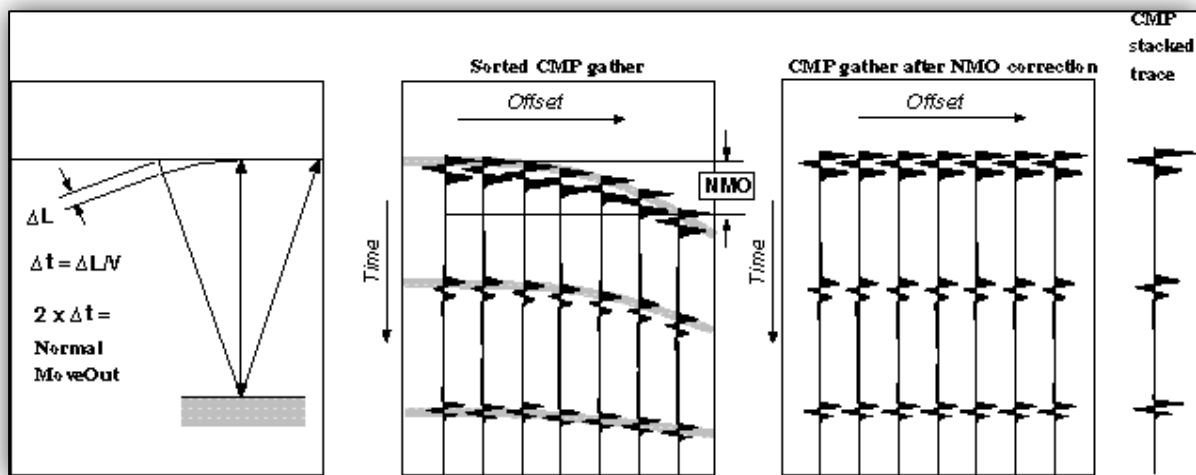
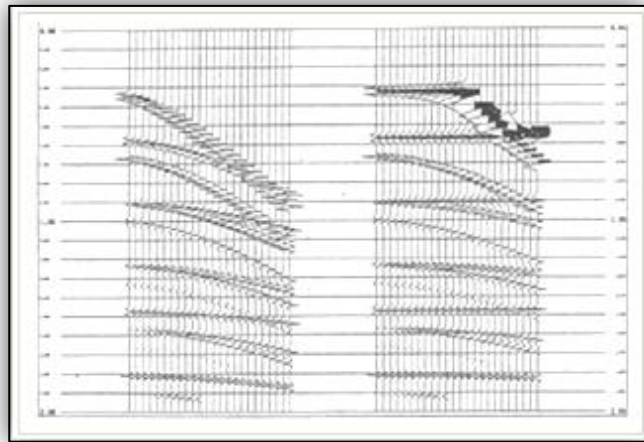


**Figure 4.20:** An example of a cmp-gather, containing reflections from three reflectors recorded by four channels. Increasing the shot-receiver distance increases the travel-time. The difference between vertical two-way travel-time and observed travel-time is called Normal-move-out

#### 4.3.2.8 Muting

The NMO correction implies stretching of the traces. This applies particularly for shallow arrivals with a large offset, where the dilation changes the pulse shape significantly. The most distorted parts are therefore replaced with zero values. This distorted part of the seismogram is removed from further use through muting (see Figure 4.21).

**Figure 4.21:** NMO correction implies differential stretching of the traces. The stretching is very large for the shallow far-offset arrivals. This distorted part of the seismogram is removed from further use through muting.



#### 4.3.2.9 Stacking

Stacking means that all traces of a common midpoint gather are summed together into one trace (see Figure 4.22). Stacking implies that primary reflections are summed constructively (in phase), while random noise is added destructively (not in phase). We have now obtained a reduction of the incoherent (random) noise by a factor  $M$ , where  $M$  is the number of channels, and we have also reduced the coherent noise considerably.

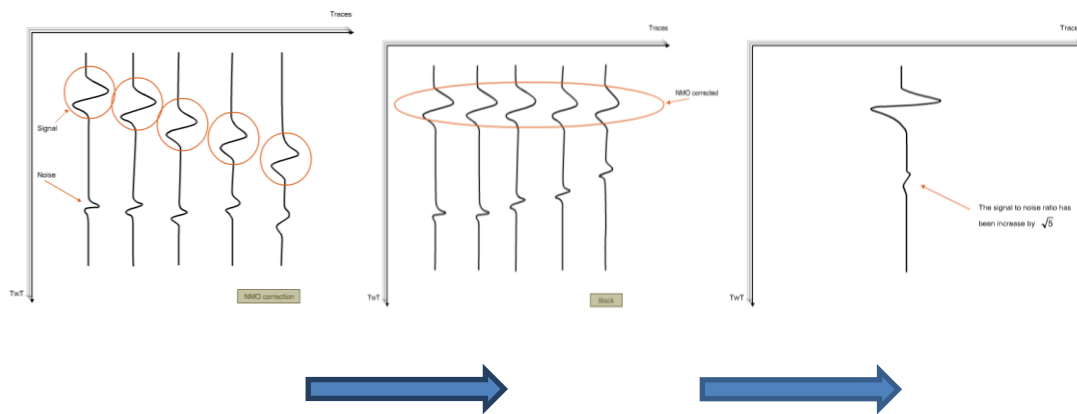


**Figure 4.22:** Stacking of the seismic traces

#### 4.3.2.10 Multiple attenuation

Since multiples have different ray-paths and stacking-velocities than primaries, multiples will be attenuated by stacking. This is shown schematically in the Figure 4.22 and 4.23, where the sea-floor multiple has smaller move-out than the primary sea-floor reflection, and larger move-out than the deeper primary reflection. After NMO correction, the two primary reflections will be horizontal, but the multiple will still show significant move-out.

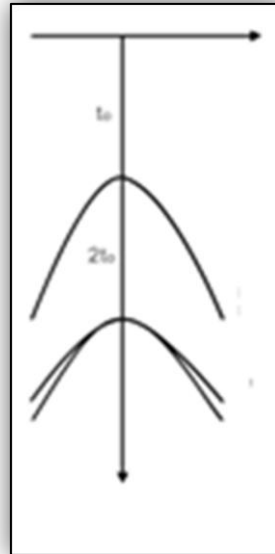


**Figure 4.23:** Multiple attenuation

#### 4.3.2.11 Migration

Migration operation is used in seismic processing to get an accurate picture of the underground layers. In the case of horizontal layer (see Figure 4.24), the reflections will occur at the same place for each common midpoint (CMP). But, in the case of dipping reflector layers (see Figure 4.25) along the survey line (inline), the true reflection points in CMP gathers are displaced in the up-dip direction and therefore gives a false impression of the reflector surface. In the migration process, the reflectors are placed in the right place in the underground. Migration can be performed with time or depth as vertical dimension, and using several different methods. Migration removes the diffraction hyperbolas generated by point reflectors such as faults, and it improves the seismic resolution by focusing the energy which is spread over the Fresnel zone . One of the drawbacks of 2D seismic data migration is the inability to deal with effects of cross-dip (crossline) features, in which the reflection points are displaced outside of the plane of the section. This can make a challenge to some degree in the interpretation of e.g. the Knipovich Ridge and the surrounding areas, which are heavily faulted and display a relatively rugged topography in more than one direction. Migration can be applied on pre-stack or post-stack sections. Pre-stack migration is extremely time consuming and is often replaced by DMO correction.

**Figure 4.24:** Reflection data is corrected for travel time and position relative to shot points which can arise due to geologic structures such as synclines and is seen as a bow tie on the stacked time series data. Migration is an inverse wave scattering calculation that relocates seismic reflections and diffractions to the location of their origin. Various methods of migration are DMO and frequency domain, ray trace and wave equation migration. ([http://perso-sdt.univ-brest.fr/~jacdev/ens/seis\\_proc05.htm](http://perso-sdt.univ-brest.fr/~jacdev/ens/seis_proc05.htm))

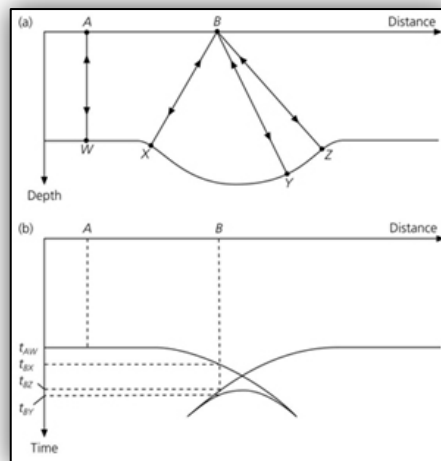
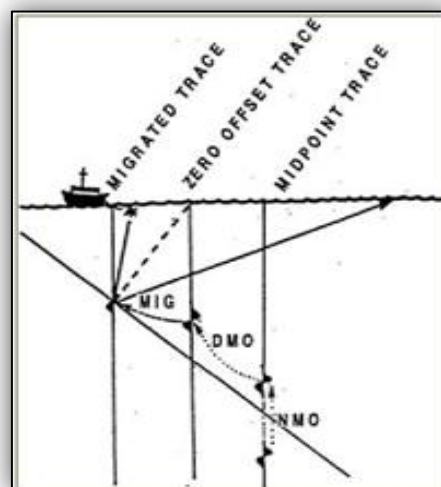


**Figure 4.25:** when the data contain dipping or diffracted events, migration must be applied in order to have a correct picture of the subsurface. Time migration is used to place events at their correct positioning time below the surface, while depth migration must be used to place events at their proper depth. The effect of NMO; DMO and migration are shown in the figure.



### 4.3.3 Seismic resolution

Seismic resolution is the ability to distinguish separate features; the minimum distance between 2 features so that the two can be defined separately rather than as one. Normally we think of resolution in the vertical sense, but there is also a limit to the horizontal width of an object that we can interpret from seismic data. In practice this means that a subsurface layer must have a certain minimum vertical thickness for the interpretation to be able to identify the upper and lower boundaries of the layer, and that a horizontally prevalent feature must have a certain lateral extent for it to be identifiable in the seismic section. Both vertical and horizontal resolution depends on the signal bandwidth (Yilmaz, 2001).

#### 4.3.3.1 Vertical resolution

Vertical resolution is the smallest distance in time or depth between two layer boundaries where they will appear as separate reflections. For two reflections, upper and lower layer boundary, respectively, the limit for how close they may be is related to:

$$\lambda = \frac{v}{f}$$

Where  $\lambda$  is the dominant wavelength,  $v$  is velocity and  $f$  is the dominant frequency (Yilmaz, 2001). In order for two nearby reflective interfaces to be distinguished well, their distance have to be about 1/4 wavelength (Rayleigh Criterion). This is also the layer thickness where interpretation criteria change. For smaller thicknesses than 1/4 wavelength we rely on the amplitude to judge the bed thickness. For thicknesses larger than 1/4 wavelength we can use the wave shape to judge the bed thickness.

However, in certain cases we may be able to discern bed thicknesses as small as 1/8 of the dominant wavelength in the signal (Widess, 1973). When the thickness of a bed is at about 1/8 of the dominant wavelength, constructive interference between the reflections from the top and the bottom of the bed builds up the amplitude to significant values.

There is a practical limitation in generating high frequencies that can penetrate deep. The earth acts as a natural filter (attenuation) removing the higher frequencies more readily than the lower frequencies. Therefore the resolution decreases with depth.

As an example: For a Shallow depth about 10 meters with the velocity of 1000 m/s and frequency of 100 Hz, the wavelength= 10 m. Whereas for a deep depth about 5000 meters with the velocity of 5000 m/s and frequency of 20 Hz, the wavelength= 250 m.

One could argue that we could simply increase the power of our source so that high frequencies could travel further without being attenuated. However, more powerful sources tend to produce lower frequencies (Sheriff & Geldart, 1995).

#### 4.3.3.2 Horizontal Resolution and the First Fresnel Zone

Horizontal resolution is the minimum distance at which two events with the same depth will appear as separate events. (Yilmaz, 1988 p. 470,71).

If we only consider rays then we never have any problems with resolving the lateral extent of features because a ray is infinitely thin and has infinite frequencies. However, the effect we see in real normal incidence data is explained better by wave concepts (Yilmaz, 1988).

A reflection is not energy from just one point beneath us. A reflection is energy that bounces back at us from a region. As waveforms are really non-planar, reflections from a surface are returned from a region and over an interval of time. Signal that comes in at about the same time may not be separated into temporally short individual components. So, we predict that reflections that can be considered as almost coincident in time interfere with each other (Yilmaz, 1988).

The area that produces the reflection is known as the First Fresnel Zone: the reflecting zone in the subsurface identified by the first quarter of a wavelength. If the wavelength is large, then the zone over which the reflected returns come from is larger, and the resolution is lower (Figure 4.26).

Horizontal resolution depends on the frequency and velocity. The width of the Fresnel zone is a function of travel-time, velocity and the dominant frequency of the signal (Figure 4.27).

**Figure 4.26:** Definition of Fresnel zone A - A' (Yilmaz 2001).

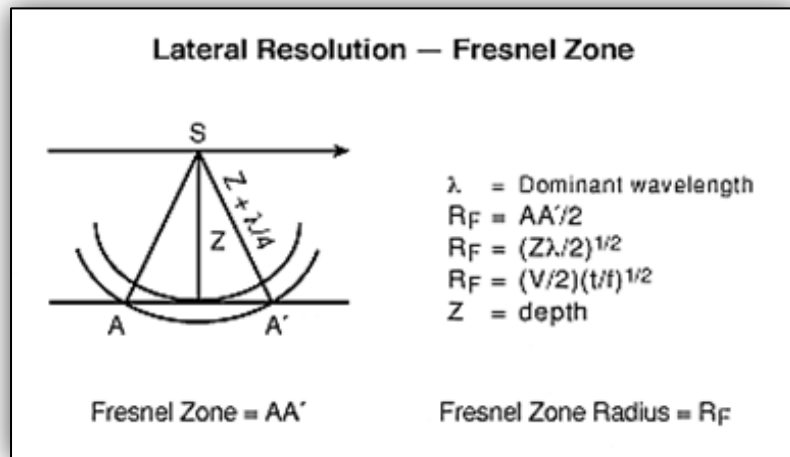
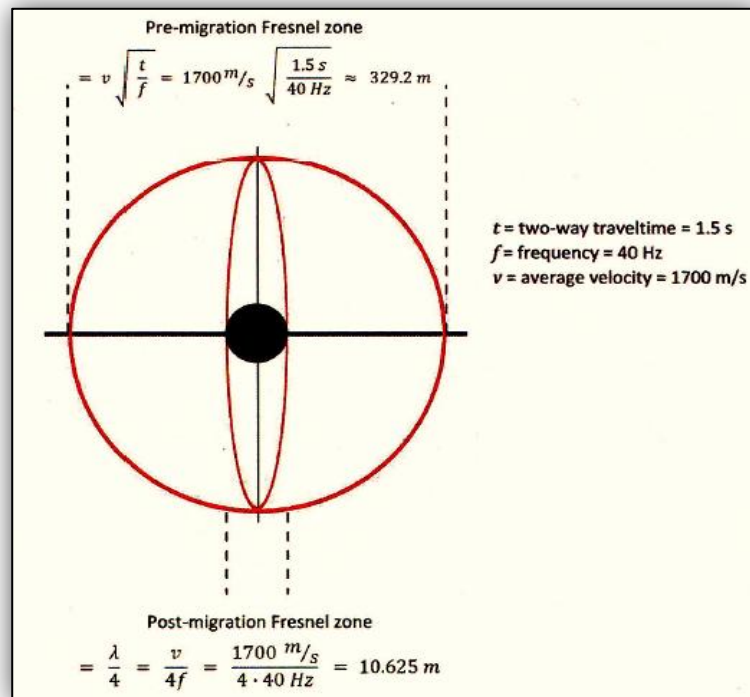


**Figure 4.27:** The effect of migration on the Fresnel zone. The example illustrates how migration reduces the width of the zone at 1.5 s (TWT) (Modified from Brown, 1999).



#### 4.4 Principles of seismic interpretation

2D seismic interpretation is a form of seismic interpretation which relies on the use of 2D surveys which provide visualizations of structures. People often use specialized software for this task, as 2D seismic interpretation requires a lot of math and a careful construction and interpretation of data. There are a number of applications for this process which includes the examination of sites to determine whether or not they would make viable oilfields, exploration of the ocean floor and general geological studies. In seismic surveys, controlled explosions are generated and the reflections of these explosions are read to generate knowledge on sub-surface structures. With 2D seismic interpretation, the data is mapped on

two dimensional representations which allow exploring the data in a number of different ways.

Interpretation of seismic data involves determining a model or prediction of geological features and structures in the subsurface, based on some fundamental geophysical assumptions (Sheriff & Geldart, 1995). General assumptions are that the coherent arrivals in the processed seismic sections are reflections from contrasts in acoustic impedance (density times velocity) in the subsurface, and then these contrasts can be related to the geological layering and structures (Sheriff & Geldart, 1995).

Seismic sections can often be divided into different units of the same seismic character, since the boundaries between different layers often are good reflectors. The units will be deposited during different geological periods under different sedimentological conditions. Layers can have angular relationships to each other that may indicate geological events, such as tectonic activity, transgression / regression, unconformities etc. (Sheriff & Geldart, 1995).

The interpretation of seismic data involves recognition and subdivision of discrete stratigraphic packages. This is primarily done by identifying unconformities in the sediments and analyzing variations in seismic characters within and between the identified units. A general methodology for describing reflection configurations of seismic facies and the termination of these facies on adjacent surfaces was established by Mitchum et al. (1977). The various reflection configurations include parallel, subparallel, hummocky, divergent, chaotic and reflection-free patterns (Figure 4.28).



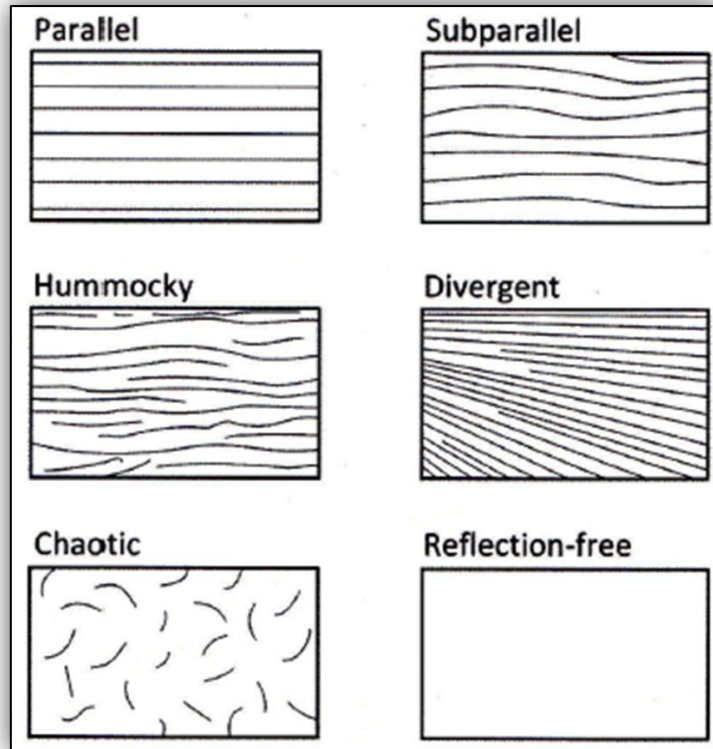


**Figure 4.28:** Reflection configurations used to describe seismic facies throughout the thesis (modified from Mitchum et al., 1977)

Figure 4.29 shows how the strata terminate against another sequence, "onlap", "downlap" and "toplap". Reflections are also often described in terms of their lateral continuity/extent, amplitude, frequency and other features that might characterize them.

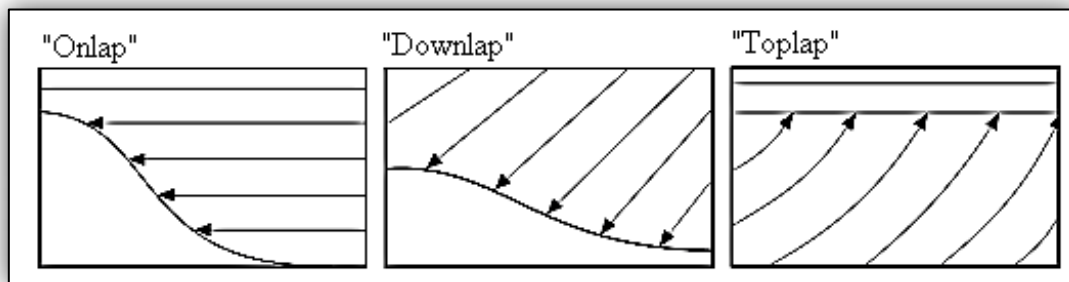


**Figure 4.29:** Termination of sedimentary strata onto surfaces.

The term "sequence" was first defined by Mitchum et al. (1977) as a relatively conformable succession of genetically related strata bounded by unconformities and their correlative conformities. The interpretation is done by defining the horizons and faults along the seismic section, thereby determining the reflector that represents the layer boundary that is desired to be identified. The horizon is followed consistently in either a positive ("peak") or a negative

amplitude (trough), representing a respectively increase and decrease in acoustic impedance. Horizons give only a two-dimensional appearance of any structures. In 2D seismic data several lines are often shot in a parallel pattern. The smaller the distance between the lines, the more accurately one can interpret the structures in the area. The lines are oriented so that the structures are best depicted. Borehole logs, previous results from geological surveys and geological history of the region are tools often used in conjunction with seismic interpretation. An example of this is plate tectonic conditions, which will characterize the fault geometry and other structures over areas on a larger scale (Sheriff & Geldart, 1995).

#### **4.4.1 Impedance**

The product of density and seismic P-wave velocity which varies among different rock layers, commonly symbolized by  $Z$ . The difference in acoustic impedance between rock layers affects the reflection coefficient. The deconvolution during seismic processing can convert data of minimum phase to zero-phase data, but is not always successful. Zero-phase data tend to provide sharper definition and less distortion between stratigraphic features in the subsurface, such as sand and shale layers (Figure 4.30).

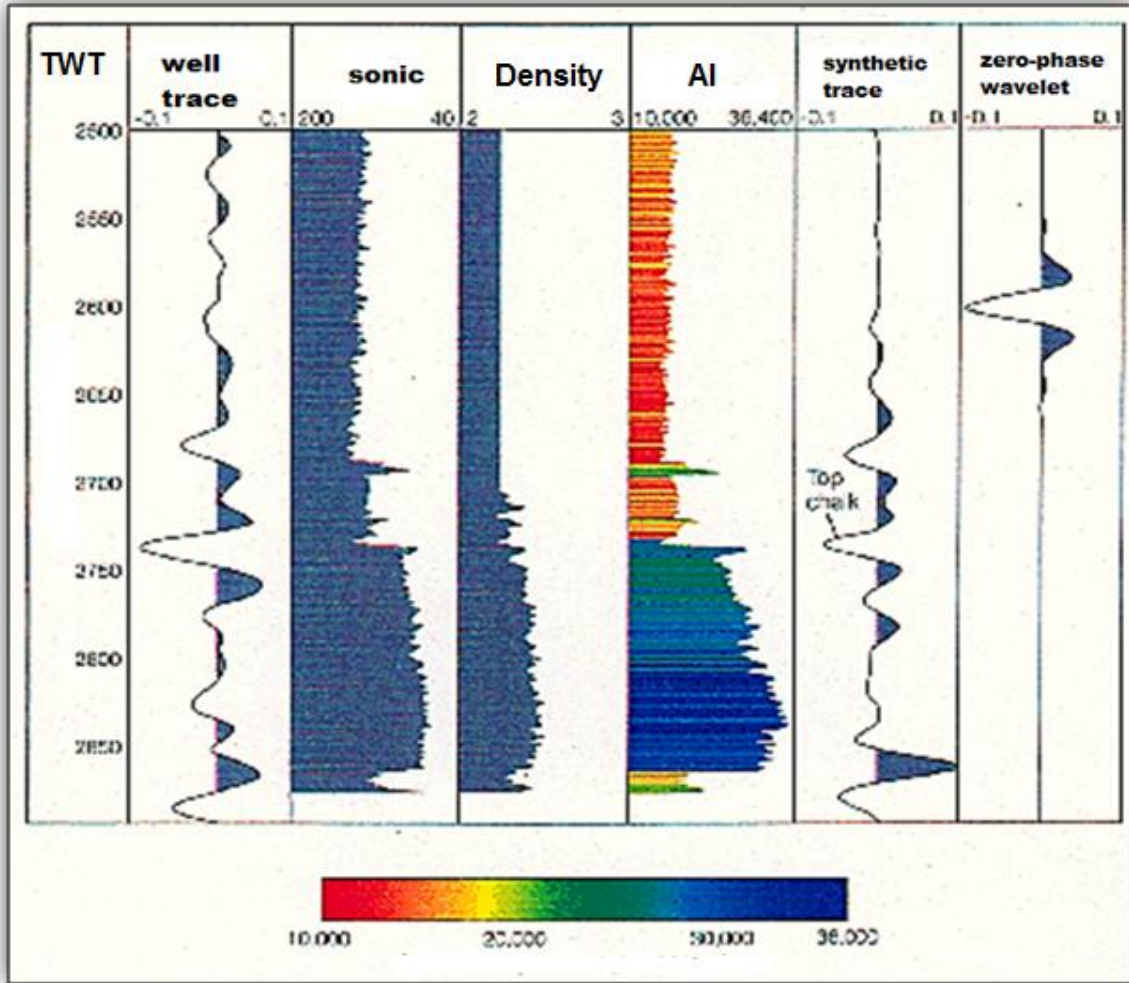


Figure 4.30: Well trace, sonic log, Density log, Acoustic impedance, Synthetic trace, Zero phase wavelet.

## 5 Acquisition and Processing of Geophysical Data

### 5.1 Acquisition data

#### 5.1.1 Svalex 2007

There are 19 seismic lines that we will use for the processing. All of the seismic lines are from Svalex 2007 except lines number 2, 4, and 6. The processing job is divided in four sequences, editing; filtering and deconvolution; velocity analysis; and stacking and migration. In order to get a consistent 3D numbering system with line numbers and crossline numbers (the CDP number is called the crossline number in 2D seismic surveys), the CDP numbers have been calculated by the following way:

For all lines running from West to East (1, 3, 7, 8, 11, 12, 15, and 16) a common formula as below were used:

$$\text{CDP} = 8 * \text{SP} - \text{CHN} - 7007$$

With the above formula, the CDP number 1000 will be directly below shot point 1000. Since the CDP number increases 8 times faster than the shot number, shot point 1100 will coincide with CDP 1800 and so on.

For the lines running from East to West (5, 9, 10, 13, 14, 17, 18, and 19) we should use different formulas for each line, and there is following formulas which gives CDP numbers consistent with other lines:

$$\text{Line 5: CDP} = -8 * \text{SP} + \text{CHN} + 13417$$

$$\text{Line 9: CDP} = -8 * \text{SP} + \text{CHN} + 13379$$

$$\text{Line 10: CDP} = -8 * \text{SP} + \text{CHN} + 13194$$

$$\text{Line 13: CDP} = -8 * \text{SP} + \text{CHN} + 12857$$

$$\text{Line 14: CDP} = -8 * \text{SP} + \text{CHN} + 12705$$

$$\text{Line 17: CDP} = -8 * \text{SP} + \text{CHN} + 12514$$

$$\text{Line 18: CDP} = -8 * \text{SP} + \text{CHN} + 12441$$

$$\text{Line 19: CDP} = -8 * \text{SP} + \text{CHN} + 12354$$

For instance, for line 5, with shot numbers running from 1006 to 1538, the first CDP number (lowest number/western end) will be

$$\text{Line 5: CDP} = -8 * 1538 + 1 + 13417 = 1114$$

And the last (highest number/eastern end) will be:

$$\text{CDP} = -8 * 1006 + 240 + 13417 = 5609$$

### 5.1.2 Svalex 2008

The remaining lines (2, 4 and 6) were shot during Svalex 2008. Line 2 and 4 were shot from west toward east and the CDP numbers can be computed as before according to the following formula:

$$\text{Line 2 \& 4: CDP} = 8 * \text{SP} - \text{CHN} - 7007$$

Line 6 was shot in the opposite direction, and for this line the following formula was used:

$$\text{Line 6: CDP} = -8 * \text{SP} + \text{CHN} + 14615$$

During Svalex 2008, the streamer was lacking one section (100m, 8 hydrophone groups), and the first 8 channels recorded unuseful data during the acquisition. Channel 9 was the first channel recording useful data, and it is also the group with the least offset (102.5m as last year). Therefore it is necessary to make some changes in the way the channels are read or in the way the offsets are set.

A possible solution is to select only channels 9 to 240 during reading, and then reduce the channel number with 8 (using MODET). This will reduce the number of channels to 232. Thereafter, the offset can be computed as before.

## 5.2 Seismic data Processing

The software used for processing of the data is Geocluster (CGG Veritas, 2006), and for velocity analysis Chronovista /Geovel has been used.

### 5.2.1 Editing

This processing sequence consists of 2 jobs, read and reformat. The steps are shown in Figure 5.1.

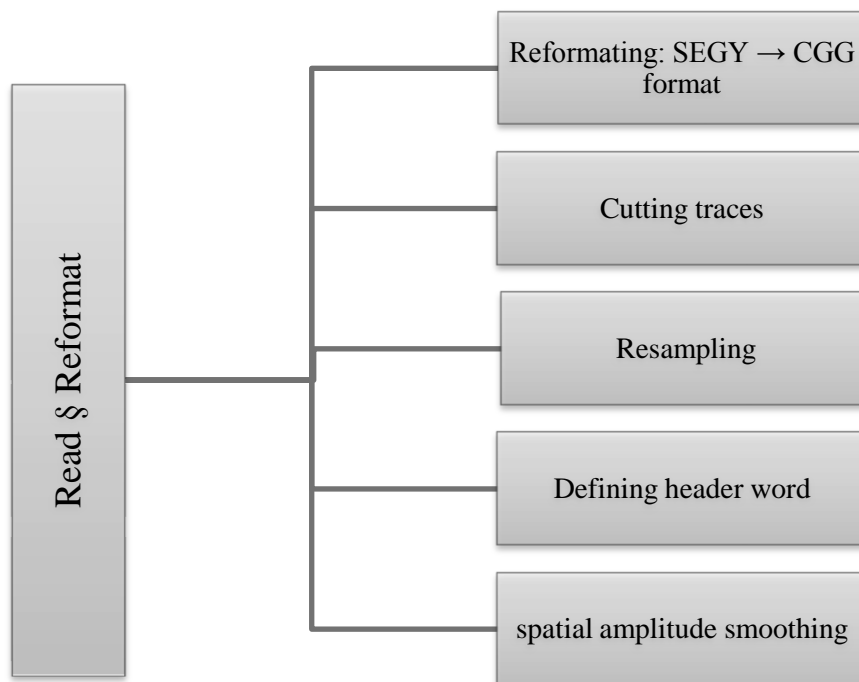


**Figure 5.1:** Read and Reformat jobs in processing sequence

The raw data were transformed to SEG-Y format and then reformatted to an internal Geocluster format. Thereafter we cut the amount of data by 6144 ms, half of the registered trace length for all the traces. Resampling from 2 to 4 ms half again the amount of data, probably without significant loss of quality with regards to the scale of the structures in the area to be mapped. The spatial amplitude thickening ("spatial amplitude smoothing") was then applied in order to reduce spikes and other loud noises. This process replaces the manual editing.

Furthermore, the header words were defined. Some headers were defined already in the raw data file such as channel and shot number. Using the header word calculation module,

MODET, CDP-number, offset, line number and CDP-position were calculated for source and receiver. Figure 5.3 shows the raw data before BP filtering.

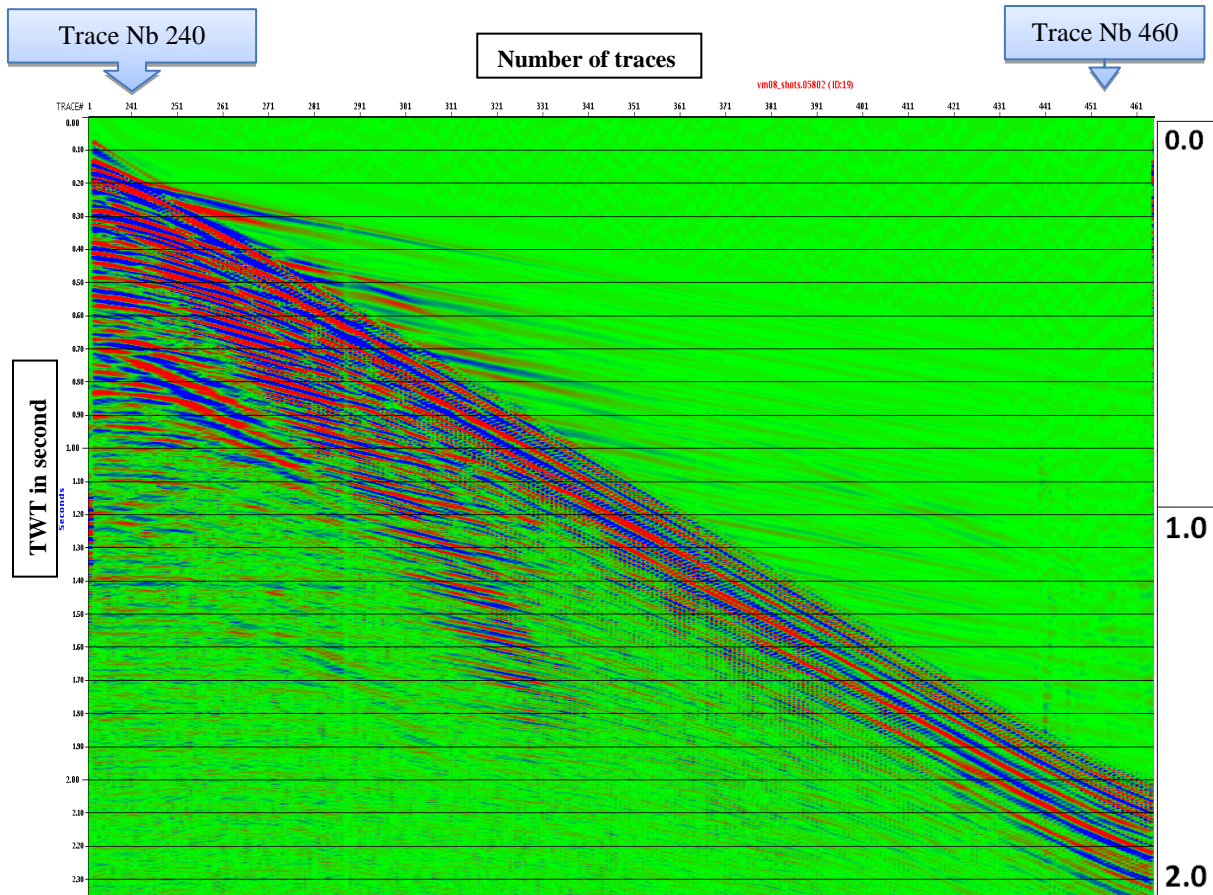


**Figure 5.3:** Line 6, name of output is Vm08\_shots\_05802, year 2008, the figure obtained after read and format jobs.

### 5.2.2 Filter and Deconvolution

The biggest challenge of processing the data is the removal of seafloor multiples. High amplitude multiples are generated as a result of abnormally high velocities in the seabed, estimated at over 4000 m/s from the ocean bottom refractions observed on the shot collections. Most of the primary reflection waves are masked by multiples, as the relatively shallow water depths (100-200 m) lead to short distances between each seafloor multiple. Multiple removals are performed using different processes which are shown in the Figure 5.4. A FK-filter was used to remove the waves that only propagate in the water layer (total reflection). After this step, a Band Pass (BP) filter was defined by 7.5 to 15 Hz to 90-115 Hz. By filtering out frequencies above 115 Hz preventing aliasing, the Nyquist frequency (at 4 ms sampling) is 125 Hz.

Then deconvolution was performed using the module "DECSC" in order to remove what is left of multiples in the water layer (pre-critical reflections / small angles) for FK and Radon filtering. This processing sequence seems to work well where there is a high velocity in the seabed and relatively shallow water.

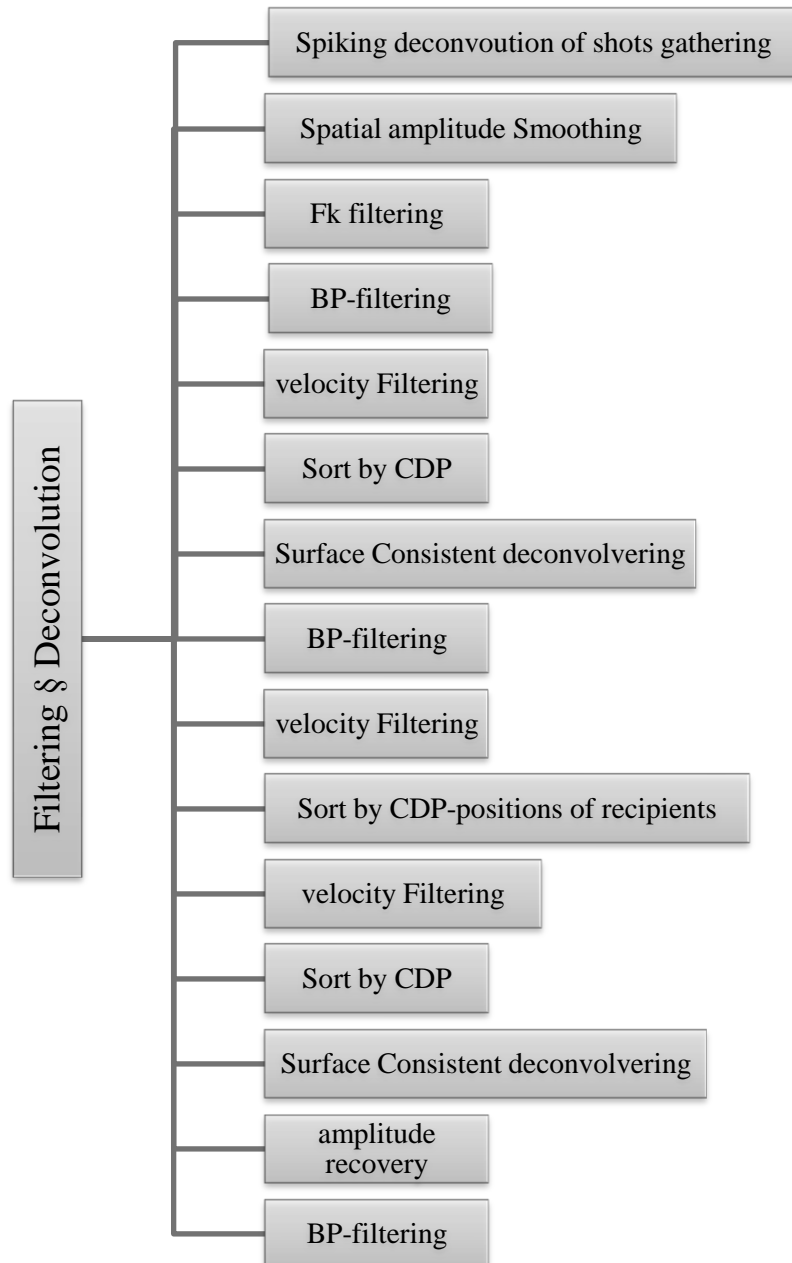


**Figure 5.4:** The schematic of filtering and deconvolution process sequence.



To remove the bubble pulse and to improve the source pulse by means of the "standard spiking multi-channel deconvolution" option, the deconvolution MCDEC module was used. The bubble pulse is common to all arrivals regardless of offset. The process applies a filter for each shot for sorted data (Figures 5.6-5.8).

Spatial amplitude smoothing is applied both before and after MCDEC. The process is used to equalize the amplitude of each

An FK filter is applied to the data before the velocity analysis. The velocity is given by  $V=F/K$ . Rates between the -4000 and 8000 m/s is maintained. These limits are determined graphically, based on the FK plot in Team view (Figures 5.5 and 5.6). In Van Mijenfjorden the velocity in the seabed is very high, over 4000 m / s. Arrivals with apparent velocities below this velocity are multiples because they must propagate only in water layer.  $V_1 = -4000$ ,  $V_2 = -6000$ ,  $V_3 = 6000$ ,  $V_4 = 9000$  and the trace spacing of 12.5 has been selected for the processing of data.

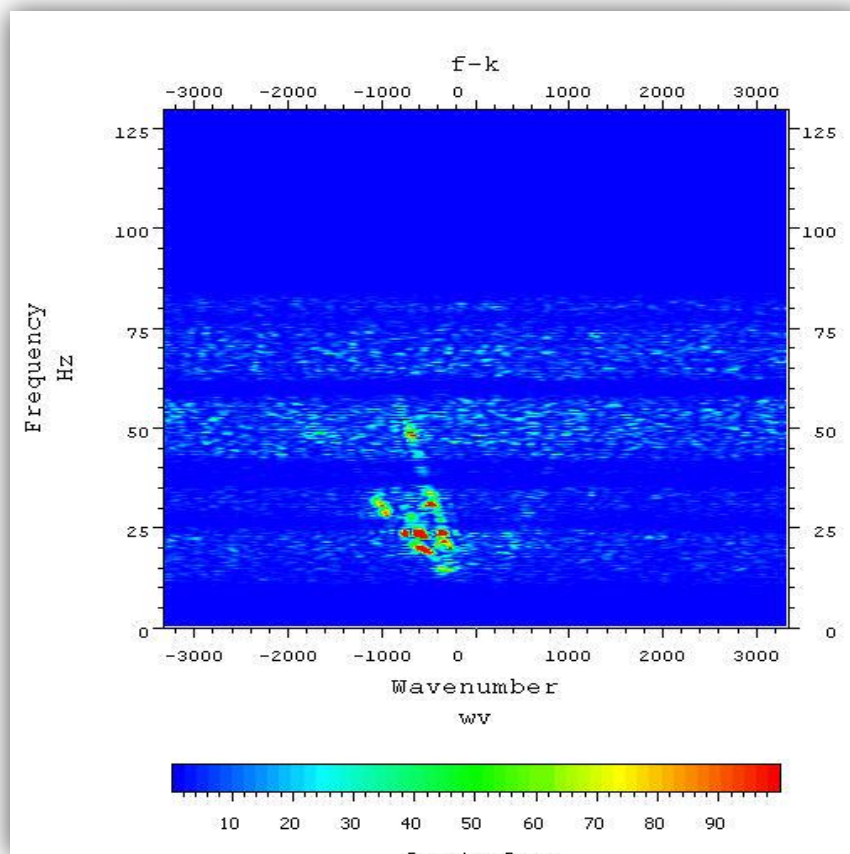
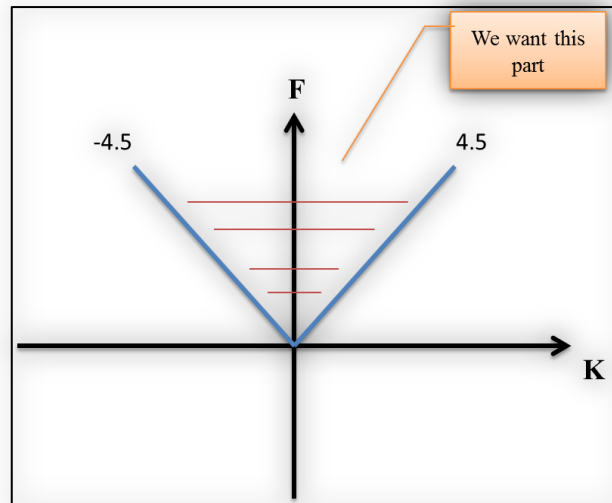


**Figure 5.5:** FK-filtering. An FK filter is applied to the data before the velocity analysis. This converts the data to the frequency ( $f$ ), wave number ( $k$ )-domain, where filtering is performed before an inverse transform back to the time offset domain (CGG, 2006).

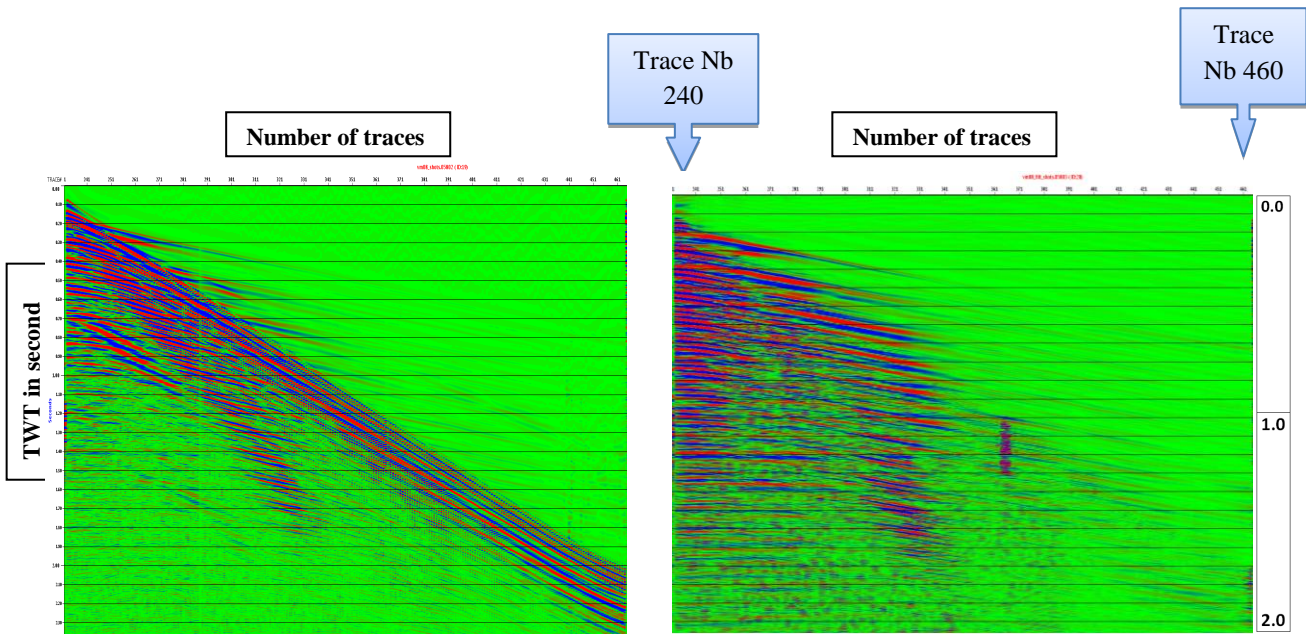


**Figure 5.6:** Line 6, VM08-filt-05802 before filtering (left), VM08-filt-5803 after filtering (right).

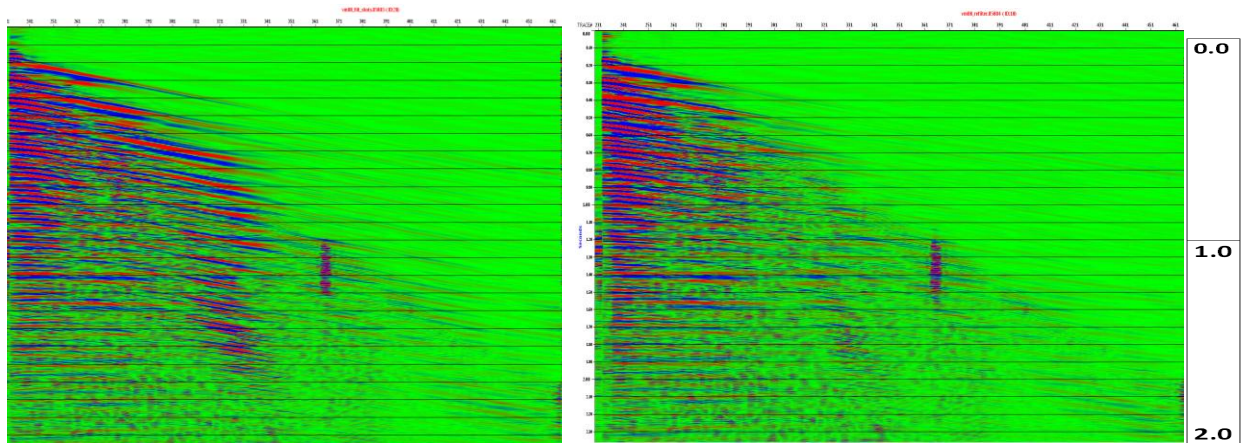


**Figure 5.7:** Line 6, VM08-filt-5803 after filtering (left), result after Refilter, VM08-filt.05804(right), CDP: 4751 to 4800, shot number :565 to 600, receiver :2491 to 2500.

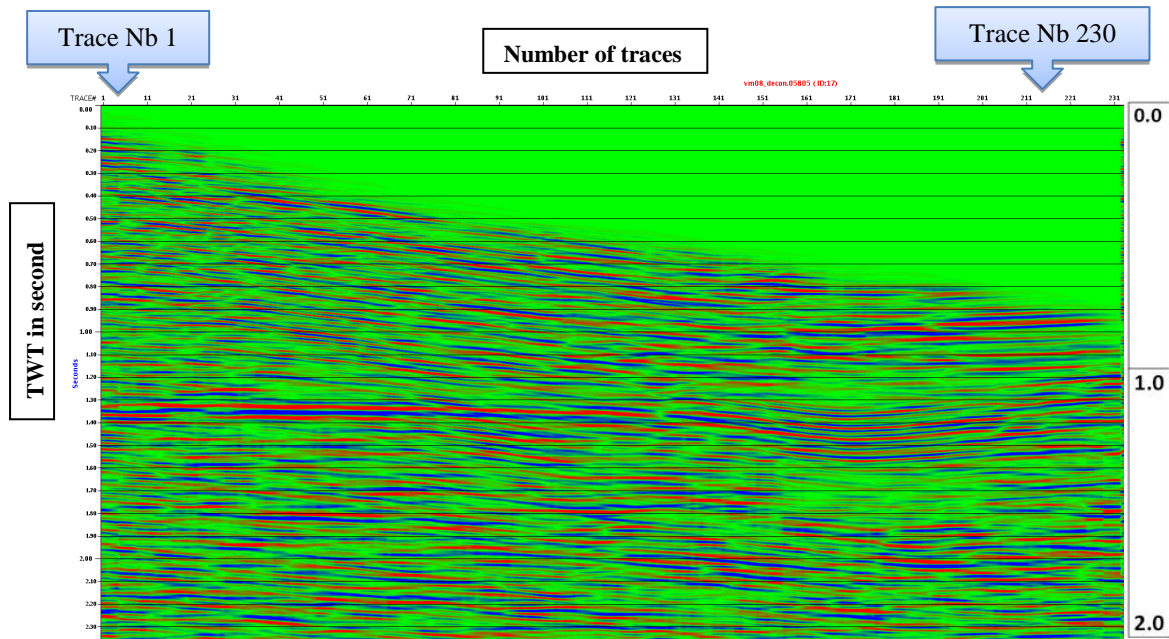


**Figure 5.8:** Result after deconvolution job, VM08-filt.05805.

Radon multiple removal is applied to the data using the module RAMUR, which uses a linear Radon transformation ("Slant Stack") to discriminate between actual arrivals and multiples. Both BC-filtering, described earlier in this chapter and linear Radon multiple removals (with the help of RAMUR) are velocity filtering with the same purpose, i.e. to remove the waves that propagate only in the water layer ("total reflection"). Radon multiple removal is used in addition to a BC-filter when the module RAMUR has higher resolution, meaning that it can distinguish sharper between small velocity differences, and that it is not as limited by spatial aliasing as the module used for BC-filtration (FKFIL). The slope of the filter in RAMUR is used to calculate a relationship between the largest offset ( $XRM = 3100$  m) and a truncation value, DTCUT in milliseconds (Figure 5.9) (CGG, 2006).  $XRM$  divided by DTCUT is equal to the inverse of the beam parameter, which also indicates the apparent velocity. DTCUT of 700 ms, which gave the best results when tested, gives an apparent velocity of 4429 m / s.

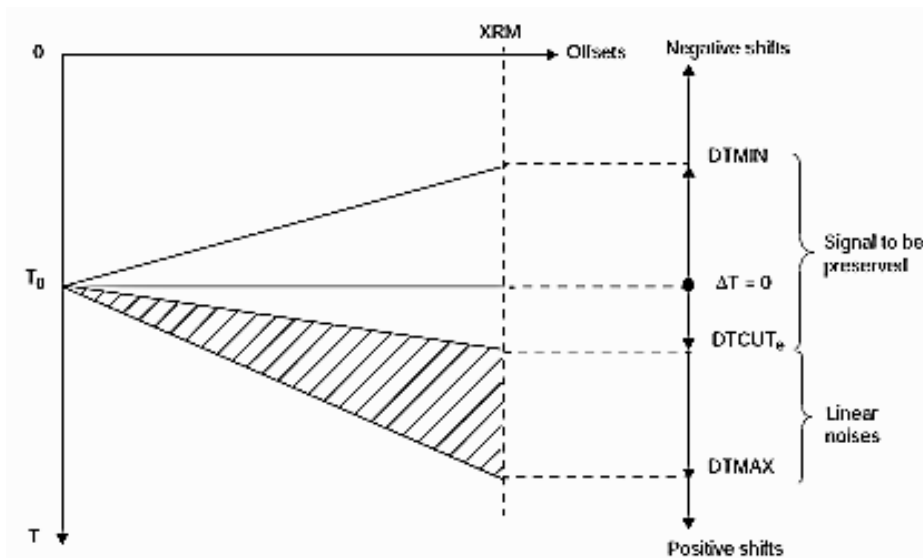


**Figure 5.9:** Graphical view of Delta T. Shaded area marks the energy muted out. By increasing the value of DTCUT the data at lower speeds are maintained. DTCUT = 700 ms and DTMAX = 1000 ms is used. Figure from CGG (2006).

By sorting the receiver gathers, one can simulate collections that are "shot" in the opposite direction, and thus have different apparent velocity than the original shot collections. Here is the principle of reciprocity used. Response time along a stream path is the same regardless of direction, and it will therefore be the same running time if we flip positions of source and receivers. Dipping layers will get the same effect as "downdip" and "up-dip" shooting. CDP-position of the recipients is calculated by

$$\text{CDP} - \frac{\text{offset}}{12.5} = \text{CDP} - \frac{1}{2} \frac{\text{offset}}{6.25}$$

Group length is 12.5 meters, but it is divided by 6.25 m, which is the interval between each CDP-point, to get the result as the CDP-point. Similarly calculated CDP-position shots by

$$\text{CDP} + \frac{\text{offset}}{12.5} = \text{CDP} + \frac{1}{2} \frac{\text{offset}}{6.25}$$

Number of traces in the collections varies with the type of sorting: Sorting Data Recipient will have 60 traces in each gathering (3 km streamer divided by 50 m shot interval), while collections sorted by shots will have all 240 traces, one for each channel of the streamer. In a CDP gather, the number of traces will be equal to the fold of the data, i.e. 30 traces per gathering (12.5 m receiver distance times 240 recipients, divided by 2 x shot distance). This

means that a Radon multiple removals will have less effect when applied to a CDP-gather, which is 100 meters between each track, than if applied to a shot collection of 12.5 meters between channels.

Deconvolution module DECSC performs surface consistent spiking deconvolution, and was applied to the data twice for Radon multiple removals of data sorted by respectively shots and after CDP-position of the recipients. DECSC perform deconvolution before stacking. Convolution model is similar to MCDEC, described in a previous section. It calculates a filter for each shot, one for each receiver position, an average filter and a filter for each offset interval. The module also has the ability to calculate a filter for each CDP location, but this is not used as the documentation warned that the CDP filter can remove the actual arrivals. Since the water depth is relatively small compared with the typical offset, and the wide-angle reflections have been removed in previous processes, the remaining data contain multiples propagating almost vertically in the water layer, either near the source or close to the recipients.

Filtration is performed for each shot and receiver position to remove multiples of both shot and receiver side, although there are differences in depth between these.

An alternative deconvolution modul (TRITA) was also tested but gave a poorer result. This may be because the module uses the water depth of the CDP-points, and thus will not be completely accurate when the seabed varies by approx. 40 ms along the lines.

Deconvolution extends the frequency band. This makes the signal narrower ("spiking"), and increases the bandwidth. Frequencies above and below the seismic signals that are believed to contain relevant information will be dampened by a band pass filter [7.5 to 15 Hz, 70-90 Hz] after each deconvolution. This is done three times, after MCDEC and after each of the two DECSC operations.

### **5.2.3 Velocity analysis**

By using the chronovista application the velocity analysis for each line can be done separately. Velocities are selected for each 160 CDP, and interpolated between them. Figure 5.10 shows, from left: 1) a velocity spectrum (coherence plot (semblance coefficient)) with



clear effects (marked with lighter colors) for misc. reflectors; 2) interval velocity is very high for short travel times: approx. 5000 m / s at 200 ms, and then only a slight increase with increasing depth is observed; 3) CPD collection, before and after NMO correction, respectively with the specified interval velocities. Hyperbolas to the reflections that are picked are relatively flat after this correction. 4) Seven mini-stacks show the results when velocities respectively decrease and increase to the left and right of the middle mini-stack (Figure 5.10).

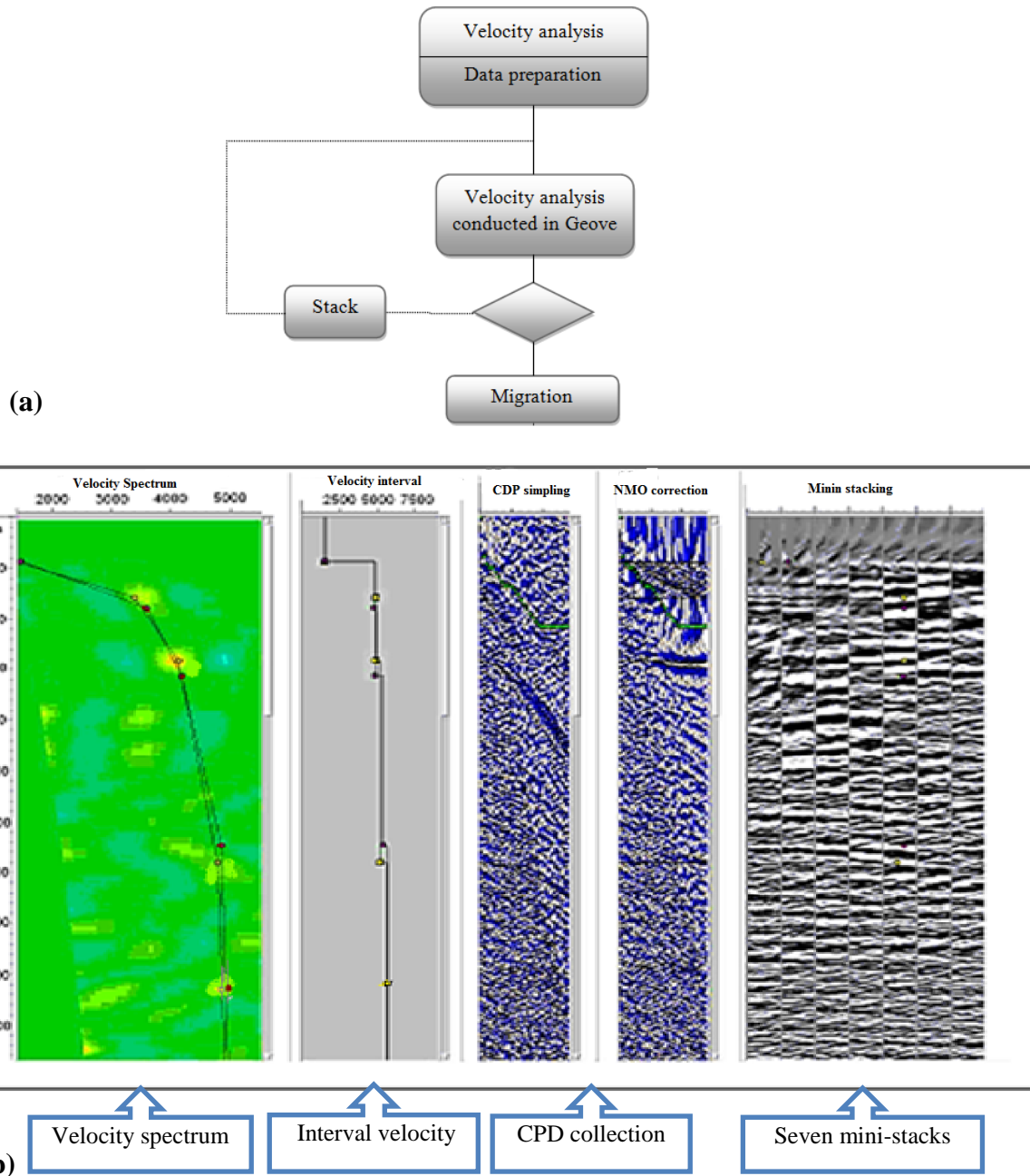


**Figure 5.10** (a) Schematic of velocity analysis job. (b) Velocity analysis of Line 6 in year 2008. Velocities are selected for each 160 CDP. ) interval velocity is very high for short travel times: approx. 5000 m / s at 200 ms.

To get a better image velocity for each line, it was adjusted several times. Stacks with scale of  $\pm 5$  percent of initial velocity was plotted (Figure 5.11), and is used as an aid to find the velocities that suits best.

The velocity field varies along the lines; generally velocities are higher in the western part of the lines than in the synclinal further east. This is true for the uppermost 2 seconds (TWT). The velocity field expresses mostly the same characteristics from line to line.

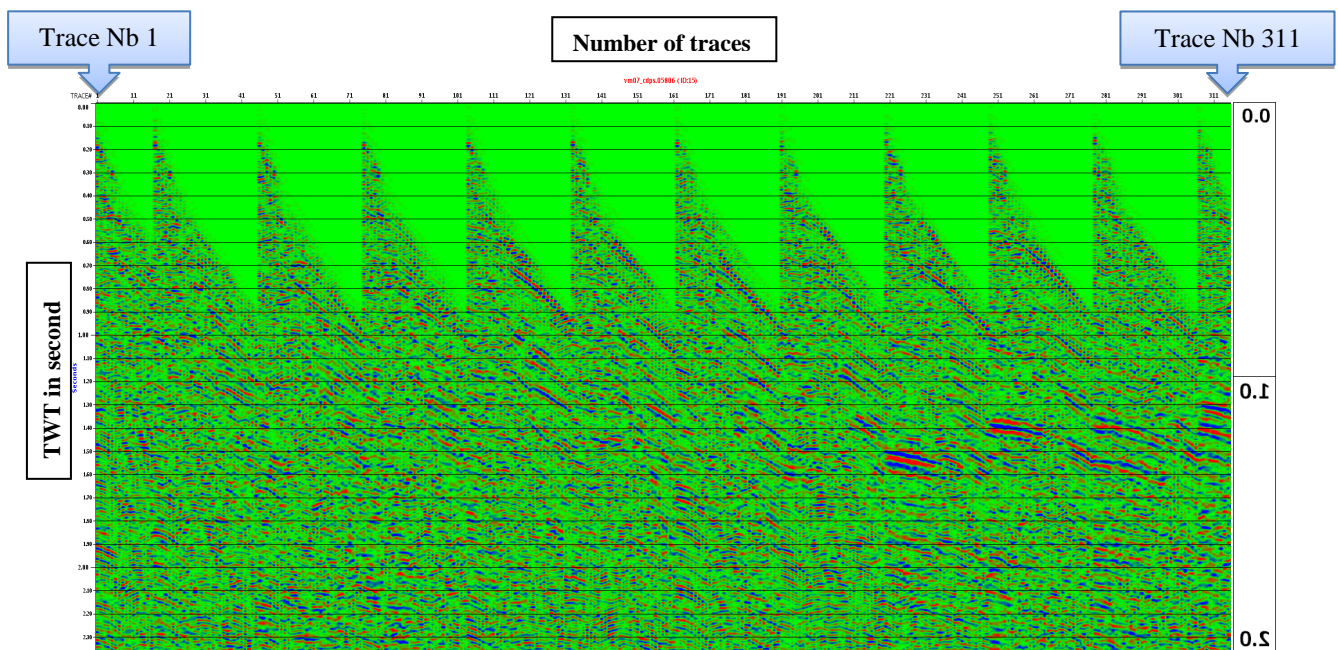


**Figure 5.11:** Line 6, year 2008, After velocity analysis we obtained vm07\_cdps.05806, with CDP: 4751 to 4800, shot number 565 to 600, receiver: 2491 to 2500.

## 5.2.4 Stacking and Migration

After velocity analysis, the data was migrated. The operation was performed in the module TIKIM, which uses 2D Kirchhoff time migration (CGG, 2006). Kirchhoff algorithm is a function where each output is treated as the highest point (apex) of a diffraction curve. Input samples are summed or spread out along the diffraction curve, which is characterized by a locally defined one-dimensional RMS velocity function (CGG, 2006). Since prestack migration was used in the processing part, DMO was not applied in the work (see Figure 5.12).



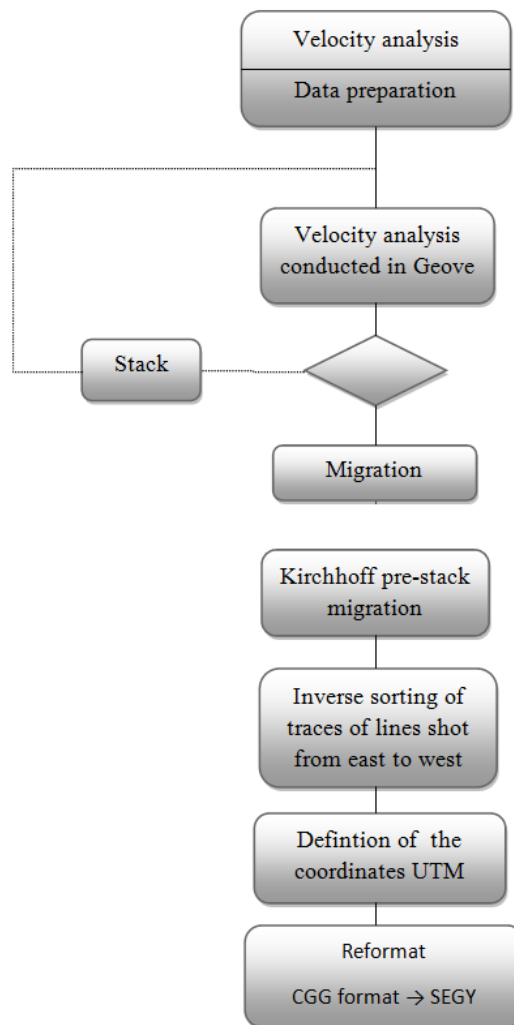


**Figure 5.12:** Stacking and Migration schematic.

Velocities defined in the previous work were used in this section. A limit on the highest apparent velocity of the layers (DIPLIM) should be defined, and all values above this will be muted by the operator. The slope of the layers in Van Mijenfjorden increases gradually westwards up to  $90^\circ$  on Akseløya, located approximately 1-3 km west of the starting point of the lines. High DIPLIM values were tested in order to map structures with large dips in the western part of the lines, with poor results. The increase of DIPLIM decreases the quality of the reflections with more moderate dip, due to noisy diagonal stripes. Too low DIPLIM values will not give reflections on the specified angle. The migration job also includes an outer mute to remove the parts of the pathways that are stretched by the NMO. This is generally far offsets for shallow arrivals. The mute is defined by the NMO-corrected CDP-collections, which are then reversed ("de-NMO"), with and without stretch mute (Figure 5.13).

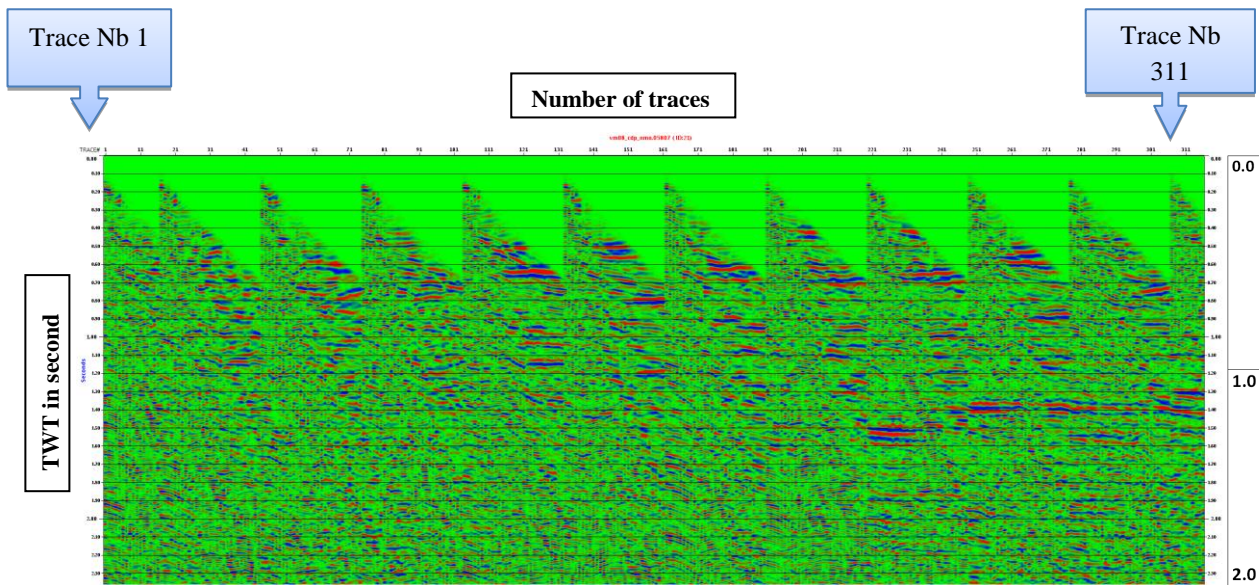


**Figure 5.13:** Line 6, year 2008, After NMO, we obtained vm08\_cdp\_nmo.05807, with CDP: 4751 to 4800, shot number 565 to 600, receiver :2491 to 2500.

Stretching the mute on the CDP-collection to the right in Figure 5.13 removes the parts of the pathways that are stretched more than 100 percent of the NMO-correction, while the collections to the left shows the effect of this stretch where mute was not applied. Figure 5.14 shows the final results after all steps of processing that will be used in the interpretation.

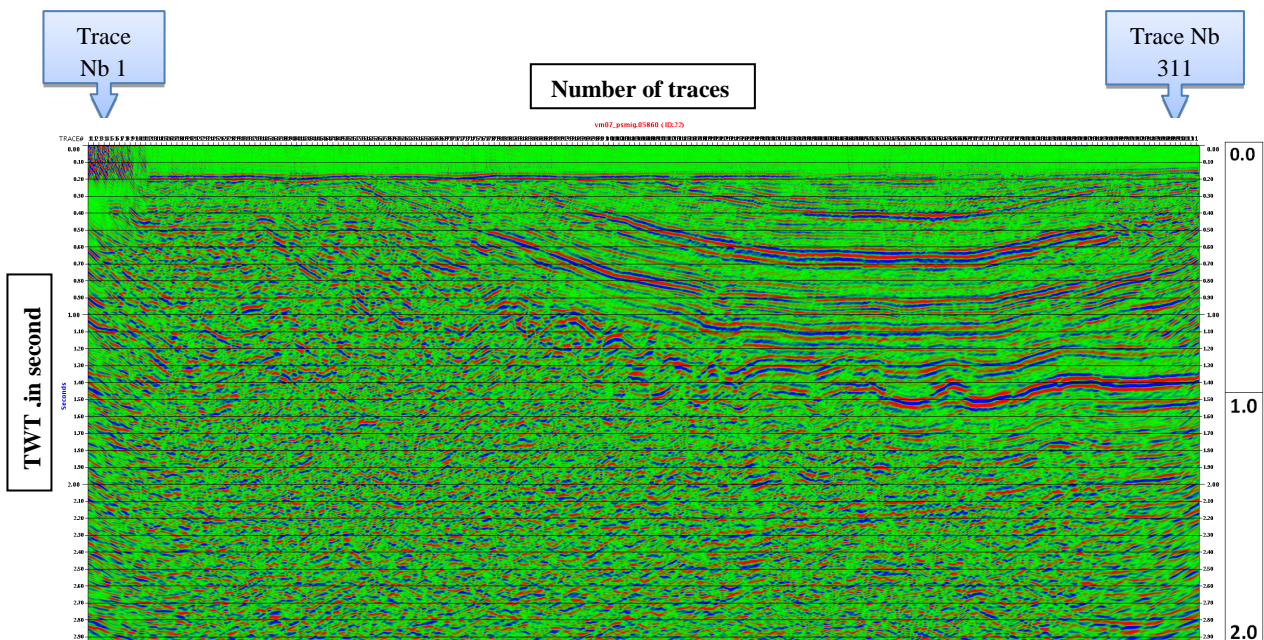


**Figure 5.14:** Line 6, year 2008, we obtained final processing line: vm07\_psmig.05860, with CDP: 4751 to 4800, shot number 565 to 600, receiver :2491 to 2500.

## 6 Seismic Interpretation

In this chapter the multichannel seismic interpretation for 19 lines will be presented.

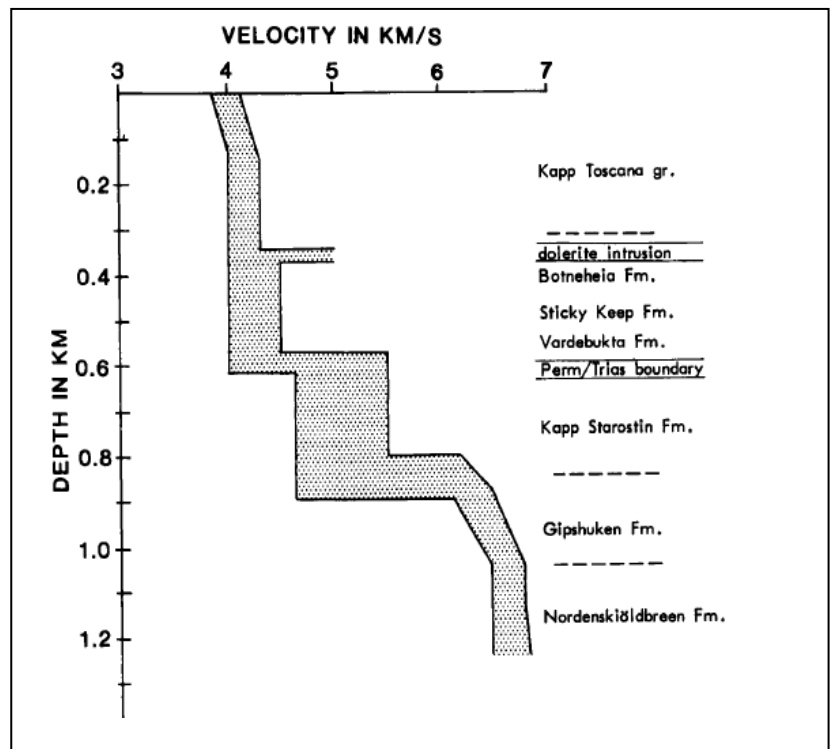
### 6.1 Interpretation frame work

The interpretation of each line is correlated with a number of previous on- and off-shore studies in the area. Since there is no available log data from any exploration well in this area to help to interpret the seismic survey, seismic interpretation from literature done by other geoscientist has been used in this study (see below).

- The results of Blinova et al. (2009) and Blinova et al. (Subm.), which describes studies of Bellsund Graben (west of Van Mijenfjorden) and Isfjorden (north of Van Mijenfjorden), respectively, mainly based on marine seismic data.
- Results from Braathen & Bergh (1995) and Bergh et al. (1997), from onshore studies in the western part of Nordenskiöld Land, mainly northwest of the study area.
- Seismic Atlas of Western Svalbard of Eiken & Austegard (1994), which includes the description and presentation of a series of seismic profiles in the study area.
- Interpretation of a 2D line from Van Mijenfjorden, interpreted by Eiken (1985). The line is located further east in the fjord than the data used in this thesis, and it apparently has lower resolution.

All horizons are interpreted on ‘peaks’, which means that each layer represents an increase in acoustic impedance. This is in agreement with the results from previous studies, and velocity distributions from measurements in Van Mijenfjorden conducted by the University of Bergen in 1981 (Eiken, 1985; Eiken & Austegard, 1994). The measurements show an increasing refraction velocity with increasing depth from ca. 4.5 km / s in the sea bed at approximately 0.1 s TWT, to approximately 6 km / s at approximately 1.45 s TWT.

Figure 6.1: Range of possible velocity-depth distributions obtained from a land-seismic survey in Agardhdalen. To the right is the geological interpretation of the velocity model (Eiken 1985)



A seismostratigraphic framework is defined, based on sources described in the next section. A sequence of Carboniferous to Tertiary represents an unconformity on Heckla Hoek and Devonian strata (Eiken & Austegard, 1994). This unconformity is interpreted as a relatively strong and continuous reflector that separates continuous and parallel reflectors of Carboniferous-Tertiary age from the more chaotic reflectors in older deposits (Eiken & Austegard, 1994). The units of Carboniferous to the Permian are characterized by continuous reflections with a locally discontinuous wavy signature and a slight slope to the southwest. Top Permian is best illustrated in the east as a strong reflection, interpreted to represent a large difference in acoustic impedance between the carbonates in the Kapp Starostin Formation and overlying slates in Sassen Dalen Group (Bergh et al., 1997).

Top Triassic is interpreted as a strong reflector representing the difference in acoustic impedance between a sandstone in the Kapp Toscana Group and overlying slate of Janusfjellet sub-group (Bergh et al., 1997), while alternating sandstone and shale in the upper Adventdalen dated to Cretaceous generate the strong reflections of Janusfjellet sub-group.



Base Tertiary in Van Mijenfjorden is interpreted as the lowest of a series of strong, continuous reflections (Eiken & Austegard, 1994). The strong reflections are associated with sandstones in Adventdalen group (Bergh et al., 1997). A correlation diagram of the seismic signatures and stratigraphic units are defined in Figure 6.2.

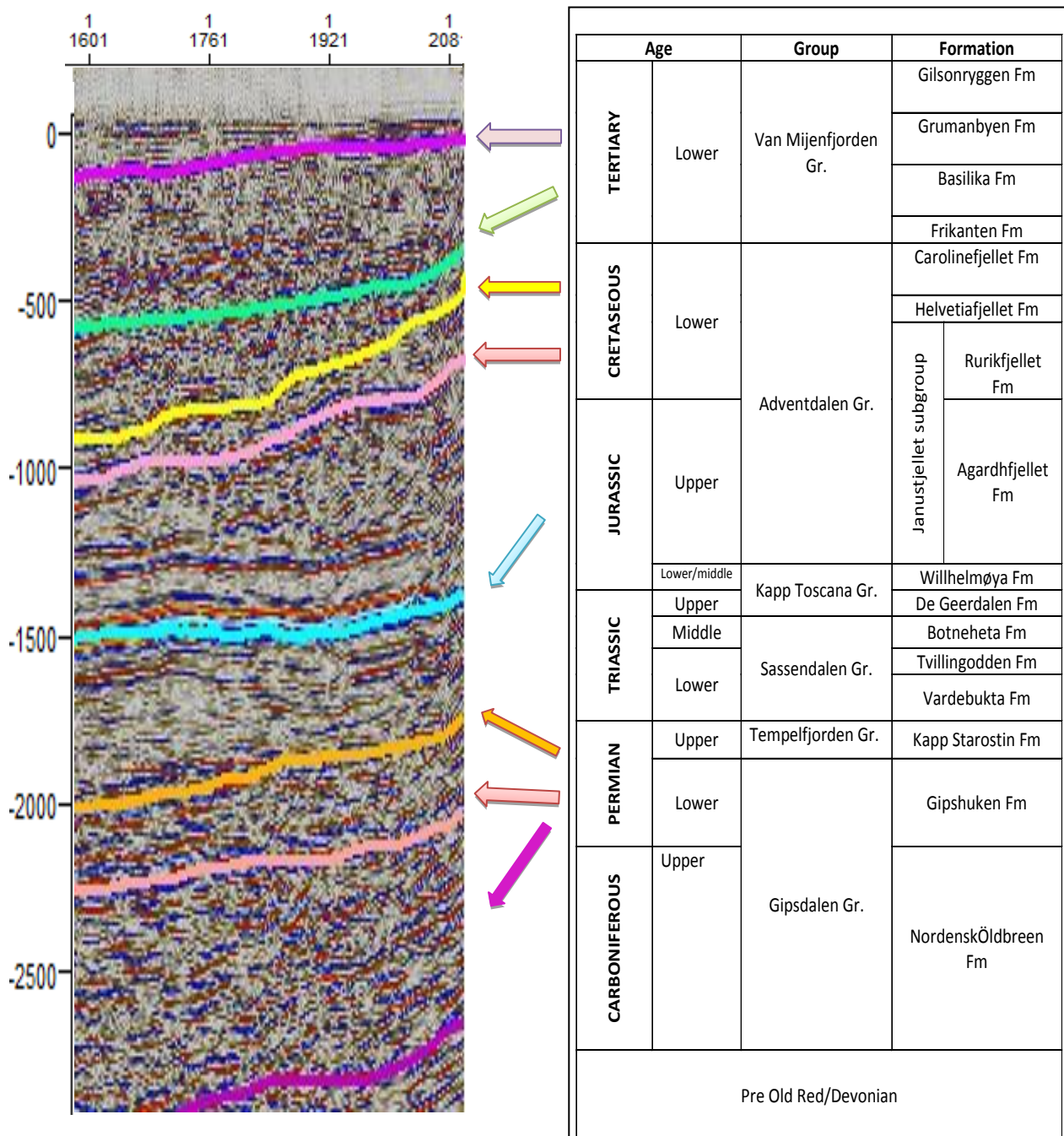


**Figure 6.2:** Correlation Diagram of seismic and stratigraphic units. Vertical axis on seismic in ms (TWT), and the view is from the deepest part of the Central Basin on line VM07-01 The stratigraphic column is from Eiken & Austegard (1994).

## 6.2 Interpretation tool

The software used for interpreting the Svalex 2007 data was Petrel (Schlumberger software) version 2009. Petrel was also used for generating maps for quality control by visualizing interpreted fault planes. The multichannel seismic profiles are presented with zero phase pulse with SEGY-standard polarity, e.g. an increase in acoustic impedance is, by convention, positive and presented as a peak, and a decrease in acoustic impedance is negative and presented as a trough. The display color in the seismic profile is red for increase in acoustic impedance and blue for decrease in acoustic impedance. Figure 6.3 shows the 19 lines of the seismic survey.

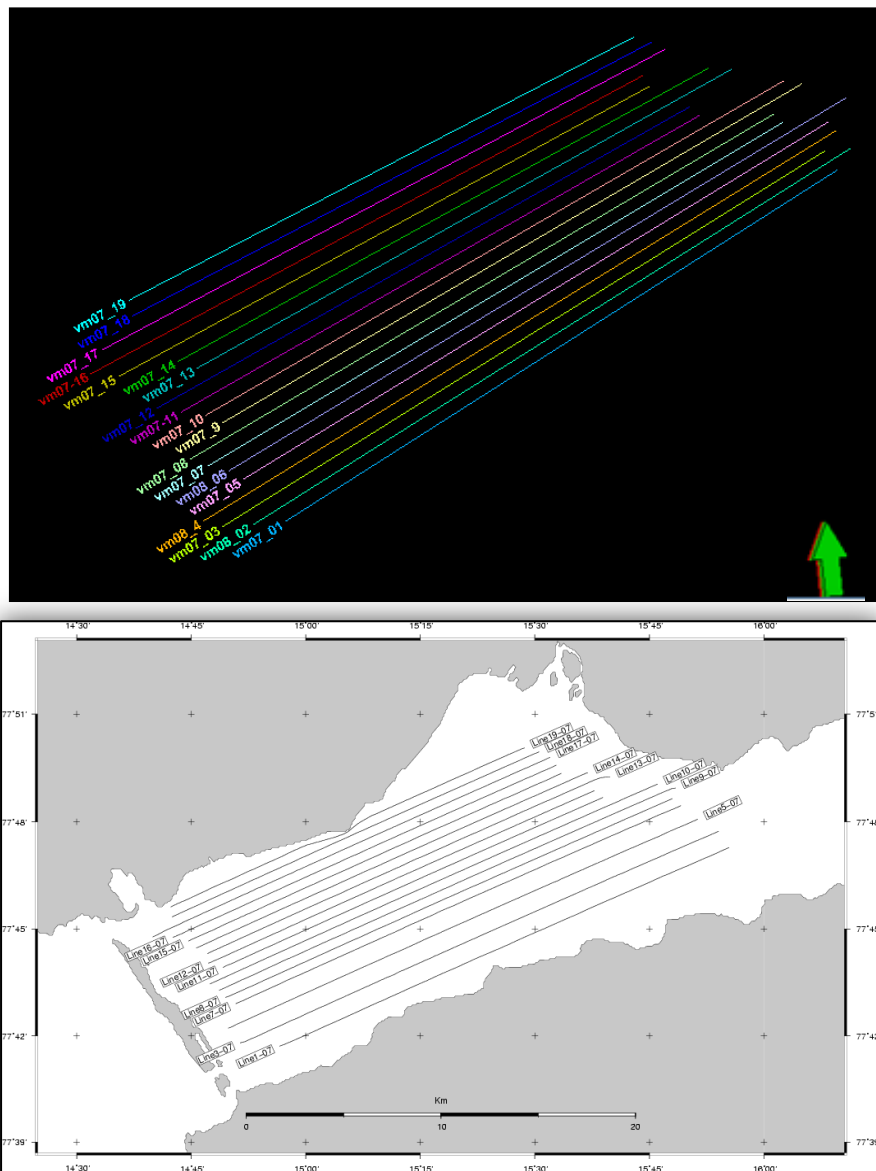


Figure 6.3: All seismic survey lines included in the thesis.

### **6.3 Data quality**

In the general processing section theoretical formulas for seismic resolution were defined. However seismic resolution depends on several factors, e.g. regarding the water depth and sea bed hardness. The seabed is hard in the study area, with velocities up to 4.5 km/s, estimated from the bottom refractions on shot collections during processing. This implies that a significant part of the energy from the source is reflected from the transition between the water layer and seabed, and thus less energy penetrates into the subsurface and depicts deeper layers and structures. In addition, several reflectors such as strata in the Tertiary, intra-Cretaceous and a sill in the Triassic unit with very strong amplitudes will affect the degree of depiction that can be obtained from deeper layers.

Also, water depth is a problem in relation to data quality, because of the short periods of time between the multiples that masks real primary reflections. Multiples are strongly attenuated in the processing, but the extensive multiple removal processes has also reduced the amplitudes of the seabed and the shallower reflectors. Despite the fact that there was a separate version of the stack aiming at interpretation of the seabed, it was difficult in some areas to follow the seafloor reflector.

The first seafloor multiple is visible on some of the stacks in the far west, which probably reflects higher seabed velocities in these areas. Otherwise, there are relatively deep multiples that are visible on the different profiles (Figure 6.4). These multiple reflections mask significantly the real arrivals.

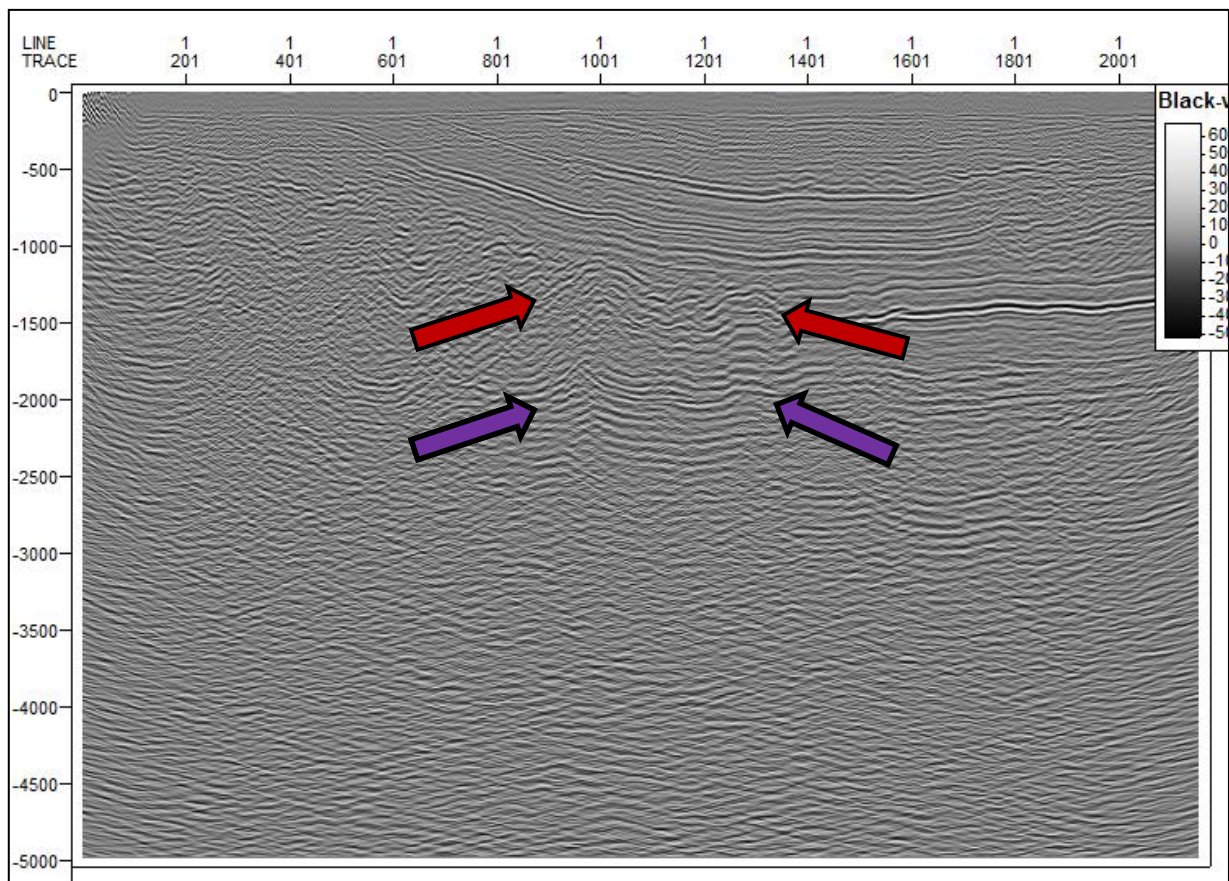


**Figure 6.4:** Multiple reflections, Red arrows show the real data and purple arrows show their multiples.

#### **6.4 Estimation of the thickness, dip, and seabed**

All measurements are from line vm01-01 or vm01-11, and are taken in a vertical line through the deepest point in the basin, unless otherwise stated. Distance and time are read from, respectively, horizontal and vertical axis in the interpretation software, Petrel, and dip estimates are calculated with trigonometric measurements. The measurements have therefore a certain margin of error. Thicknesses in meters are based on average speeds of 1500 m/s in the water layer, 4500 m/s in the tertiary layer and 5000 m/s for underlying units. These are only rough estimates, but votes along with good velocity analysis made in the processing, as well as the velocity used in previous studies, for example, in Eiken & Austegard (1994). All measurements in seconds or milliseconds are given in two-way travel time.



The ocean floor is mostly flat, with a slight slope down to the west. The shallowest areas are east and south in the fjord, with a water depth of approx. 120 ms (about 90 m). The deepest areas are in the north-western part, with water depth of approx. 210 ms (about 150 m).

Any geological structures along the ocean floor is not interpreted as the data have relatively poor resolution, and because there is a high degree of uncertainty in the oceanic interpretation related to problems with data quality in the shallow parts of the stacks. In further studies bathymetry collected along the profiles could be used to develop a better seabed map.

## **6.5 Interpretation of seismic lines**

The following section describes the interpretation of line vm07-11. The profile is representative of structures and features that are present on all profiles, and it has relatively good data quality. Figure 6.5 shows the final migrated stack of line vm07-11.

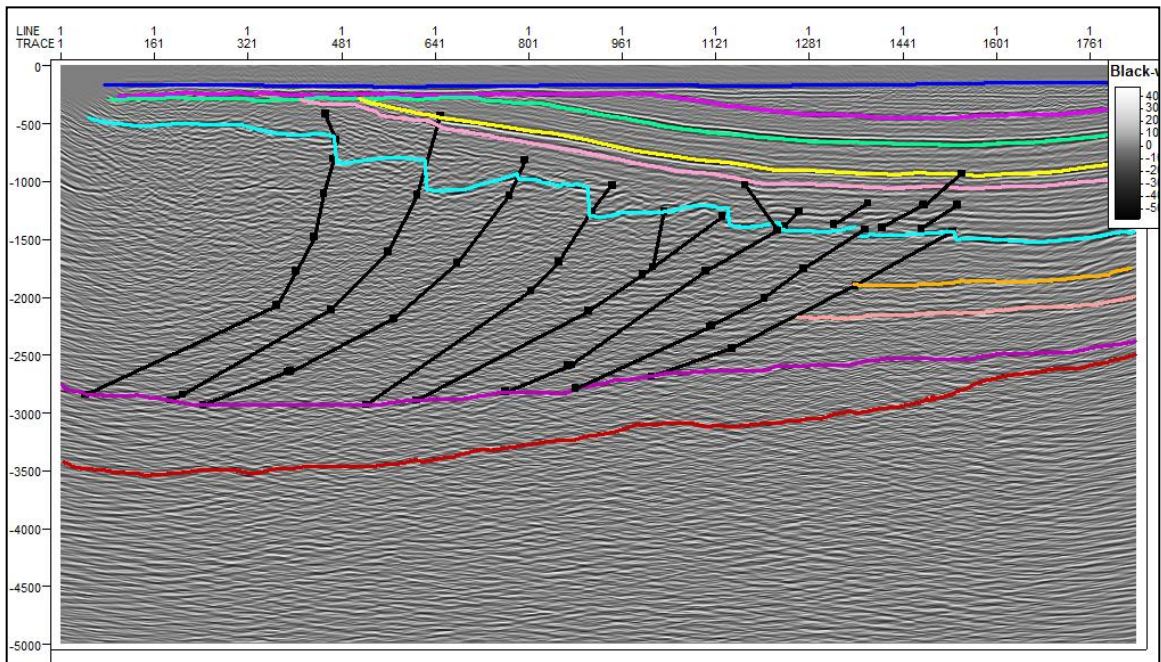
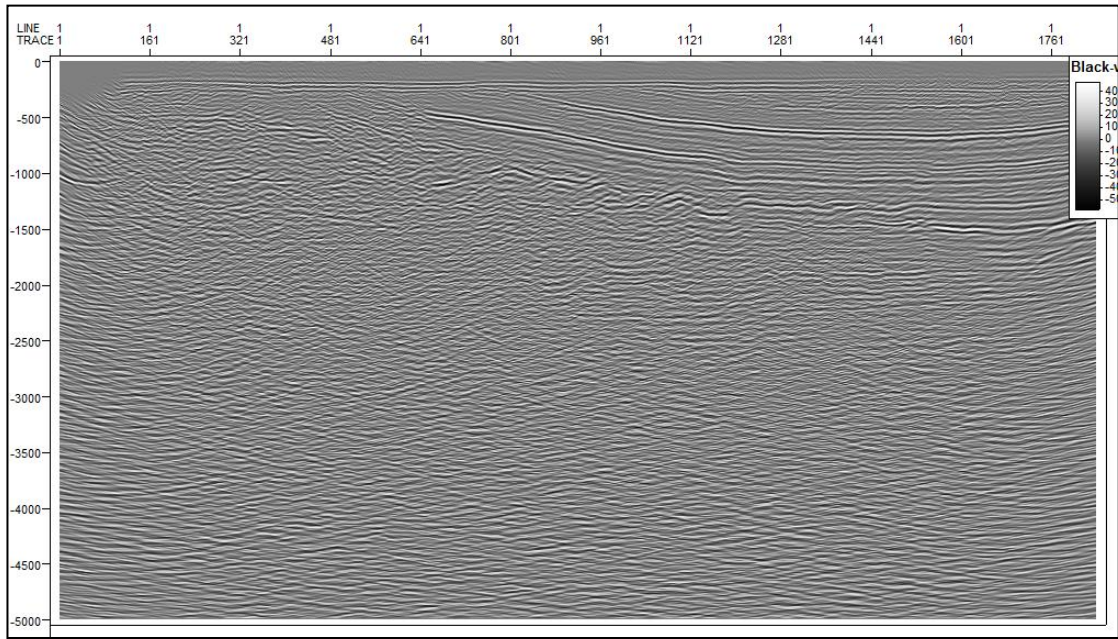


Figure 6.5: Line vm07-11. Top figure is the seismic line with effect color of white, grey, black, without interpretation, middle figure is with interpretation and the below figure is the same seismic survey with effect of seismic (default in Petrel). Horizons mark the following reflectors

- Sea bed
  - Lower Tertiary
  - Lower Cretaceous
  - Top Perm
  - Lower Perm
  - mid Tertiary,
  - mid Cretaceous,
  - Lower Jurassic
  - mid Perm
  - Basement.
- F1-8 is reverse Faults in black colors

### 6.5.1 Unit 1: Tertiary

A series of continuous reflectors in Van Mijenfjorden depicts a broad, asymmetric syncline, interpreted as central Spitsbergen Basin with deposits of Tertiary age in the Van Mijenfjorden group. The horizon which is interpreted as the base Tertiary is placed in the bottom of two strong reflectors. The upper approximately 150 ms of the unit is characterized by low amplitudes and reflections that are "smeared" (Figure 6.6), probably as a side effect from operations in the processing. The unit includes two sequences of strong reflections, interpreted to represent sandstone units in Van Mijenfjorden group.

The top of these sequences have at least three continuous reflections with thickness of approximately 100 ms. Below mid-Tertiary remnants of multiples can be seen (yellow arrow in Figure 6.9), while the bottom layer has one clear reflection. Between these two layers is a thick layer of more transparent seismic character and weaker amplitudes. There are also some artifacts near the sides of the stacks that are probably not real structures, but the result of low-fold in the beginning and end of lines.

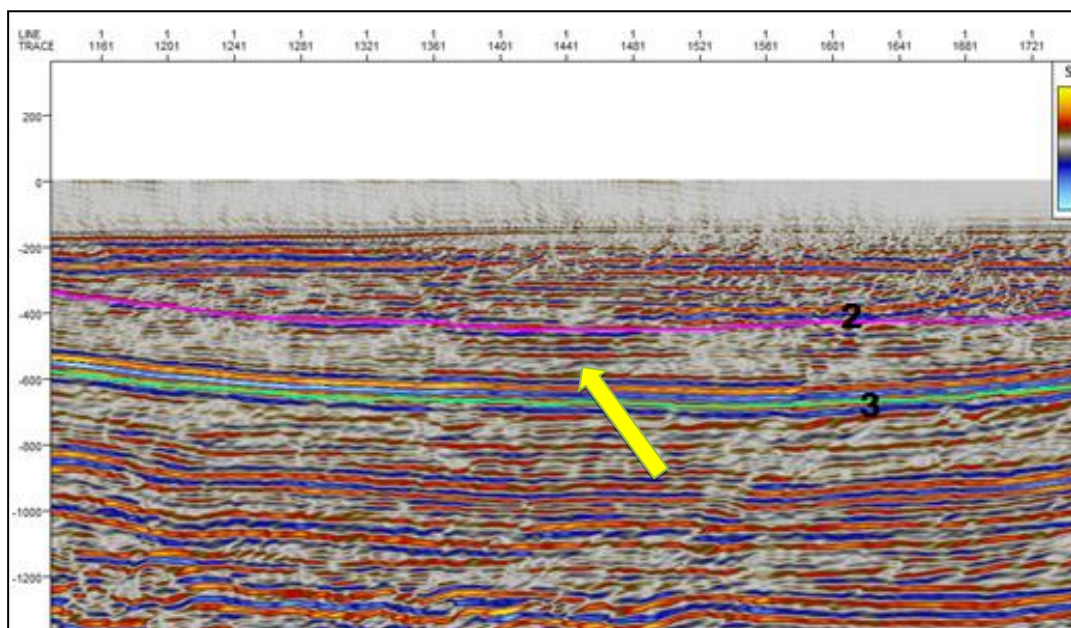


Figure 6.6: There are 2 layers of Tertiary, purple: mid Tertiary and green: lower Tertiary. Yellow arrow shows remnants of a multiple.

### 6.5.2 Unit 2 - Cretaceous

The unit is approximately at 500-1050ms in the deepest part of the basin, and is divided by a continuous, strong reflection, mid-Cretaceous, at approximately 600ms (Figure 6.10 line



number 4). The unit is restricted by the horizons of Lower Cretaceous (Figure 6.10 line number 5) and base Tertiary, and has a generally uniform thickness of about 550ms. The upper part of the unit is characterized by parallel, weak reflectors, and has a progressively more chaotic seismic character to the east. The mid-Cretaceous reflections are narrower and have higher amplitude (Figure 6.7).

The upper part of the sequence is characterized by weak, parallel layers above a reflector with very high amplitudes, interpreted as mid-Cretaceous. This represents probably the Festningen section, a sandstone unit in Helvetiafjellet formation dated to the early Cretaceous.

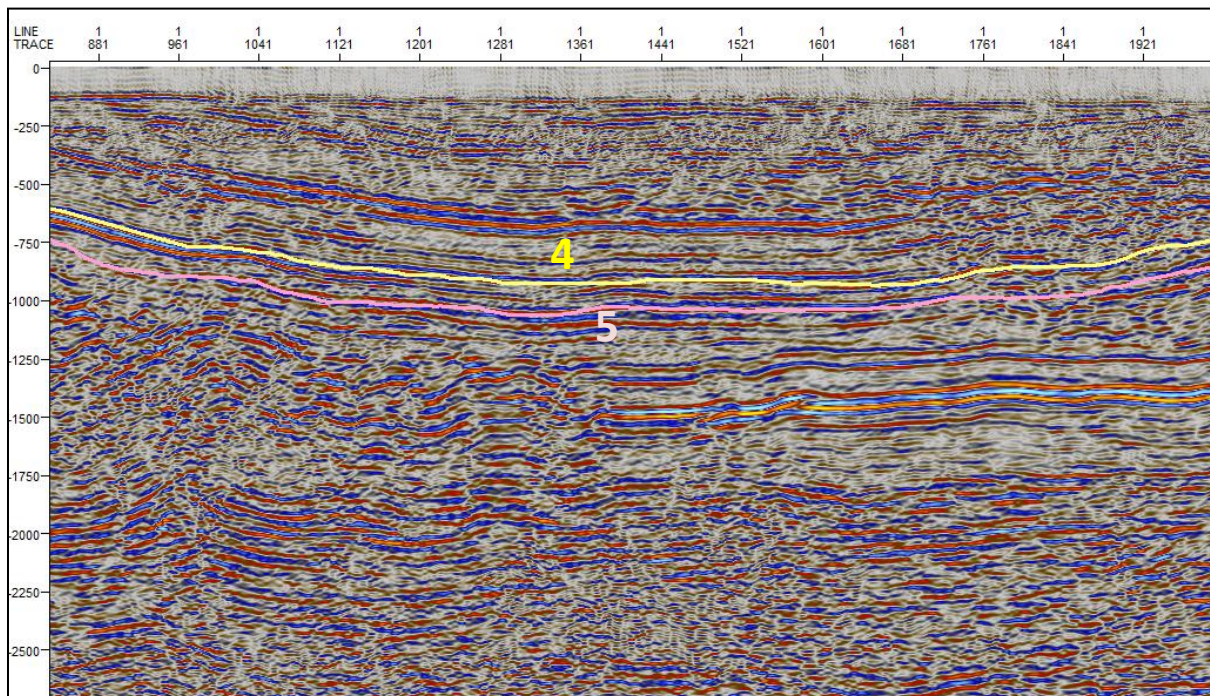


Figure 6.7: Cretaceous units. Yellow line (number 4) shows mid Cretaceous, pink line (number 5) shows lower Cretaceous

### 6.5.3 Unit 3 - Jurassic

The unit is interpreted as deposits from Jurassic, based in the Lower Jurassic and the upper limit is defined up to Lower Cretaceous. The thickness of the unit is approximately 300 ms in the bottom of the basin, with an increase in thickness towards the east (Figure 6.8).

High degree of deformation makes it difficult to follow the unit west of the fault number 1, where the base Jurassic horizon is strongly faulted (see Figure 6.8). It seems that the unit

gradually thins from the west and the middle of the line, but this is difficult to determine because of the large uncertainty in the interpretation of the horizon in the heavily deformed area in the west.

East of fault 1 the sequence is characterized by continuous, parallel stratification with lower amplitudes than in the Cretaceous sequence. In the east, the unit has obvious faults with approximately 500 m interval. Four of these faults can be followed further up into the overlying clay unit, and terminates at the mid-Cretaceous horizon. The faulted reflectors are interpreted as possible duplex structures. The faults propagate along a reflector interpreted as a slate of Janusfjellet sub-group that acts as a sliding plane for tertiary contraction deformation.

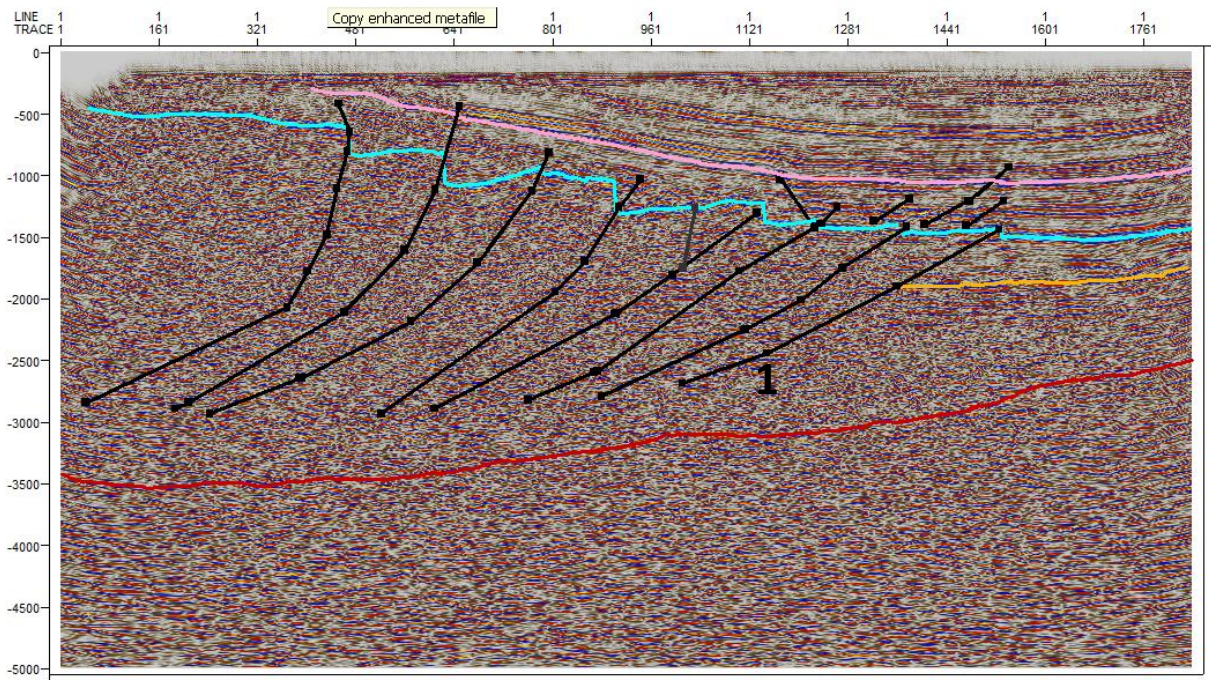


Figure 6.8: Jurassic unit. Blue line shows the lower Jurassic. Fault number 1 indicated.

#### 6.5.4 Unit 4 - Triassic

The unit is interpreted as deposits from the Triassic, bounded by top Permian and Lower Jurassic (Figure 6.9). The unit is not interpreted west of fault number 1, due to poor imaging. The unit has, in contrast to over and underlying units, generally uniform thickness. East of Fault number 1 the lower parts of the unit is characterized by discontinuous reflectors, interpreted as shales associated Sassendalen Group.



The upper part of the sequence expresses chaotic and weak parallel layered seismic signature, with some small-scale reverse faults. This is interpreted as the upper part of shale in the Sassendalen Group and the reflections with higher amplitude are interpreted as Cape Tuscan sandstone near the Lower Jurassic.

Some reflectors with very strong amplitudes and approximately 150 and 200 ms thick, paralleling the stratification near the Lower Jurassic horizon, are interpreted as top and bottom of sills, respectively. These are mapped from white arrow in Figure 6.9 eastwards to the end of the line.

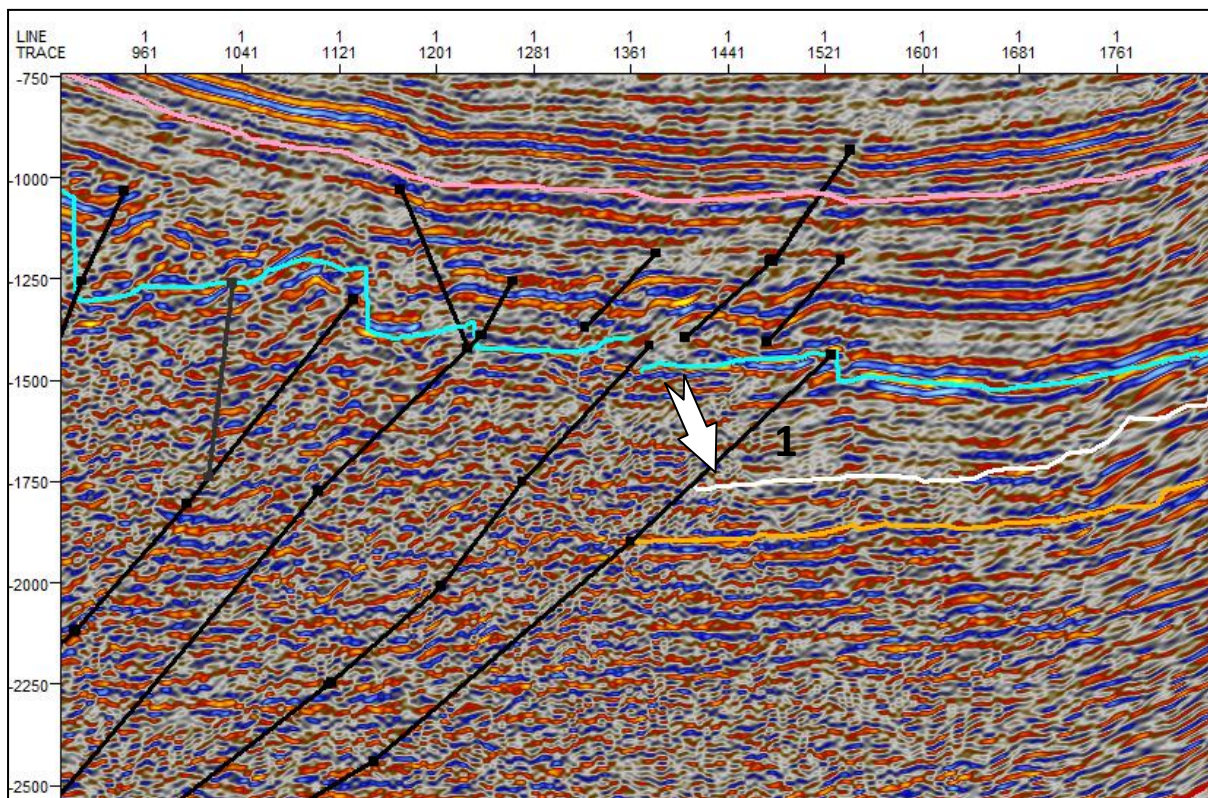


Figure 6.9: white line is the Triassic. Number 1 in figure is Fault number. Arrow shows the sills.

### 6.5.5 Unit 5 – Permian

Unit 5 is interpreted as deposits from the Permian, based in Lower Permian and the upper limit is defined by the top Permian, associated with the transition between the slate in Sassendalen Group, and carbonates in the KappStarostin Formation. The layer is

characterized by slightly folded, parallel reflections with low amplitude. It gradually thickens towards the west, from approx. 450 ms in the east to 600 ms at Fault number 1 (Figure 6.10). A relatively strong reflection that parallels the top-Permian at approximately 100 ms distance is interpreted as mid-Permian. This possibly represents a high velocity layer in the upper part of the KappStarostin Formation (Figure 6.10). Top - and mid-Permian is not interpreted in the west of Fault 1 due to the lack of imaging.

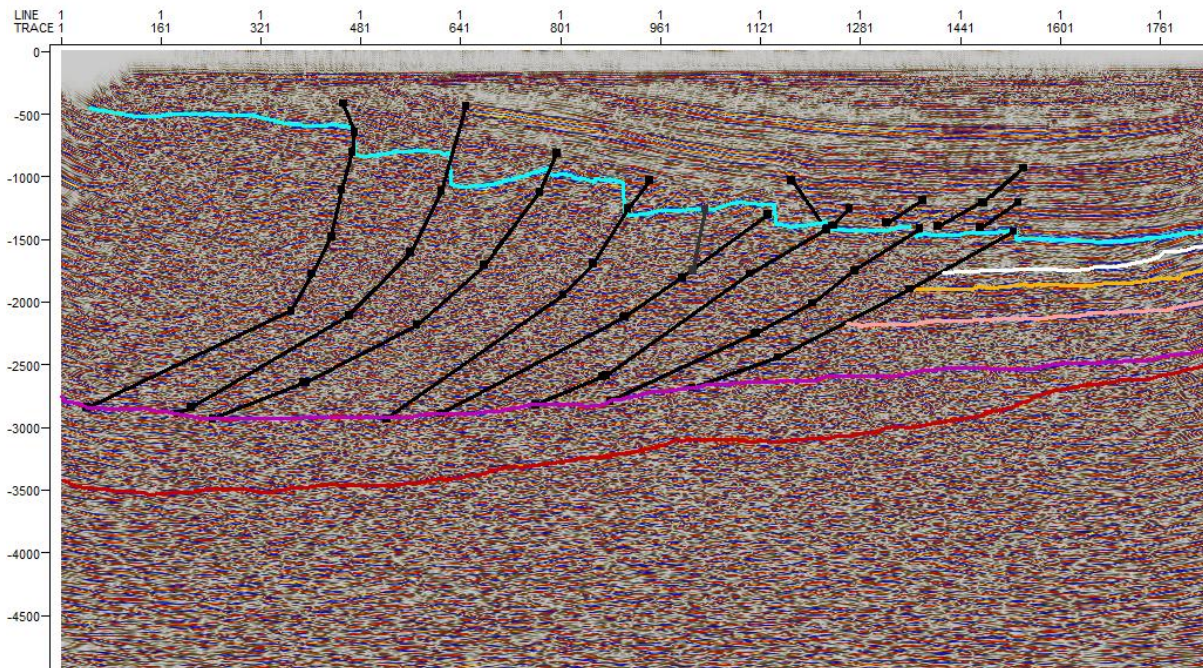


Figure 6.10: Interpretation of Permian unit

### 6.5.6 Unit 6: Carboniferous and older

The unit is interpreted as deposits older than the Permian, deeper than approx. 2.3 s. The deepest horizon that is followed through all the profiles is interpreted as Lower Permian, and defines the upper limit of the unit in the eastern part of the profile. Lower Permian is interpreted with great uncertainty to the west of Fault number 2, because of its low amplitude and non-continuous imaging. The horizon is here broken based on the weak reflections. The unit is mostly transparent, but has some weak reflections in the east that probably represent fragments of layered rocks (Figure 6.11).



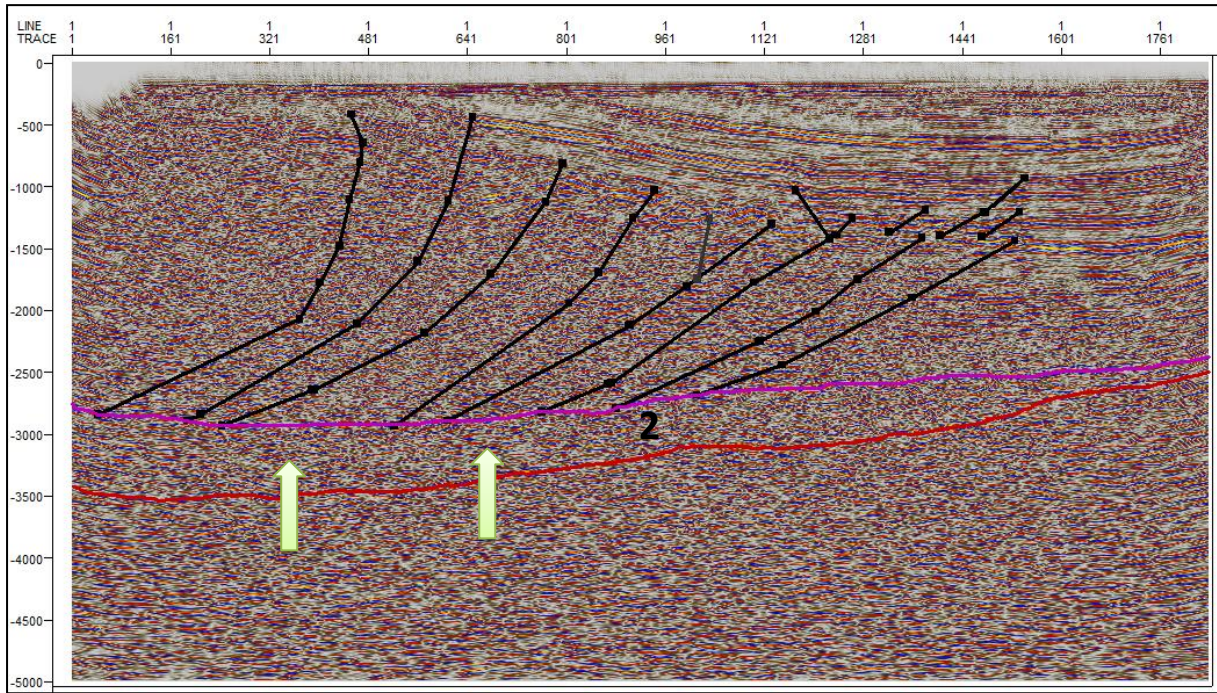
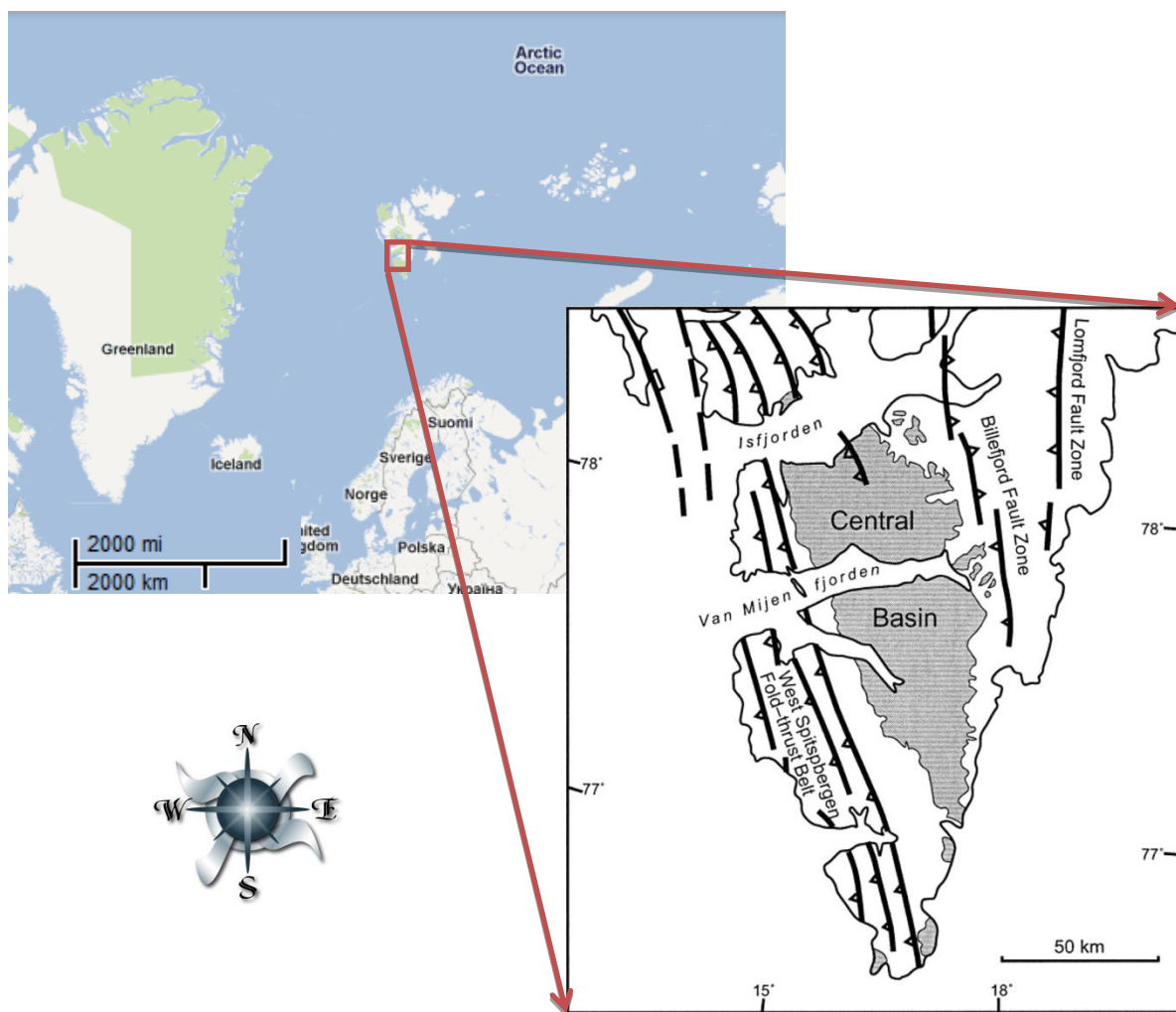




Figure 6.11: Some traces of weak reflections within the carboniferous unit



## 7 Discussion

The following section describes the correlation of the units from Carboniferous to Tertiary and large-scale structures with earlier studies in western Spitsbergen. The study area is dominated by a large-scale syncline, Spitsbergen Central Basin (CSB) in the east, and west Spitsbergen fold-and fault belt (WSFTB) in the west (eg. Bergh et al, 1997; Blinova et al., 2009). WSFTB can be divided into zones with different structural nature. In the study area, we can expect to see much of the CSB and the Foreland-oriented part of the fold and fault belt (see Figure 7.1).



**Figure 7.1:** Svalbard map. Right figure shows the central basin with  marks Paleogenic sediments, and the line  is fold thrust Belt.

In this chapter we discuss the sedimentological units and interpretation of faults.

## **7.1 Sedimentary units**

### **7.1.1 Tertiary unit**

The Tertiary sequence defines a broad, asymmetric syncline that corresponds to the central Spitsbergen Basin. Base Tertiary is in several studies from Isfjorden defined as a transparent zone within a series of strong reflections (e.g. Bergh et al. 1997; Blinova et al. Subm.). However, in this study it is interpreted as the lowest of a number of strong reflections, corresponding with the seismostratigraphic definition of Eiken & Austegard (1994). It is therefore taken into account that the base Tertiary in reality can be somewhat deeper than the lower Tertiary horizon. The thickness of the unit at the bottom of the basin is measured to about 500 ms (1125 m), consistent with Eiken & Austegard's (1994) estimation of about 1.1 - 1.2 km. The reflection configuration seems to be parallel, weak for mid-Tertiary and strong for lower-Tertiary. The uniform thickness may indicate that the unit of the Tertiary has not been subjected to large degree of deformation however it has been folded into a syncline (See Figure 6.9).

### **7.1.2 Cretaceous unit**

The upper portion of the unit is characterized by parallel, weak reflectors and a progressively more chaotic seismic character towards the east (see Figure 6.10). Over mid-Cretaceous, the unit has a uniform thickness (Figure 6.8), which may be due to the Tertiary deformation propagating preferably along the weaker layers of shale from the Lower Jurassic. Thickening eastward as described for the Jurassic unit is less present in the lower Cretaceous unit, which may indicate that thickening of deformed material of the Lower Jurassic glide plane also has affected the lower Cretaceous unit.

At least three major reverse faults in the eastern part of the basin can be followed from the sliding zone in the Lower Jurassic, stopping within the mid-Cretaceous (see Figure 6.8). It thus appears that the strata of mid-Cretaceous consist of tougher, more competent sandstones, which corresponds to the interpretation of the reflector as within the Fortress formation. This is consistent with both Eiken (1985) and Blinova et al. (subm.), who interpret the horizon as a significant impedance contrast between the low-velocity slate of Janus mountain subgroup and the overlying high-velocity sandstone of the Helvetiafjellet formation. Eiken (1985)

based their interpretation of the mid-Cretaceous on geological arguments, that there are thick layers of slate with apparently very small velocity contrasts both above and below this unit (Flood et al., 1971, reprinted in Eiken, 1985). The weak reflections in the upper part of the clay unit are interpreted as shale of the Caroline Mountain Formation, based on seismic reflection patterns and seismostratigraphy.

### 7.1.3 Jurassic unit

The overall thickness of the sequences from Jurassic and Cretaceous is approximately 700 ms in the west, and ca. 850 ms in the east due to the presence of an inverse fault (see Figure 7.2). This is equivalent to 1400 and 2000 m, respectively, and corresponds to a total thickness of 1500-2000 m (increase toward east) as described in Eiken (1985), and is slightly thicker than the measurements at 1350 m of the same units taken from a borehole in Grumantbyen north of the study area (Skola et al., 1980, reprinted in Eiken, 1985).

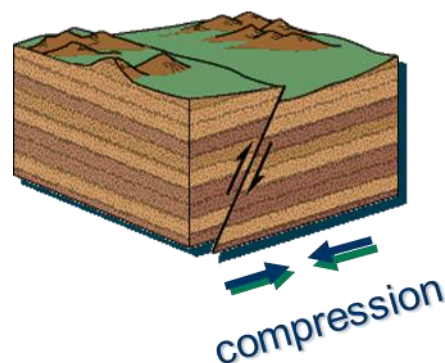


**Figure 7.2:** definition of the reverse fault

The thickness increase in the eastern part is mainly related to the Jurassic sequence (see Figure 7.3). A series of thin skinned reverse faults propagate from a weak but continuous reflector just above the horizon that defines lower Jurassic, interpreted as a slate of Janusfjellet sub-group that acts as a sliding plane for Tertiary contraction deformation. Faulted rocks accumulate in a stack on the east, thus causing the increase in thickness of the unit. A number of structures in the eastern part of the unit is interpreted as possible duplex

faulting, and is a further indicator of compression deformation of the unit. This corresponds to the interpretation of a sliding plane in Janusfjellet sub-group of Blinova et al. (subm.), and the interpretation of the Jurassic sequence in Nøttvedt et al. (1993a), where eastern thickening of the unit is justified by the tectonic thickening of weak slate of Janus mountain subgroup.

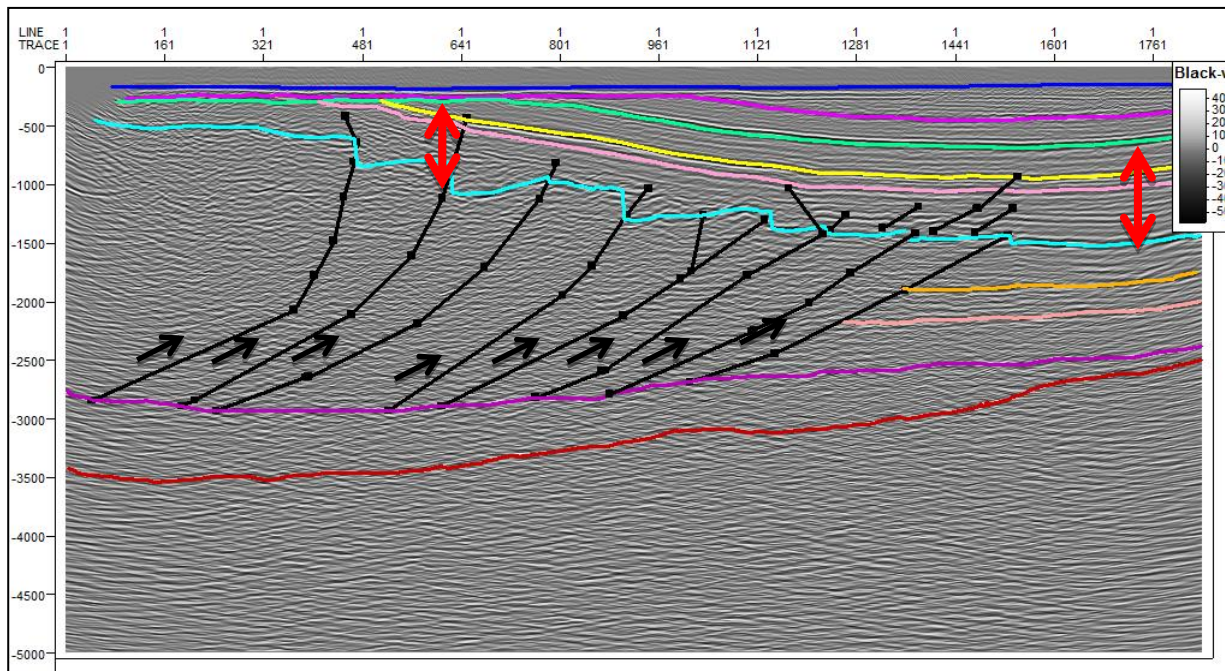
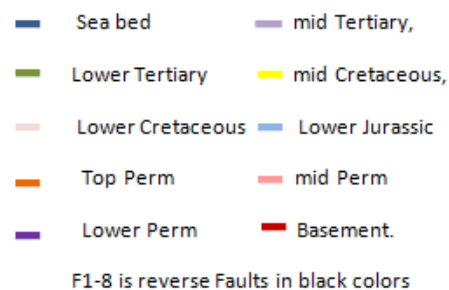


**Figure 7.3:** Sequences from Jurassic and Cretaceous are approximately 700 ms in the west, and ca. 850 ms in the east. We can see in Figure because of inverse fault, the West part is more compact Vertically but east part is more compacted horizontally due to aging inverse fault..



#### 7.1.4 Triassic unit

The unit from the Triassic is characterized by weak, discontinuous reflections from shales in Sassendalen Group, over reflections with higher amplitude, interpreted as sandstone layers in the KappToscana Formation. Blinova et al. (subm) describes the seismic character as typical for strata from Triassic and Lower Jurassic. In contrast to the over and underlying units, the Triassic unit has uniform thickness in the east, indicating that there has been no compaction of faulted rocks in the unit. A sliding plane in the upper Sassendalen Group in the Middle Triassic is interpreted in several studies from Isfjorden (e.g. Blinova et al. Subm.; Bergh &



Andresen, 1990). It is, however, found no indications of sliding planes in the Triassic unit in the data from Van Mijenfjorden.

### 7.1.5 Permian unit

The interpretation of top Permian reflector is related to the strong impedance contrast between carbonates in KappStarostin Formation and overlying low velocity shale in the Sassendalen Group (Triassic), which generates weak, discontinuous reflections. This is consistent with the interpretation of Bergh et al. (1997). The Permian unit is not interpreted west of Fault number 1 or F1 (see Figure 7.4), where a high degree of deformation leads to poor seismic imaging. The unit thickens gradually towards the west, which may be due compaction of fragments of layers in the context of tertiary deformation.

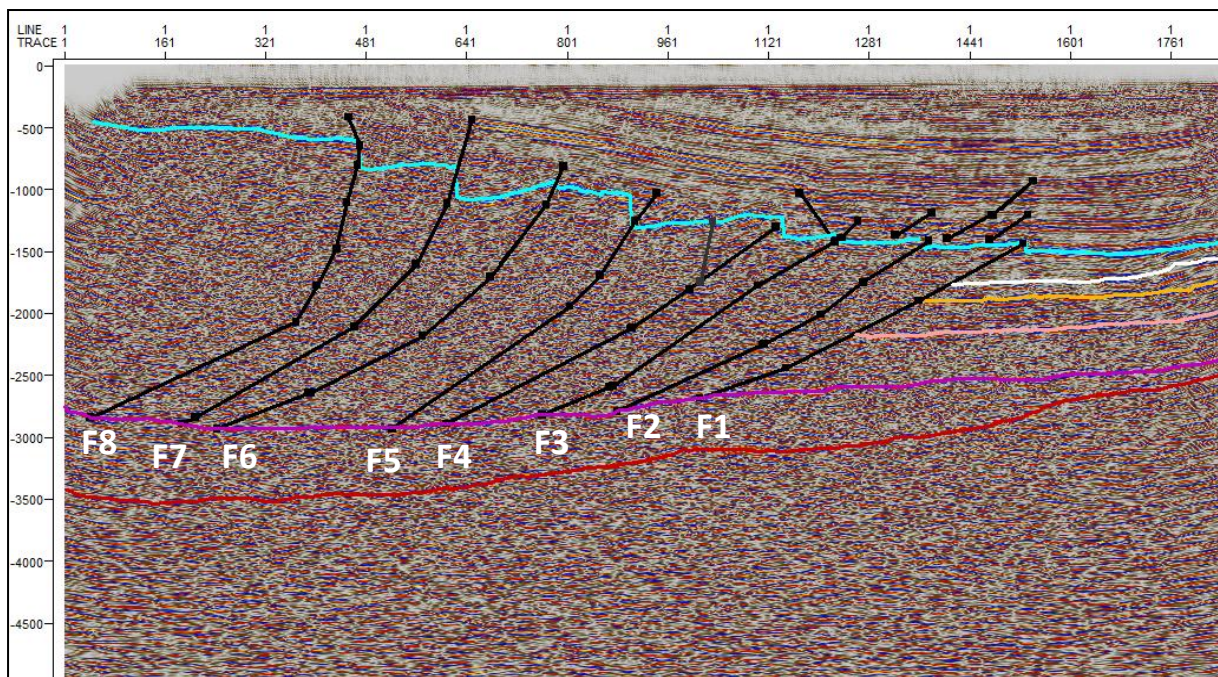


**Figure 7.4:** The Permian unit is not interpreted west of Fault number 1, where a high degree of deformation in the area leads to poor seismic imaging.

- Sea bed
  - Lower Tertiary
  - Lower Cretaceous
  - Top Perm
  - Lower Perm
  - mid Tertiary,
  - mid Cretaceous,
  - Lower Jurassic
  - mid Perm
  - Basement.
- F1-8 is reverse Faults in black colors

### **7.1.6 Carboniferous and older units**

Lower Permian, which defines the upper limit of Unit 6 (see Figure 7.4), is interpreted as a relatively strong reflector associated with the transition between low-velocity porous evaporates of the Gipshuken formation and underlying dolomite layers with higher velocities in the Nordenskioldbreen formation. This interpretation corresponds with seismostratigraphy from Isfjorden in Bergh et al. (1997). Lower Permian is in the previous studies described as an angular unconformity (eg. Eiken & Austegard, 1994; Blinov et al. Subm.), but the resolution along the present profiles is not sufficient to determine whether this also applies here. A reflector that corresponds to the depth of the lower Permian is by Eiken & Austegard (1994) defined as top basement. A certain degree of uncertainty is therefore associated with the interpretation of the reflector.

The seismic signature in the unit is characterized by diffuse and discontinuous reflectors, which probably represents the basin deposits of Devonian and Carboniferous age. Relatively strong dip of reflections at approximately 2.7 s is observed in some of the profiles (Figure 7.5), and interpreted as top Heckla Hoek. Eiken & Austegard (1994) describes the seismic response of the Heckla Hoek as relatively poor, with few and scattered visible reflections, with the possible exception of the central to eastern Spitsbergen and the northern Storfjord, where strong dip of reflections to less than 3 s is observed and interpreted as lower Paleozoic sediments and Devonian basins. These basins are located, however, east of the study area, and are thus not contradictory to the interpretation of the deep reflection in Van Mijenfjorden as top Heckla Hoek. Bergh et al. (1997) describes the seismic signature of the units in the Devonian and Heckla Hoek as scattered, strong and irregular reflections, and an overlying unit with diffuse and discontinuous reflections is interpreted as the basin deposits of Devonian and Carboniferous age. Such a division between the Lower Permian and top Heckla Hoek is not observed in profiles from Van Mijenfjorden.



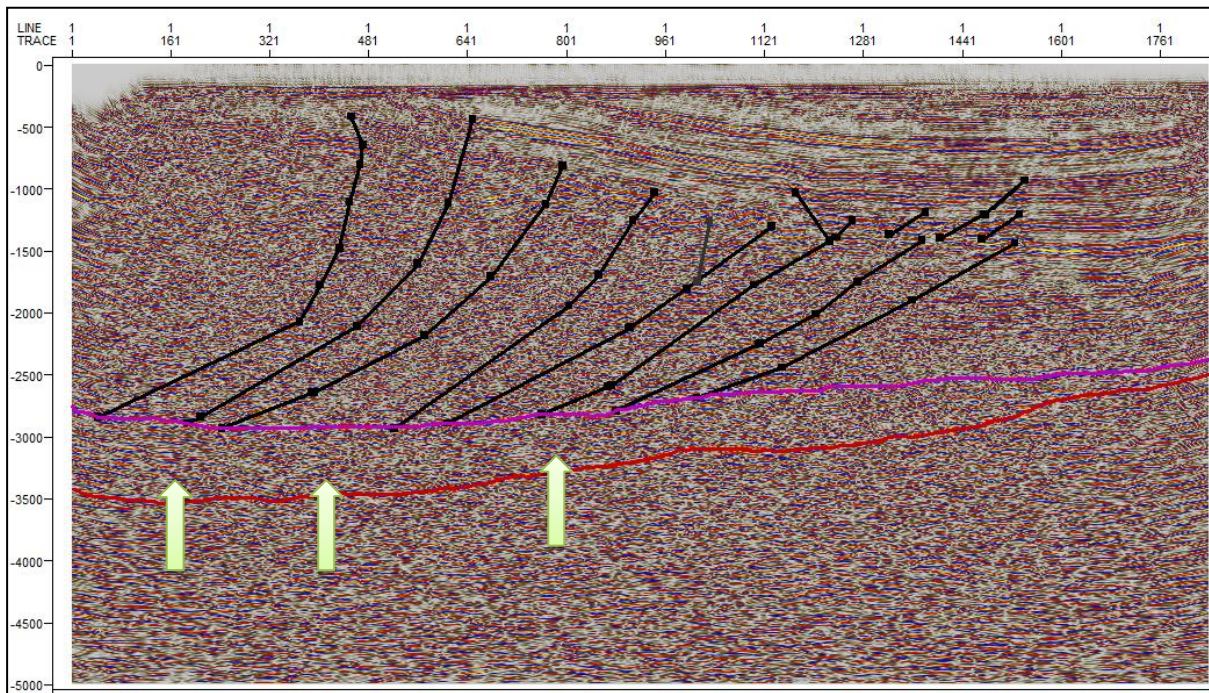


**Figure 7.5:** The seismic signature in the unit is characterized by diffuse and discontinuous reflectors, which probably represents the basin deposits of Devonian and Carboniferous age.

## 7.2 Interpretation of faults

A number of studies from western Spitsbergen (e.g. Birkenmajer, 1981; Braathen & Bergh, 1995, Bergh et al., 1997, Blinova et al., 2009) divides WSFTB in different tectonic zones, where the western part of the fold belt is characterized by a bedrock folding and faulting stack, and the eastern part of the fold belt is characterized by a thin skin Forelands fold and fault belt. Interpreting the model in Figure 7.4 implies that it is mainly the units from Permian to Jurassic that is deformed by F1-F8. No bedrock faulting is observed. It is therefore believed that the study area mainly covers the eastern, Foreland oriented part of WSFTB ("western zone" in Figure 7.6), as well as a zone characterized by a smaller degree of deformation ("eastern zone" in Figure 7.6), which is associated with the Foreland, Spitsbergen central basin.

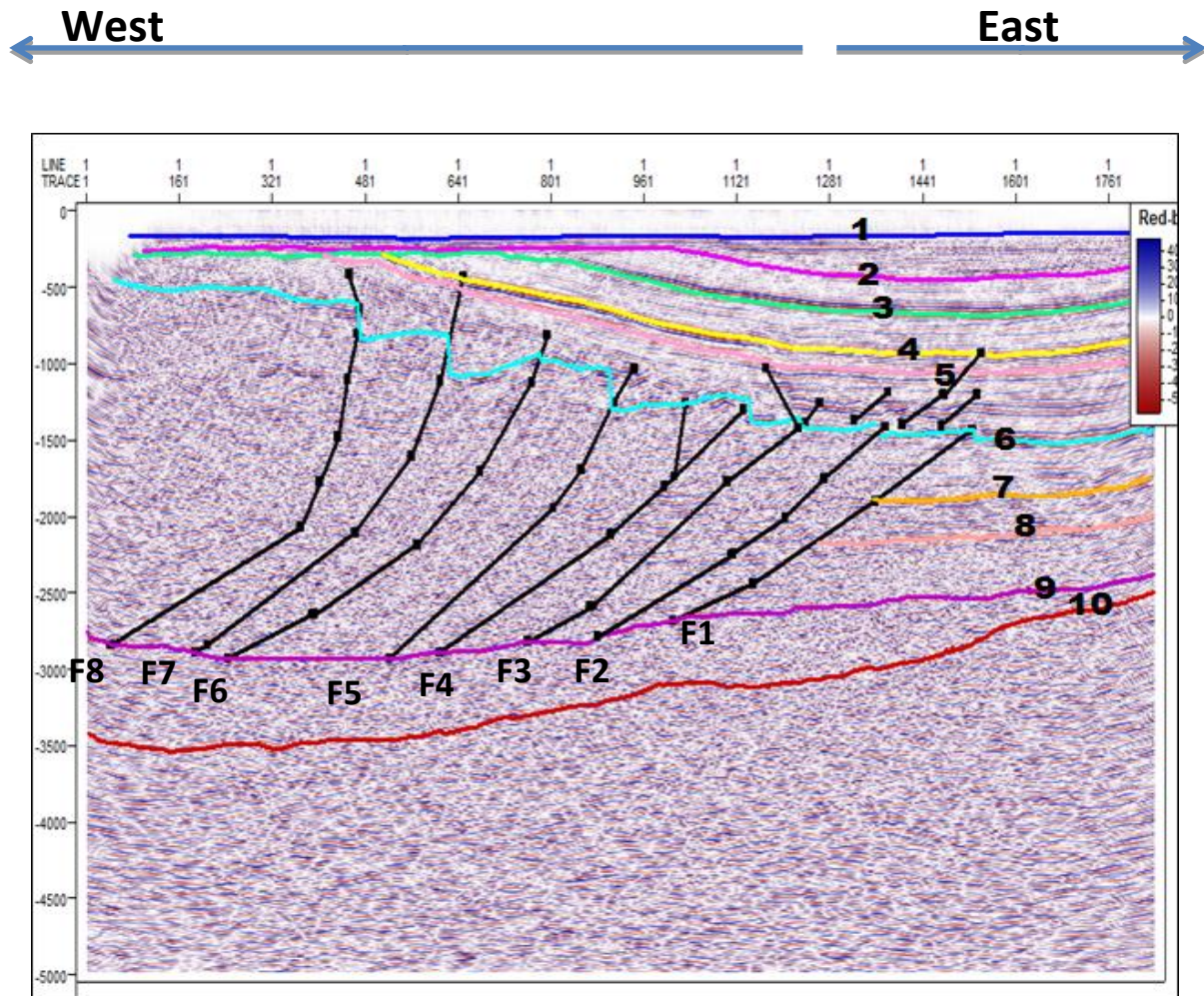


**Figure 7.6:** Horizons mark the following reflectors: 1- blue= sea bed, 2-light purple: mid Tertiary, 3-green: lower Tertiary, 4-yellow: mid Cretaceous, 5-pink: lower Cretaceous, 6-light blue: lower Jurassic, 7-orange: top Perm, 8-orange-pink: mid Perm, 9-dark purple: lower Perm, 10-red: basement. F1-8 is reverse Faults.

Faults F1 - F8 (Figure 7.6) are followed through all the profiles with fault planes striking northwest, corresponding with, for example Blinova et al. (subm.).

Due to poor imaging there is a large degree of uncertainty in the interpretation of the profiles in the west. F1 - F8 is interpreted along the most pronounced breaks in the illustrated reflectors as well as the Gypshuken formation in the Lower Permian that works as sliding zone for faults (Figure 7.6). Since Gypshuken is assumed to represent low-velocity porous evaporites that will not generate clear seismic reflections, the faults are followed down to the



relatively strong lower Permian reflector, which is interpreted as the transition to underlying dolomite layers with higher velocities in Nordenskiöld breen formation .

Lack of imaged units from Permian to Jurassic in the western part of the profiles is probably due to severe deformation of the area interpreted as the eastern part of CSFTB. A possible interpretation model may be introduced for the western part of the lines: In the model defined in Figure 7.6 units are faulted from Permian to Jurassic by large reverse faults (F1-F8) that propagates from Gypshuken across the Lower Permian.

All the interpretation that have been discussed so far is according to 2D data. The reason is that only 2D data were available for the thesis and there are no cross-line data to help us make a 3D image of the stratification of study area. But in order to better visualize the faults in the area, one may use 2D imaging for different parallel lines and map changes in layers and fault systems along the lines. With this regard Line 1 and Line VM07-11 have been chosen and are interpreted in 2D as seen in Figure 7.7. Moving from Line VM-07-1 toward Line VM-07-11, this figure demonstrates that there are some obvious structural changes (circles in figure 7.7). Traces between 801 and 961 (green circle in the figure) in line VM-07-1 and VM-07-11 indicate some changes in reflective pattern. In line VM-07-11 there are some discontinuities which may be related to the Cretaceous unit. Also traces between 1441 and 1601 (red circle in the figure) show some strong and more continuous Jurassic reflectors compared with line VM-07-1.

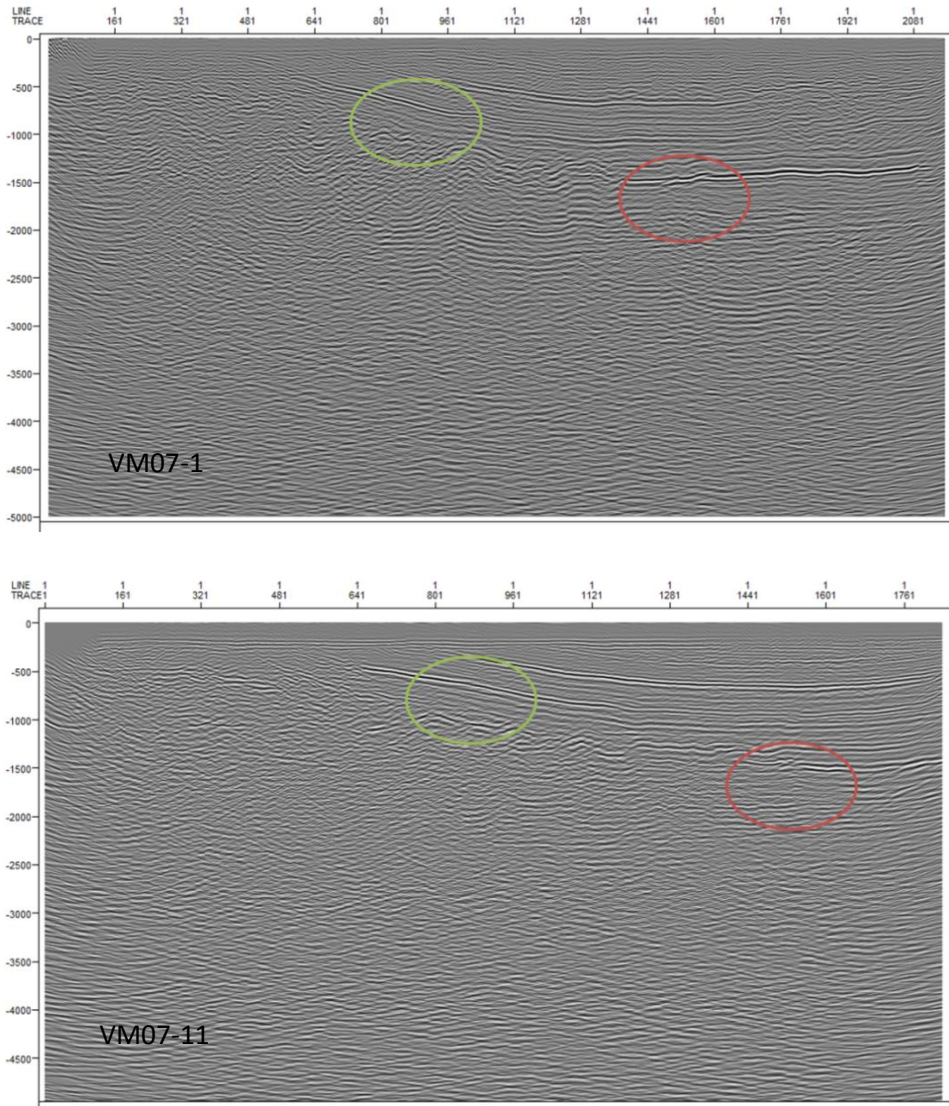


**Figure 7.7:** Traces between 801 and 961 (green circle in the figure) in line VM-07-1 and VM-07-11 indicate some changes in reflectors. In line VM-07-11 there are some discontinuity which may be related to the Cretaceous unit. Also traces between 1441 and 1601 (red circle in the figure) shows stronger and more continuous reflectors than line VM-07-1, related to the Jurassic unit.

Figure 7.8 shows all 19 seismic lines in this study. Lines VM-07-1 and VM-07-11 have been displayed in this 3D figure. Figure 7.9 shows the same from a different viewpoint. The figure demonstrates that the interpretation of the different reflectors in is consistent and show continuity. Figure 7.10 shows the direction of the faults between the interpreted lines. The 3D shape of the fault planes can be easily seen in the figure (e.g. fault No. 8 which is in red colour). As discussed above, the units are faulted from Permian to Jurassic by large reverse faults (F1-F8) that propagates from Gypshuken across the Lower Permian.

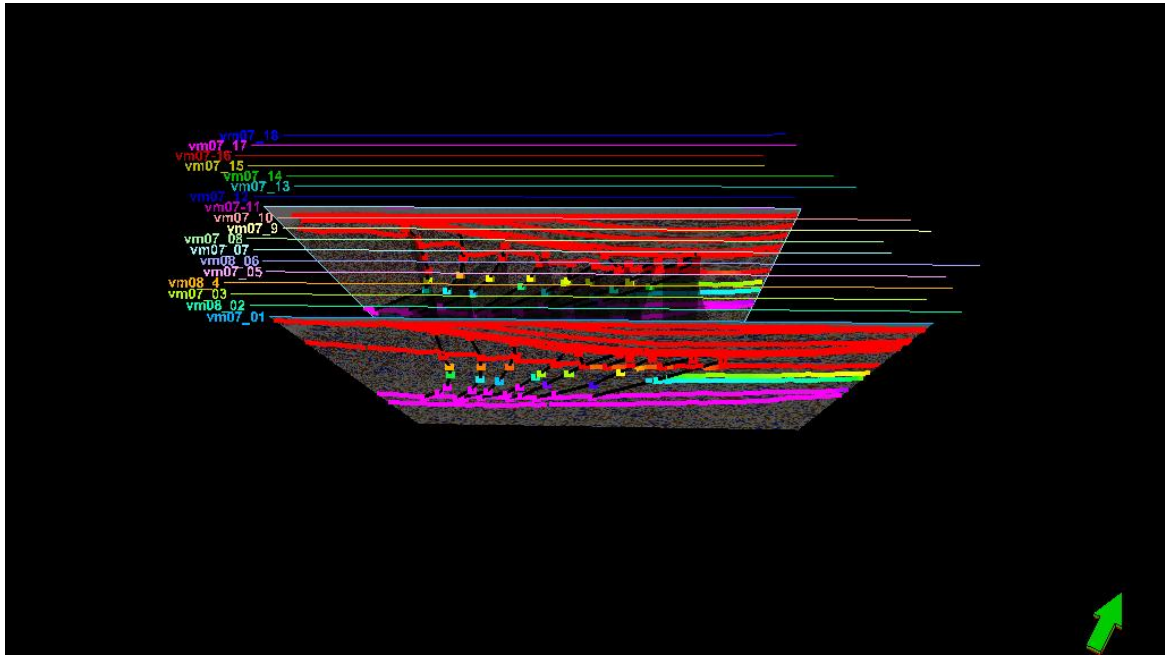


**Figure 7.8:** Top view of all 19 seismic lines in this study, the arrow shows north east

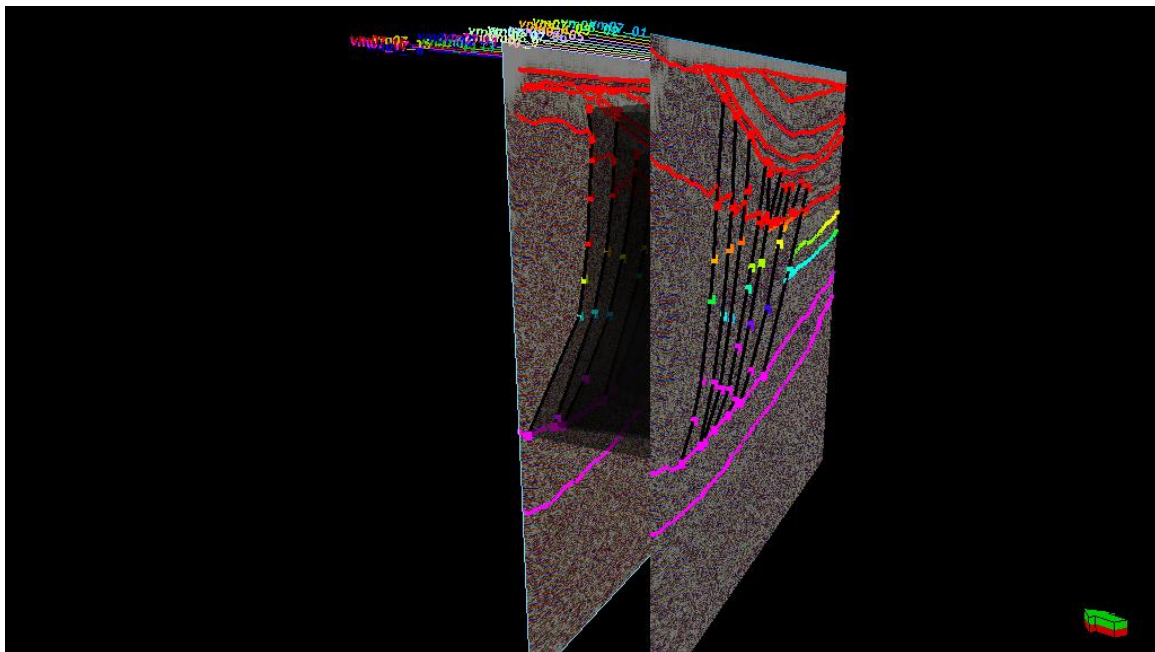


**Figure 7.9:** Seismic lines VM-07-1 and VM-07-11 displayed in 3D

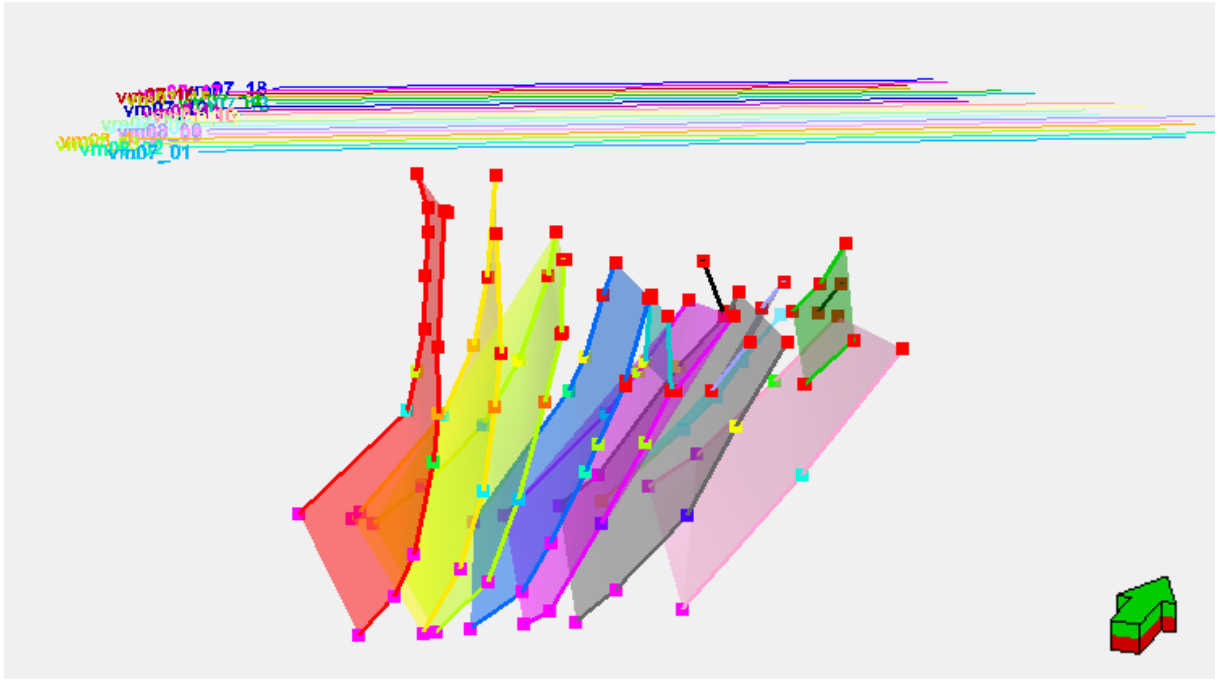


**Figure 7.10:**Direction of the faults between the lines.

## 8 Concluding Remarks

19 seismic profiles from Van Mijenfjorden on Svalbard have been processed. The main focus of the processing has been the removal of multiples, which represents a major challenge in the seismic data due to hard seabed and low water depth in the study area.

Several different processes have been used to remove multiples. Waves that are only in the water layer (total reflection) were removed by FK and linear radon filters. Deconvolution and stacking were then applied to remove the remains of multiples.

Velocity filtering was applied to three different sorts of data: the standard CDP collection, as well as data sorted according the CDP-positions, shot and receiver collection. By sorting the CDP-positions of receivers, collections that are shot in the opposite direction were simulated. It means that travel time along a ray path is the same regardless of direction, but apparently velocity will vary depending on the shot direction. This method has given good results: only in the top parts of some profiles there are indications of seabed multiples.

When the seabed and the top reflectors were weakened in the processing an alternative version of the stacks was generated. These show much clearer imaging of the upper 0.5 s. These stacks were used to support the interpretation of the seabed and the upper parts of the profiles.

The profiles were interpreted, with emphasis on the correlation of sedimentary strata from Permian to Tertiary with an already established seismostratigraphic framework, and to provide an overview of large-scale fault geometries in the area. These are mainly formed by transpressive deformation related to the opening of the Norwegian and Greenland Sea.

A number of strong reflections depict an asymmetric syncline, interpreted as Tertiary deposits in Spitsbergen Central Basin. Furthermore, one can follow the reflections corresponding to the sedimentary sequence of Carboniferous to Cretaceous.

A reflector interpreted as shale from Janusfjellet sub-group in the Lower Jurassic acts as sliding plane for Tertiary contraction deformation. This is indicated by the eastern thickening of the formation and potential duplex structures within the unit.

Eight major reverse faults, F1 - F8, were interpreted in the western parts of the profiles, with a certain degree of uncertainty. These appear to propagate along a sliding zone in evaporite layers in the lower Permian. Transparent seismic character and reflections from fragments of strata with different dip, indicate significant deformation which increases towards the west.

The Permian unit has a clear thickening from east to west and from north to south in the study area, probably due to stacking of faulted materials related to the faults F1-F8.

The study area can be divided into two zones with different deformation pattern:

The Western Zone is characterized by a high degree of deformation, and is associated with the Foreland-oriented part of the West Spitsbergen fold and fault belt. The units from Permian to Jurassic are probably strongly deformed in this zone.

The Eastern zone has a lower degree of deformation, and is dominated by a syncline that corresponds to the Spitsbergen main basin.

## References

- Bergh, S. G., Braathen, A. & Andresen, A. (1997). Interaction of Basement-Involved and Thin-Skinned Tectonism in the Tertiary Fold-Thrust Belt of Central Spitsbergen, Svalbard. *AAPG Bulletin*, 81(4), 637-661.
- Bergh, S. G. & Andresen, A. (1990). Structural development of the Tertiary fold-and-thrust belt in east Oscar II Land, Spitsbergen. *Polar Research*, 8(2), 217-236.
- Birkenmajer, K. (1981). The geology of Svalbard, the western part of the Barents Sea, and the continental margin of Scandinavia. *The Ocean Basins and Margins*, 5, 265-329.
- Blinova, M., Thorsen, R., Mjelde, R. & Faleide, J. I. (2009). Structure and evolution of the Bellsund Graben between Forlandsundet and Bellsund (Spitsbergen) based on marine seismic data. *Norwegian journal of Geology*, 89, 215-228.
- Blinova, M., Faleide, J. I., Gabrielsen, R. H. & Mjelde, R. (subm.). Seafloor expression and shallow structure of a surfacing fold-and-thrust system. An example from Isfjorden, West Spitsbergen. *Submitted to Polar Research*.
- Braathen, A., Bergh, S. G. & Maher Jr, H. D. (1995). Structural outline of a Tertiary basement-cored uplift/inversion structure in western Spitsbergen, Svalbard: Kinematics and controlling factors. *Tectonics*, 14, 95-119.
- Braathen A., Bergh, S. G., & Maher, H. D. (1999). Application of critical wedge taper model to the Tertiary transpressional fold-thrust belt on Spitsbergen, Svalbard: Kinematics and controlling factors. *GSA Bulletin*, 111 (10), 1468-1485.
- Brown, A. R. (1999). *Interpretation of Three-Dimensional Seismic Data*. American Association of Petroleum Geologists (AAPG).
- CGG Veritas (2006). *Geocluster Release Notes*.
- Dallmann, W. K. (ed.) (1999). *Lithostratigraphic Lexicon of Svalbard: Review and recommendations for Nomenclature Use: Upper Palaeozoic to Quarternary Bedrock*. Norsk Polarinstitutt.
- Eiken, O. (1985). Seismic mapping of the post-Caledonian strata in Svalbard. *Polar Research*, 3, 167-176.
- Eiken, O. & Austegard, A. (1994). *Seismic atlas of Western Svalbard: A selection of regional transects*. Norsk Polarinstitutt, 73 p.
- Faleide, J. I., Vågnes, E. & Gudlaugsson, S. T. (1993). Late Mesozoic-Cenozoic evolution of the southwestern Barents Sea in a regional rift-shear tectonic setting. *Marine and Petroleum Geology*, 10, 186-214.

Faleide, J. I., Tsikalas, F., Breivik, A. J., Mjende, R., Ritzmann, O., Engen, Ø., Wilson, J. & Eldholm, O. (2008). Structure and evolution of the continental margin of Norway and the Barents Sea. *Episodes*, 31, 82-91.

Fossen, H., and R. H. Gabrielsen, 2005, structure geology: Bergen, book., 375 s. p.

geo.uib.no. <http://www.geo.uib.no/eworkshop>

Hart, B. (2000). *3-D Seismic Interpretation: A Primer for Geologists*. SEPM Short Course Notes 48, 124 p.

Hatton, L., Worthington, M. H. Makin, J. (1986). *Seismic Data Processing*. Blackwell Scientific Publications, 1., 175 p.

Hjelle, A. (1993). *Geology of Svalbard*, Norsk Polarinstitutt.

Jackson, J.A., 1997, Glossary of Geology: Alexandria, Va., American geological Institute, XII, 769 s. p.

Kearey, P., Brooks, M. & Hill, I. (2006). *An Introduction to Geophysical Exploration*. Blackwell Publishing, 3, 262 p.

Kellogg, H. E. (1975). Tertiary stratigraphy and tectonism in Svalbard and continental drift. *AAPG Bulletin*, 59, 465-485.

Mitchum, R. M., Vail, P. R. & Thompson, I. (1977). Seismic Stratigraphy and Global Changes of Sea Level, Part 2: The Depositional Sequence as a basic Unit for Stratigraphic Analysis. *Seismic Stratigraphy-application to hydrocarbon exploration, AAPG*, 26, 53-62.

Mjelde, R. (2008) Cruise report, Svalex (unpublished).

Mjelde, R. (2007) Cruise report, Svalex (unpublished).

Mjelde, R. (2003). "Seismic Equipment", e-læringsmodul fra [www.lg.eage.net](http://www.lg.eage.net).

Nøttvedt, A., Livbjerg, F., Midbøe, P. S. (1993 a). Hydrocarbon potential of the Central Spitsbergen Basin. *Norsk Petroleumsforening (NPF) Special Publications*, 2, 333-361.

Ohta, Y. (1994). Caledonian and Precambrian history in Svalbard: A review and an implication of escape tectonics. *Tectonophysics*, 231, 183-194.

Pluijm, B. V. D. & Marshak, S. (2004). *Earth Structure*. Norton & Company Press, 2., 656 p.

Sengbush, R. L. & Hu, S.-T. (1986). Wiener-Levinson Deconvolution of Nonminimum Phase Seismic Data. Offshore Technology Conference, 93-102.

Sheriff, R. E. & Geldart, L. P. (1995). *Exploration Seismology*, Cambridge University Press, 592 p.



Steel R. J. & Worsley, D. (1984). Svalbard's post-Caledonian strata – An atlas of sedimentational patterns and palaeogeographic evolution. *Petroleum Geology of the North European Margin*, 109-135.

Steel R. J., Gjelberg, J., Helland-Hansen, W., Kleinspehn, K., Nøttvedt, A. & Larsen, M. R. (1985). The Tertiary strike-slip basins and orogenic belt of Spitsbergen. *SEPM, Special publication*, 37, 339-359.

Worsley, D. (2008). The post-Caledonian development of Svalbard and the western Barents Sea. *Polar Research*, 27, 298-317.

Yilmaz, O. (2001). *Seismic Data Analysis*. Doherty, S. M. (ed.), Society of Exploration Geophysicists, Tulsa, Oklahoma. 2027 p.

[www.slb.com](http://www.slb.com)

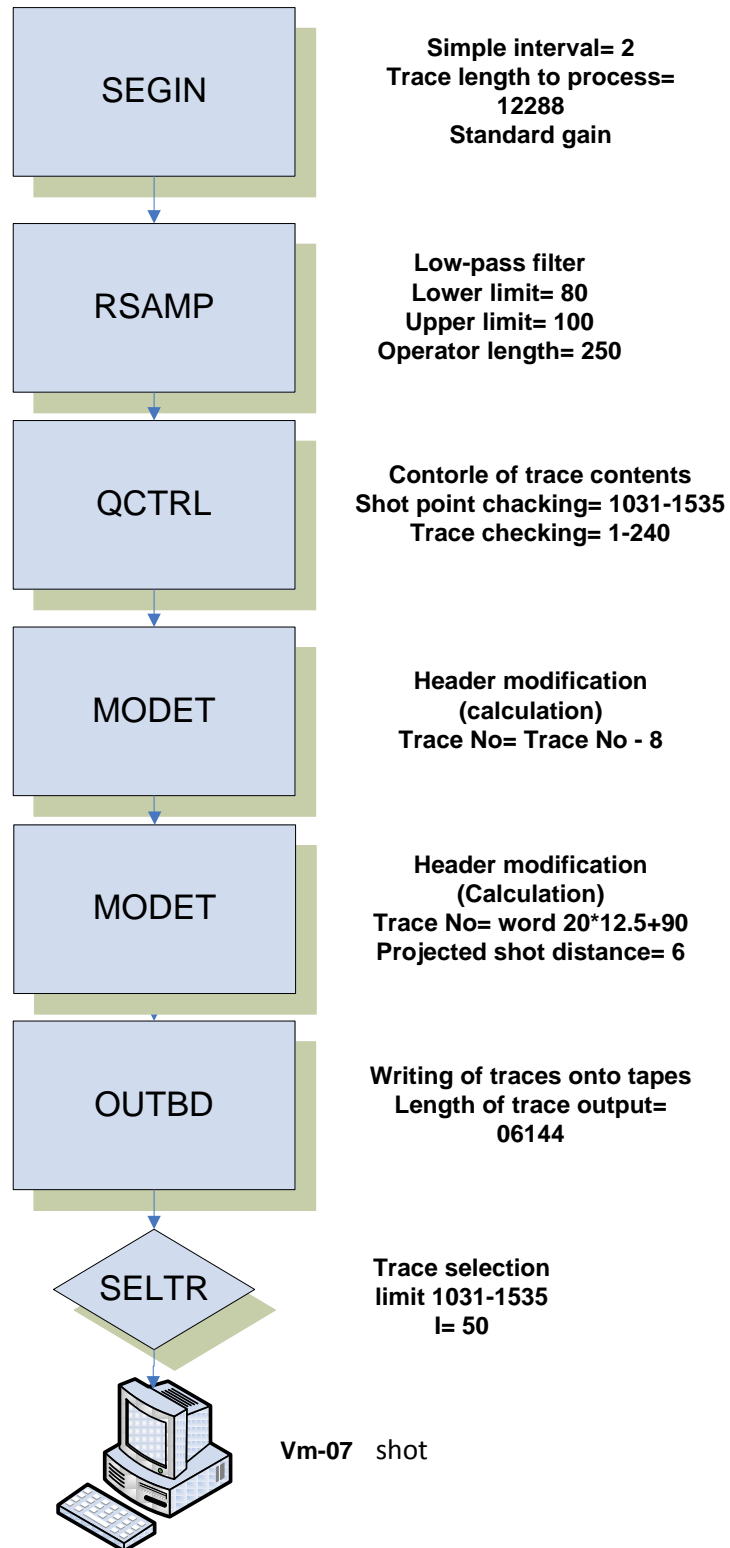
[http://perso-sdt.univ-brest.fr/~jacdev/ens/seis\\_proc05.htm](http://perso-sdt.univ-brest.fr/~jacdev/ens/seis_proc05.htm)

Reservoir Geiophysic course (GEOF294) material, GeoClasse,UIB 2008 .

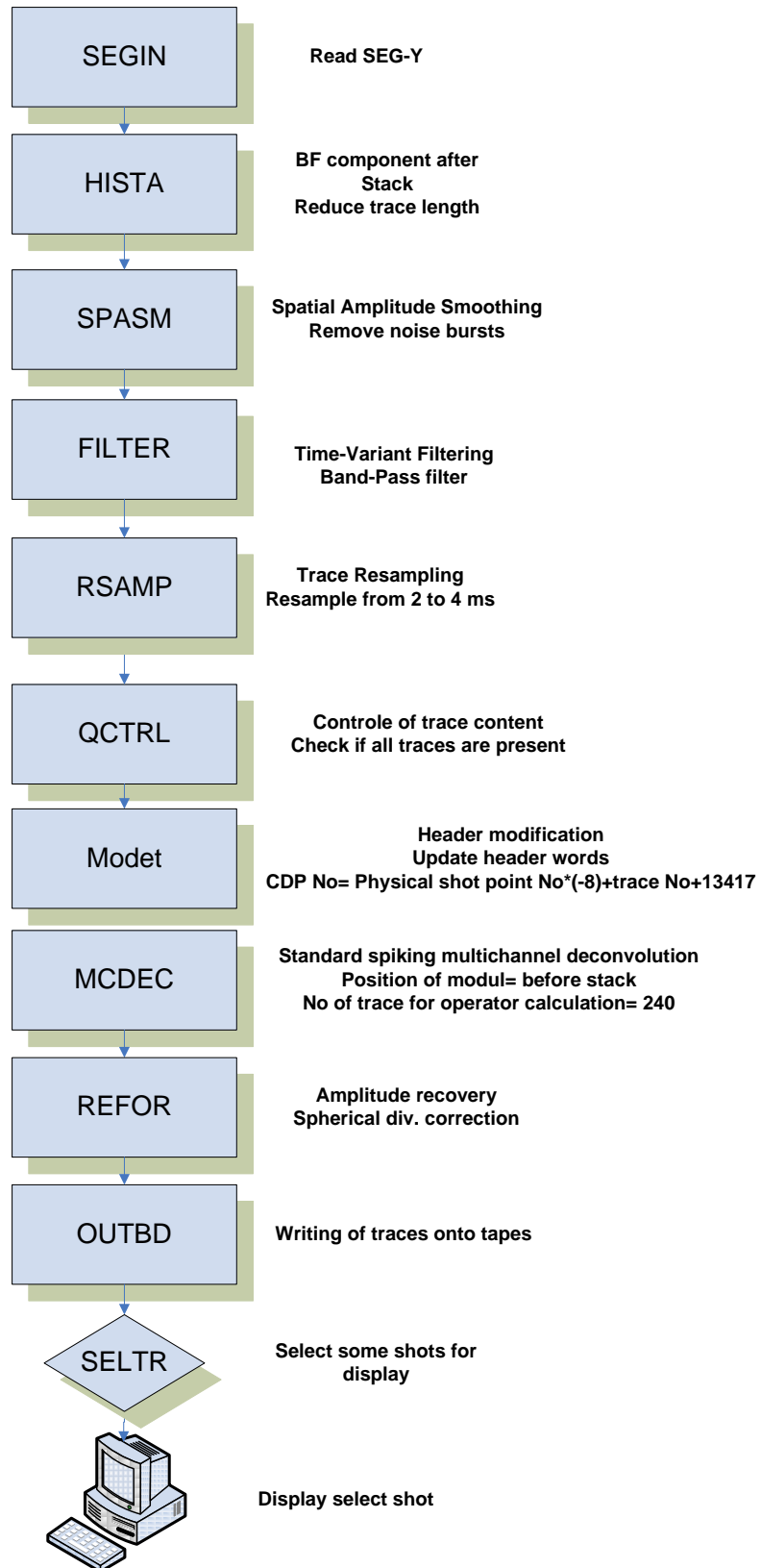
<http://www.xsgeo.com/course/basic.htm>

**Appendix 1**  
**Schematical of processing steps**

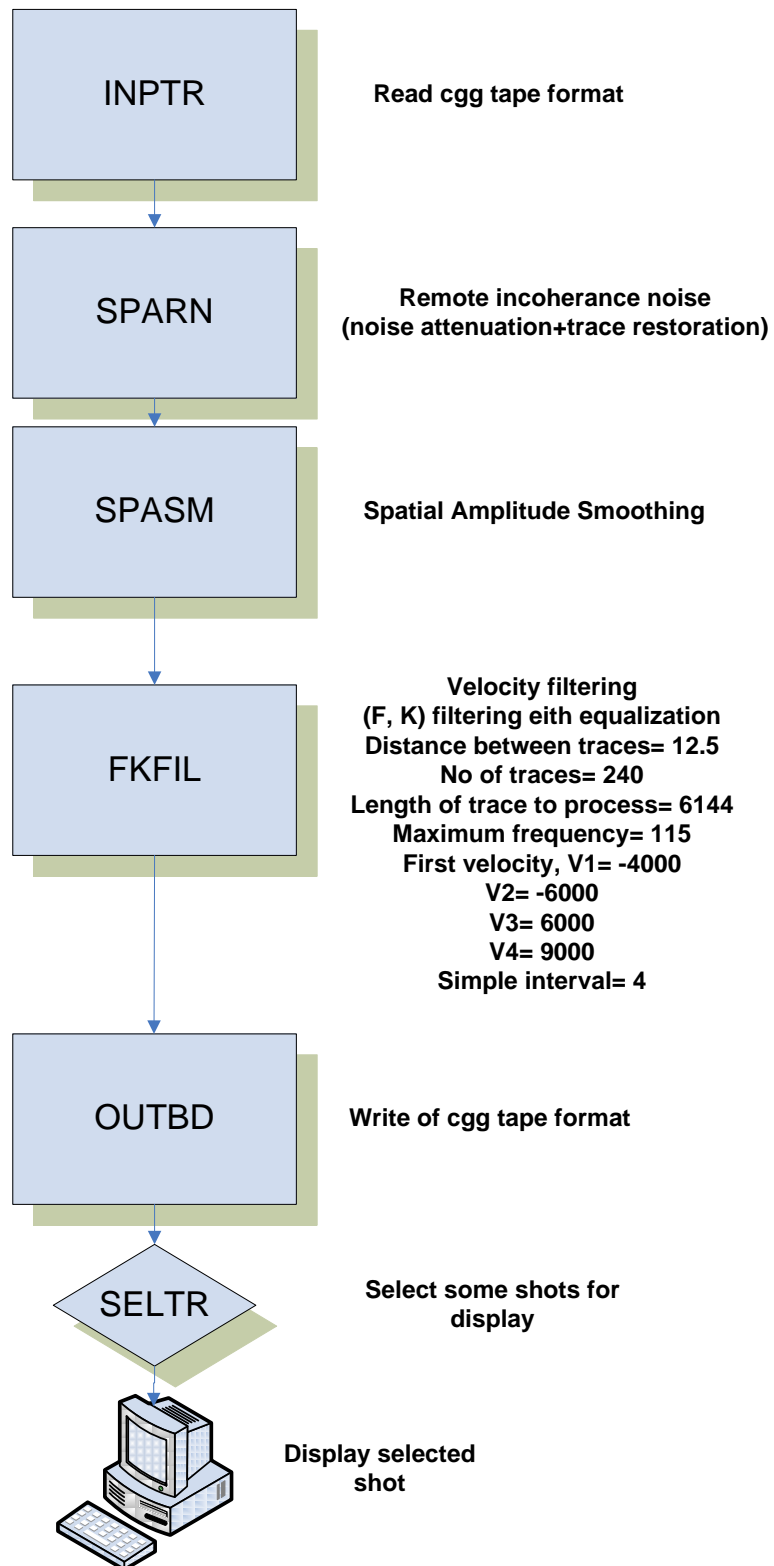
## Read Job for Line 6:



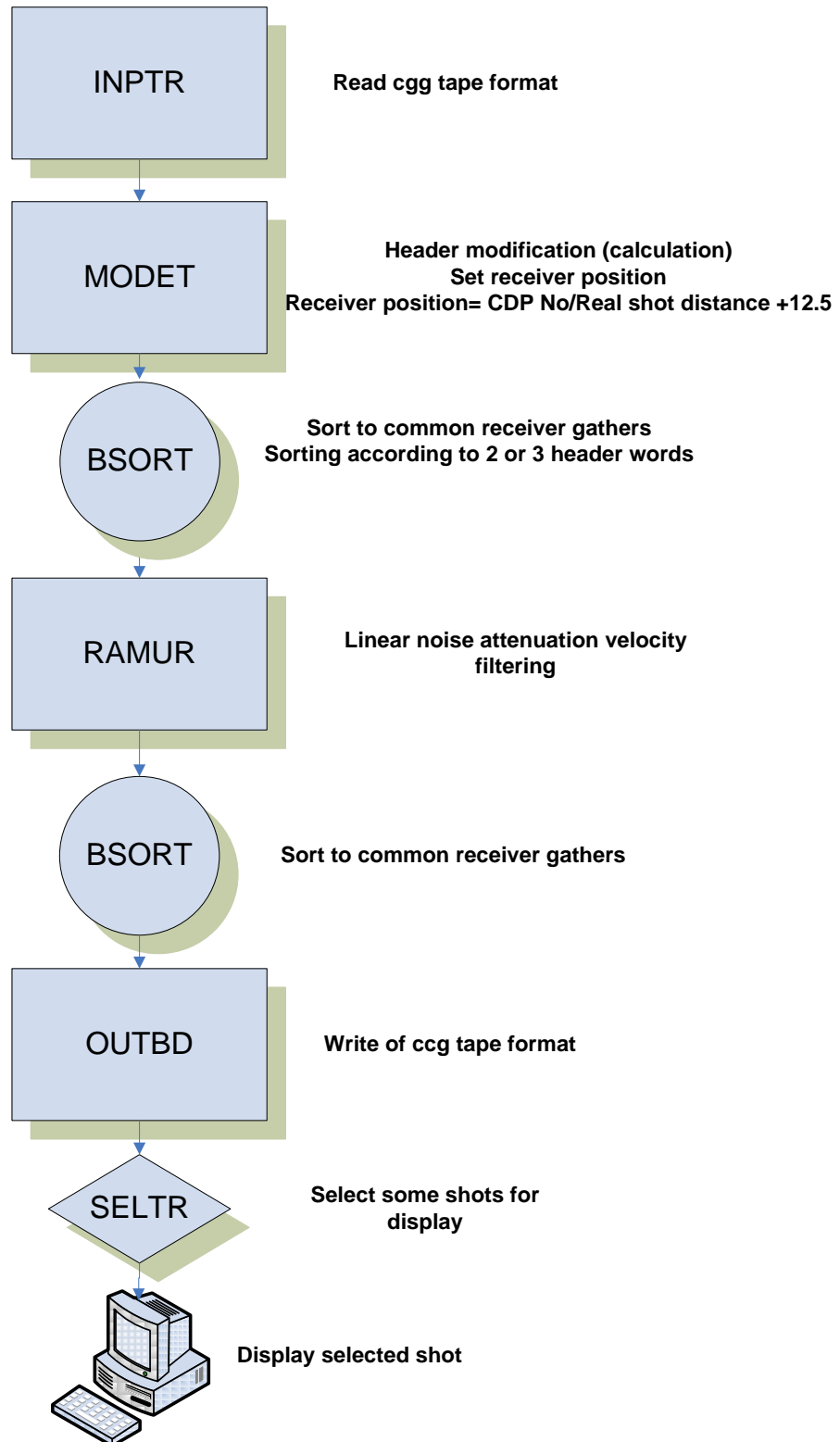
**Reformat job:**



## Filter Job:

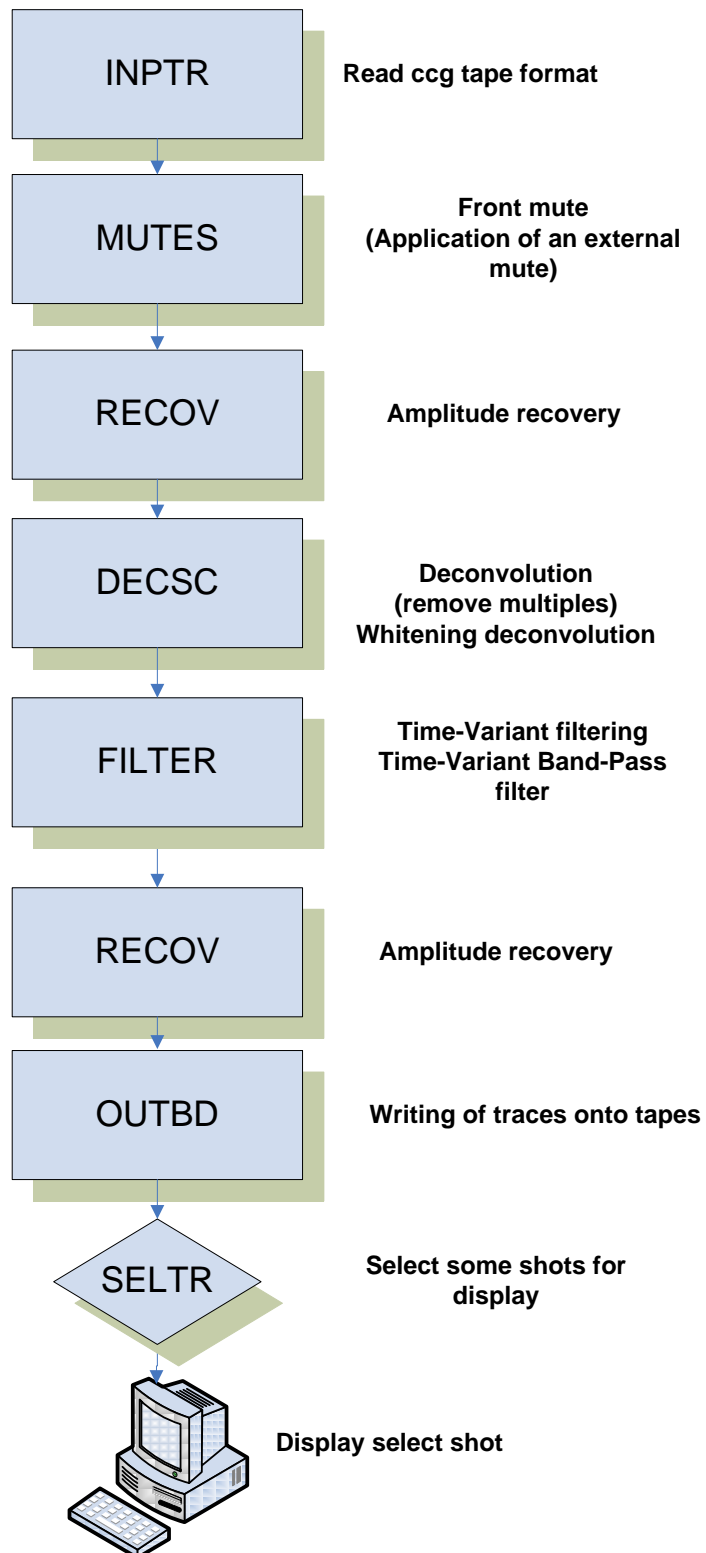


## Refilter Job:

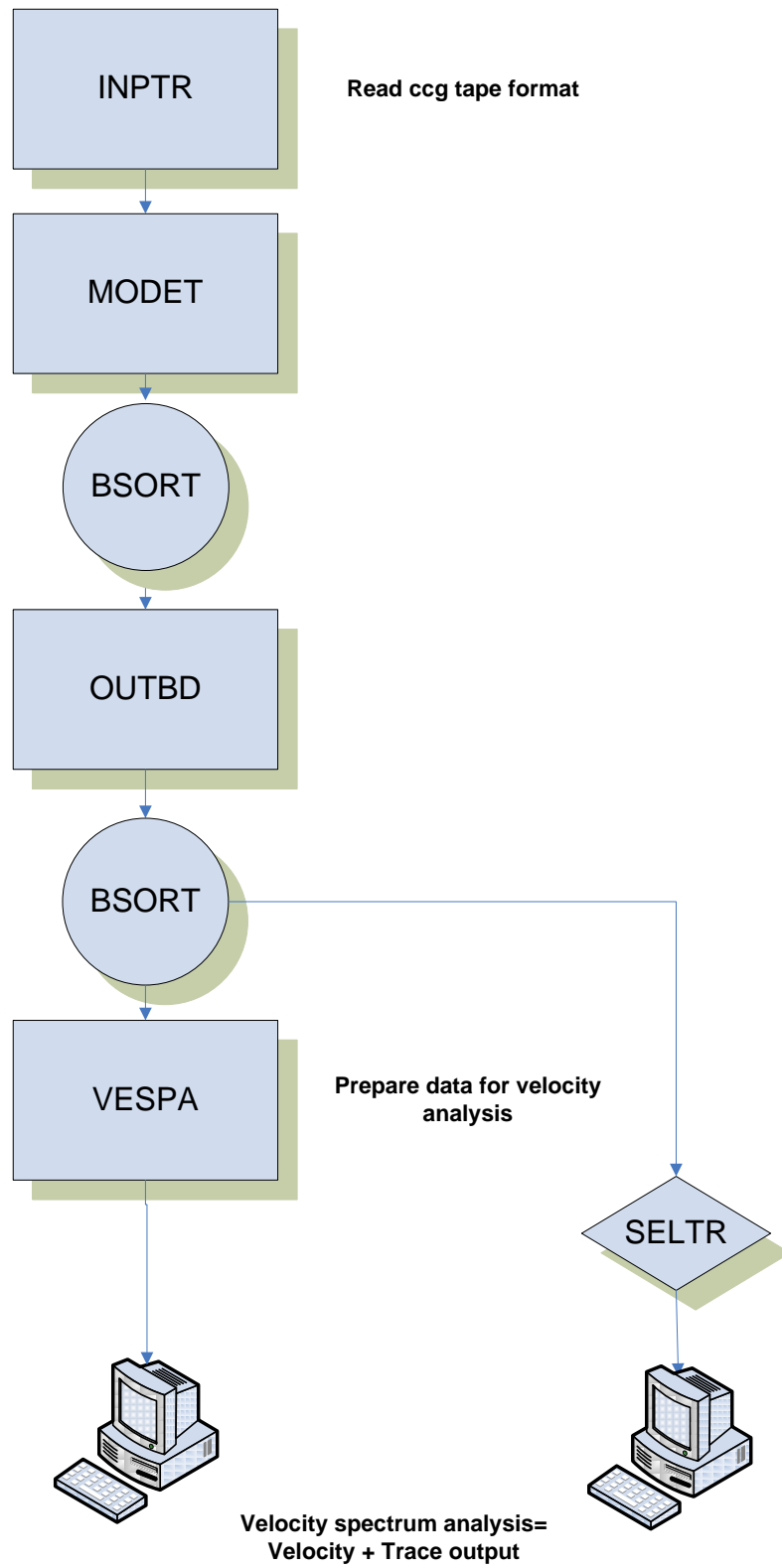




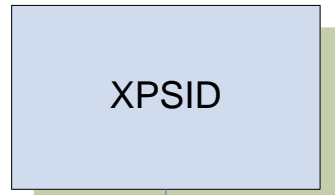
## Deconvolution Job:



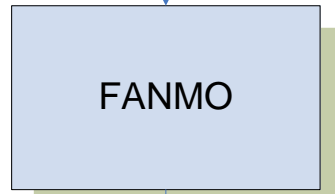
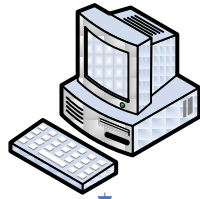
**Vespa Job:**



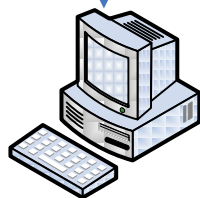
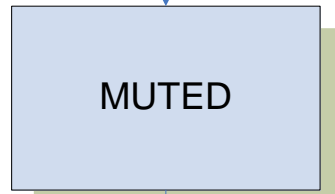
**NMO Job:**



**Read cgg tape format**

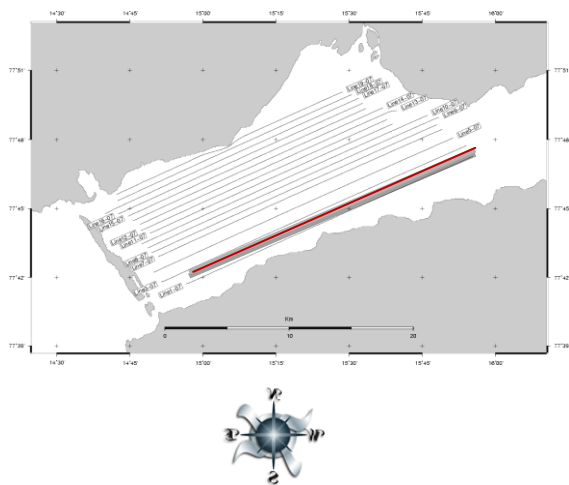
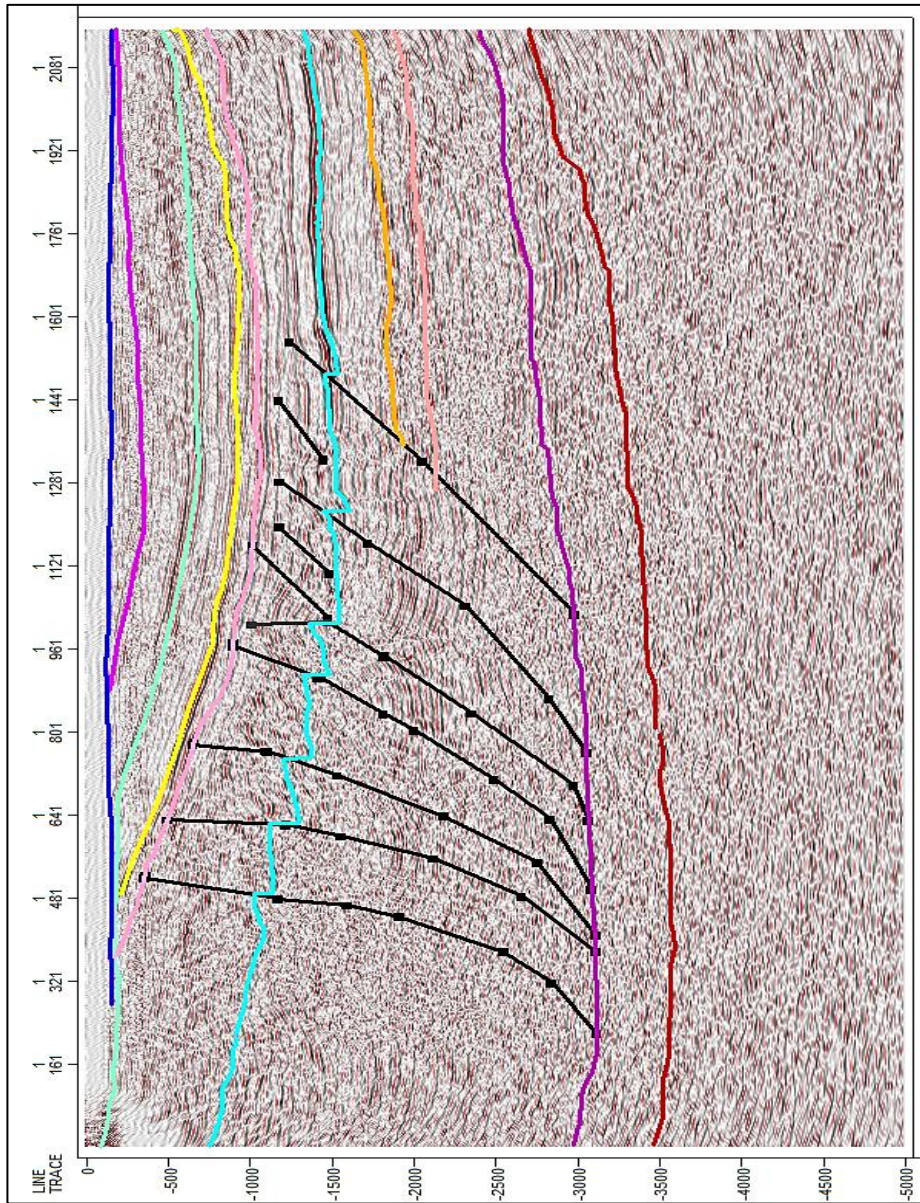


**Dynamic correction (NMO)**



## **Appendix 2**

### **Seismic profile**

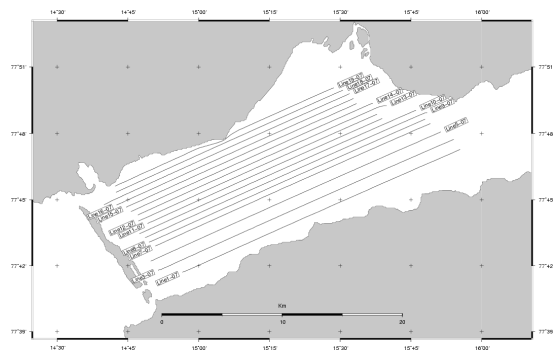
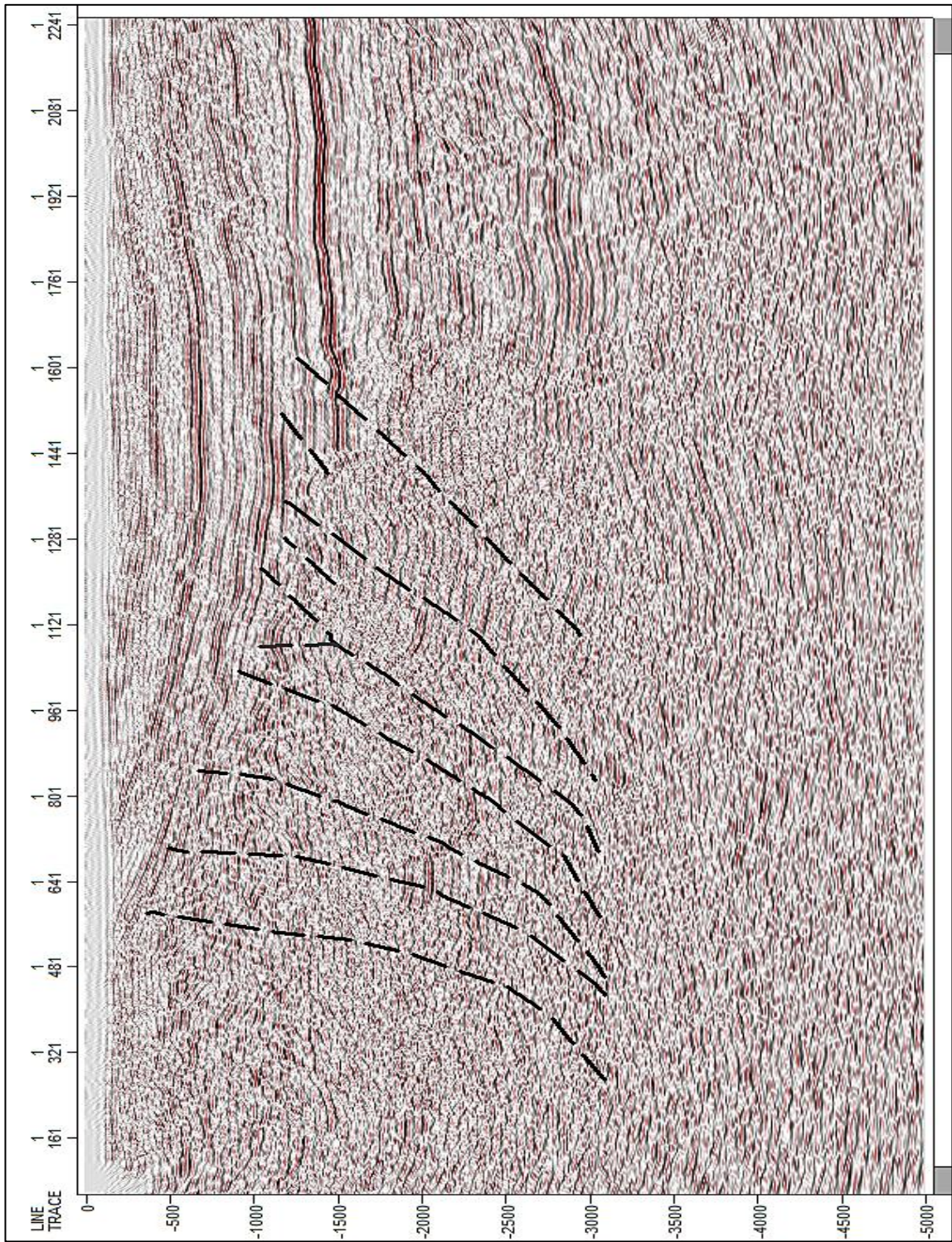


Profile VM-07-1. Trace number versus TWT.  
Horizons mark the following reflectors:

- |  |                  |  |                 |
|--|------------------|--|-----------------|
|  | Sea bed          |  | mid Tertiary,   |
|  | Lower Tertiary   |  | mid Cretaceous, |
|  | Lower Cretaceous |  | Lower Jurassic  |
|  | Top Perm         |  | mid Perm        |
|  | Lower Perm       |  | Basement.       |

F1-8 is reverse Faults in black colors

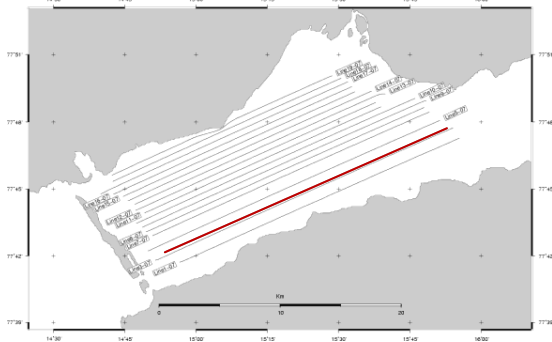
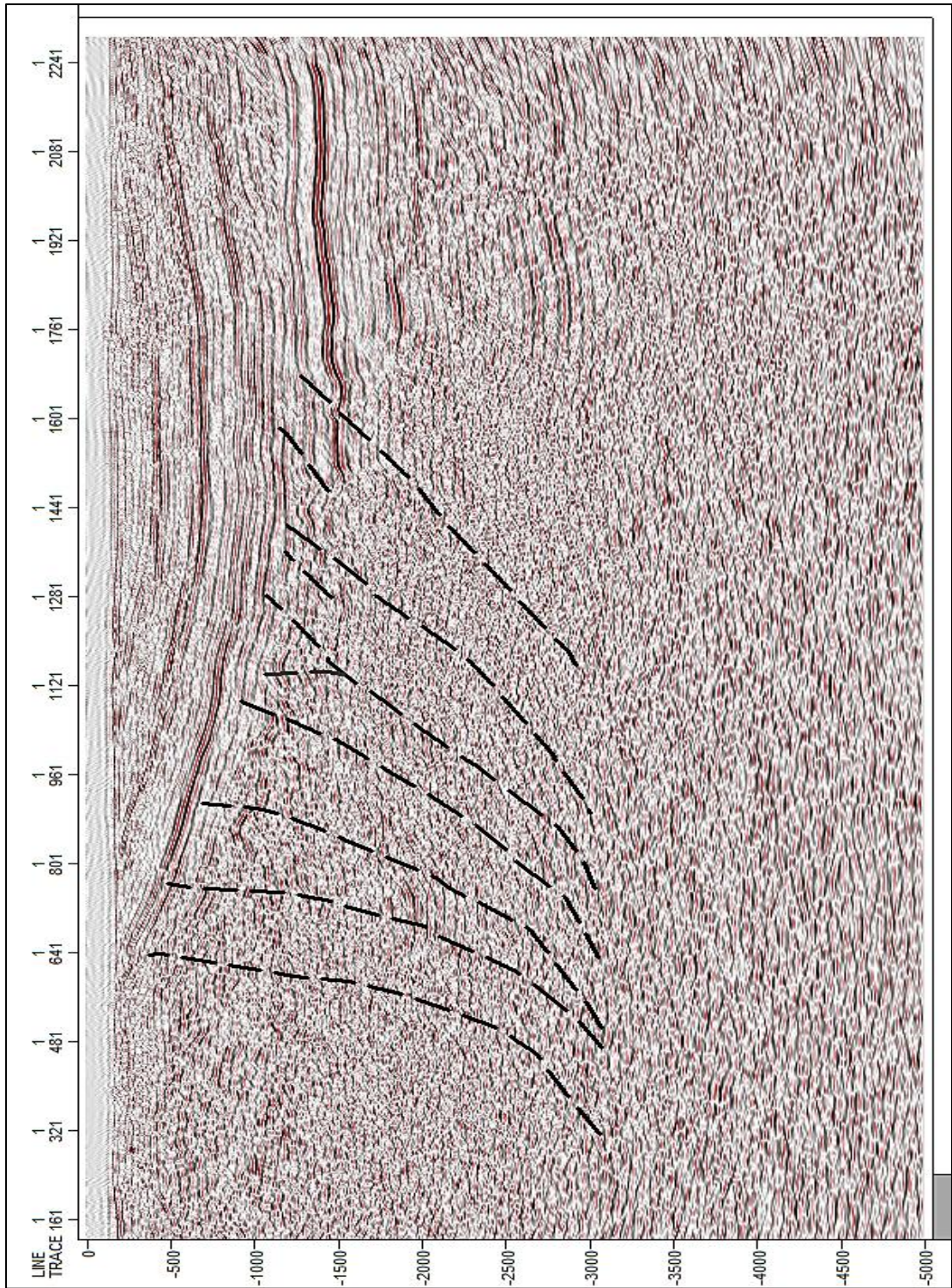




Seismic profile VM-08-2. This survey is for 2008. Trace number versus TWT.



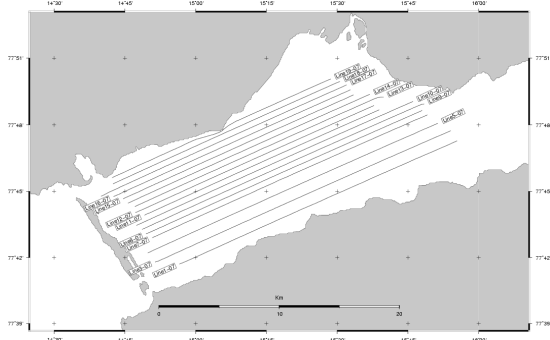
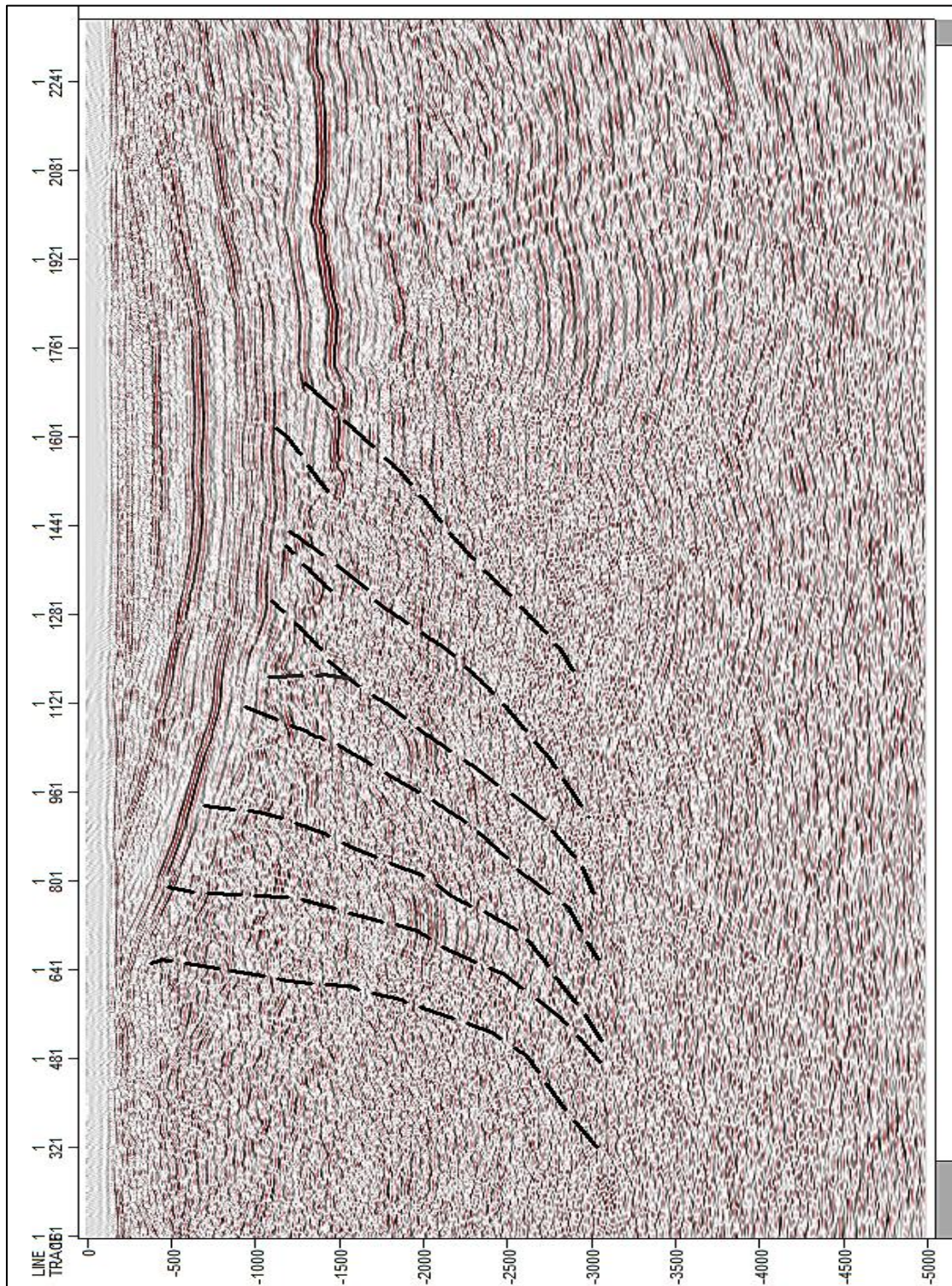




Seismic profile VM-07-3. Trace number versus TWT.



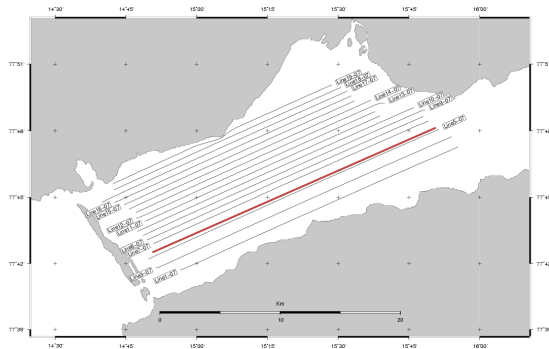
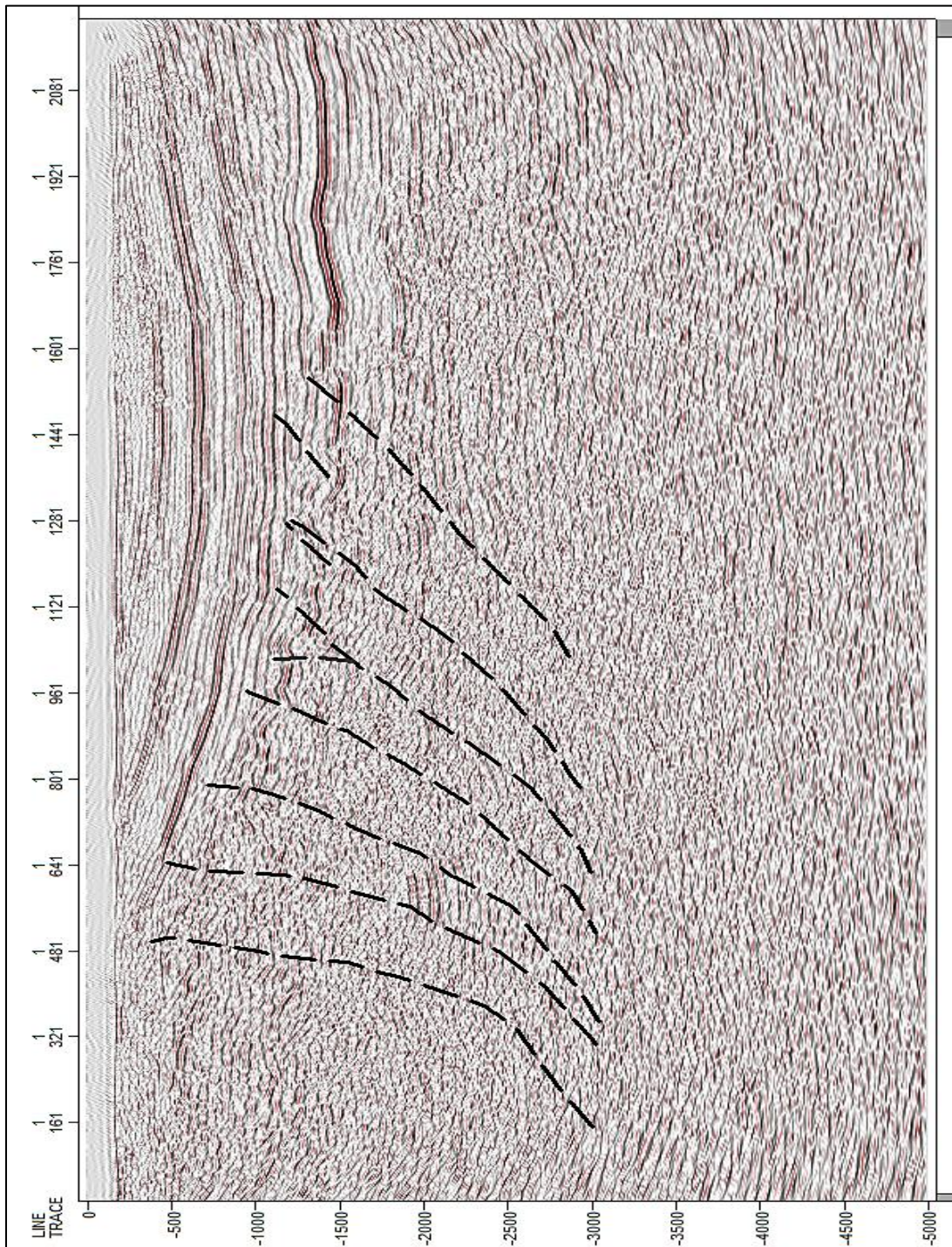




Seismic profile VM-08-4. Trace number versus TWT.







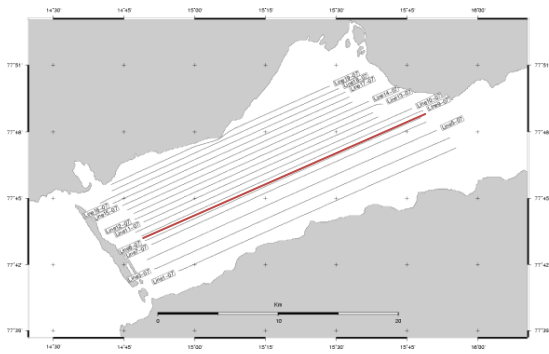
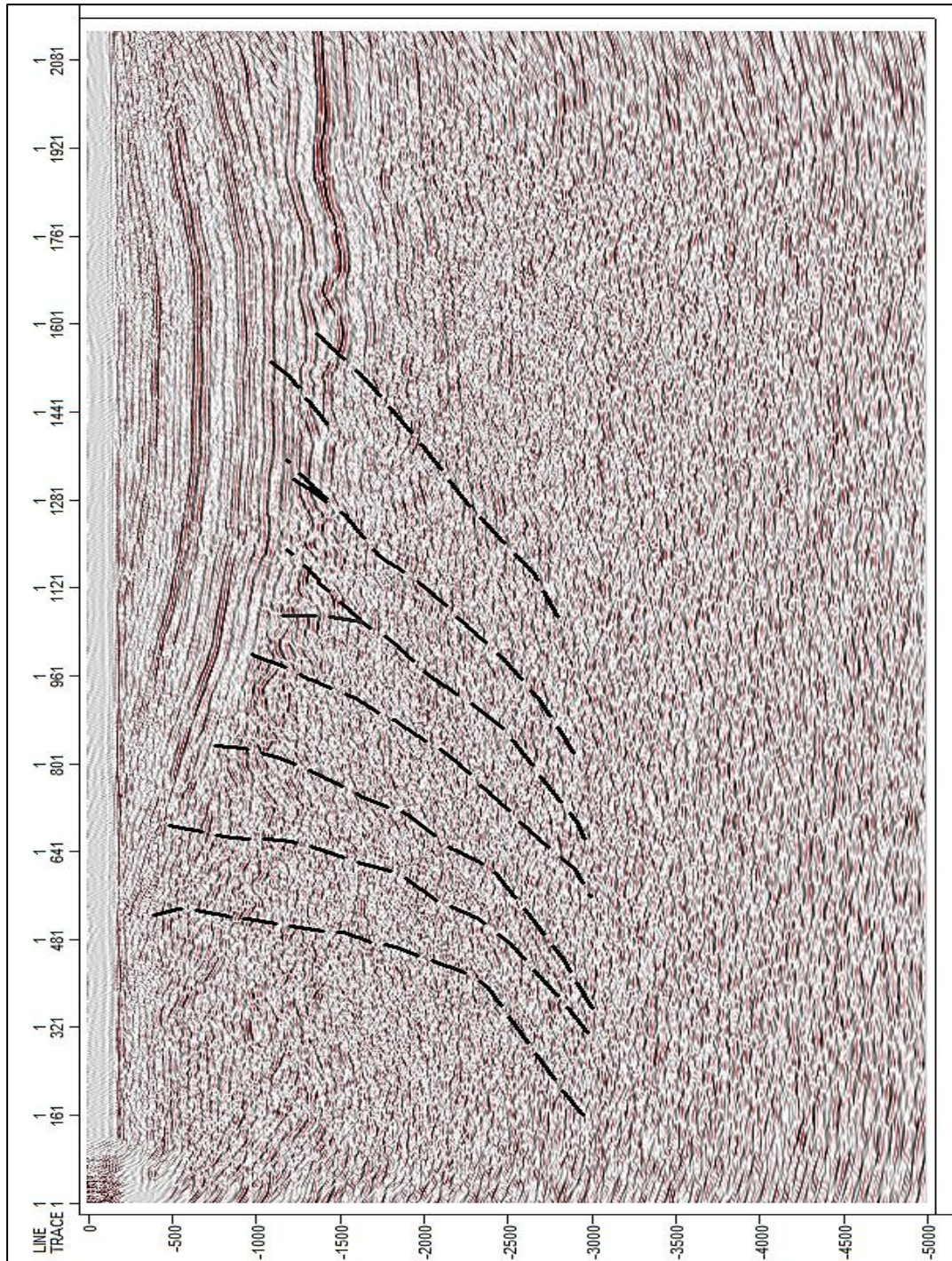
Seismic profile VM-07-5. Trace number versus TWT.







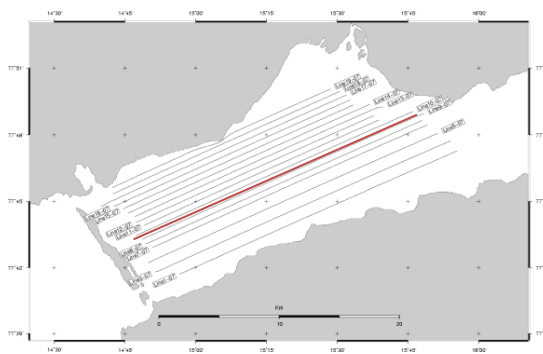
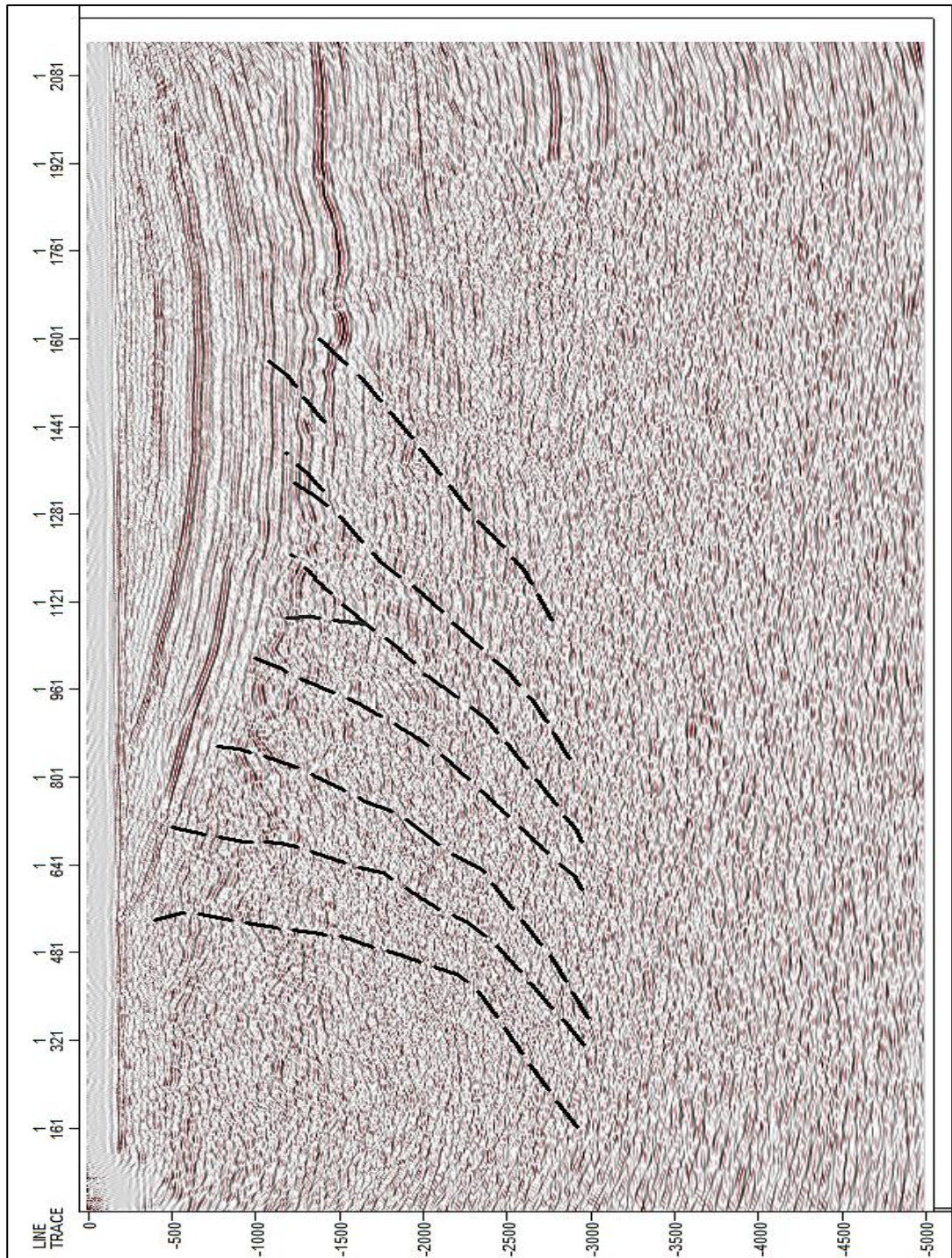




Seismic profile VM-07-7. Acquisition of this This survey was in 2007. Trace number versus TWT.



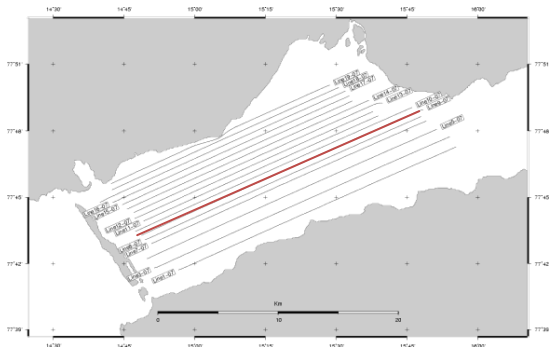
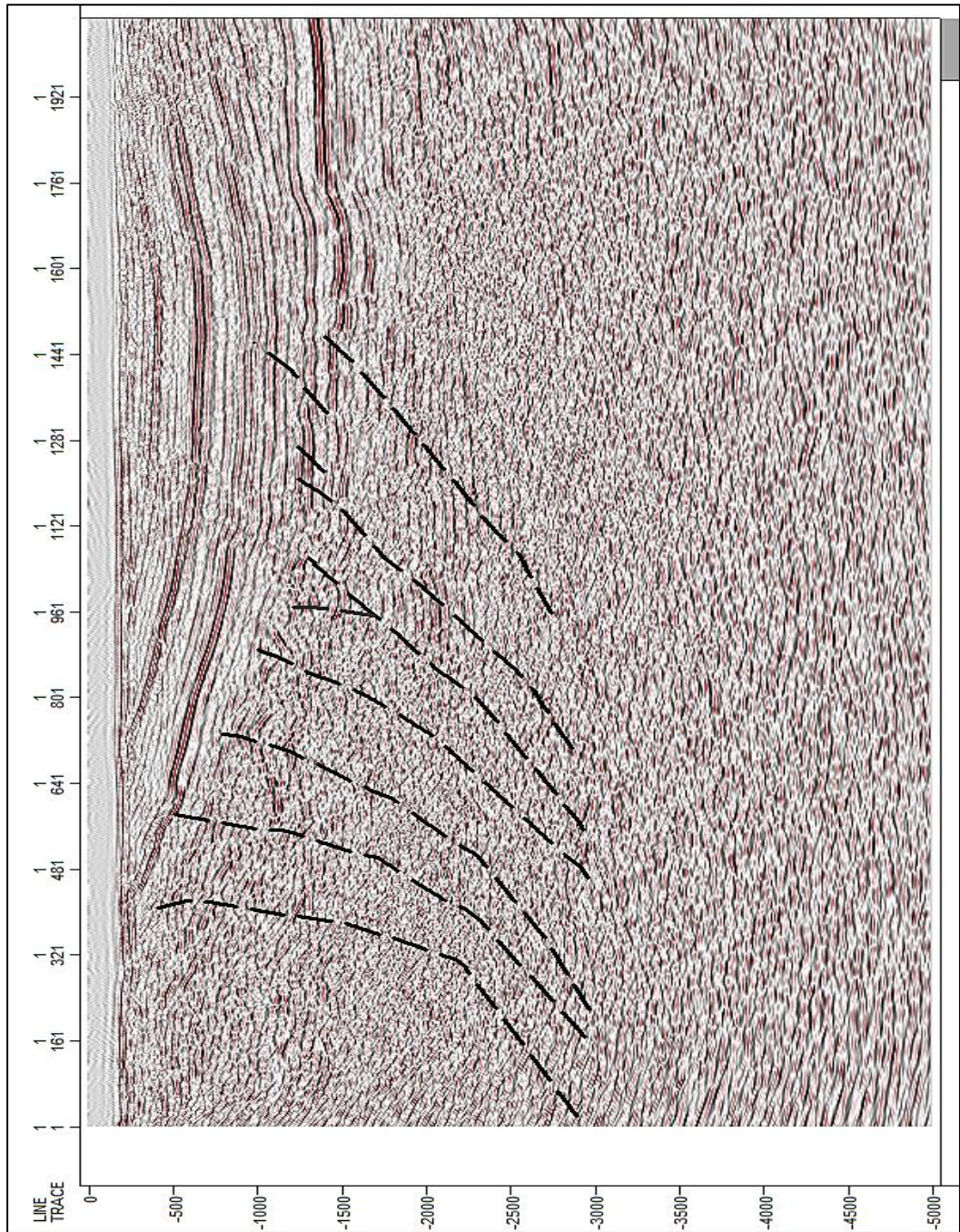




Seismic profile VM-07-8. Acquisition of this This survey was in 2007. Trace number versus TWT

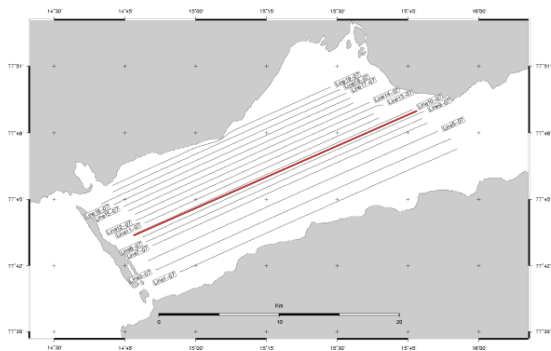
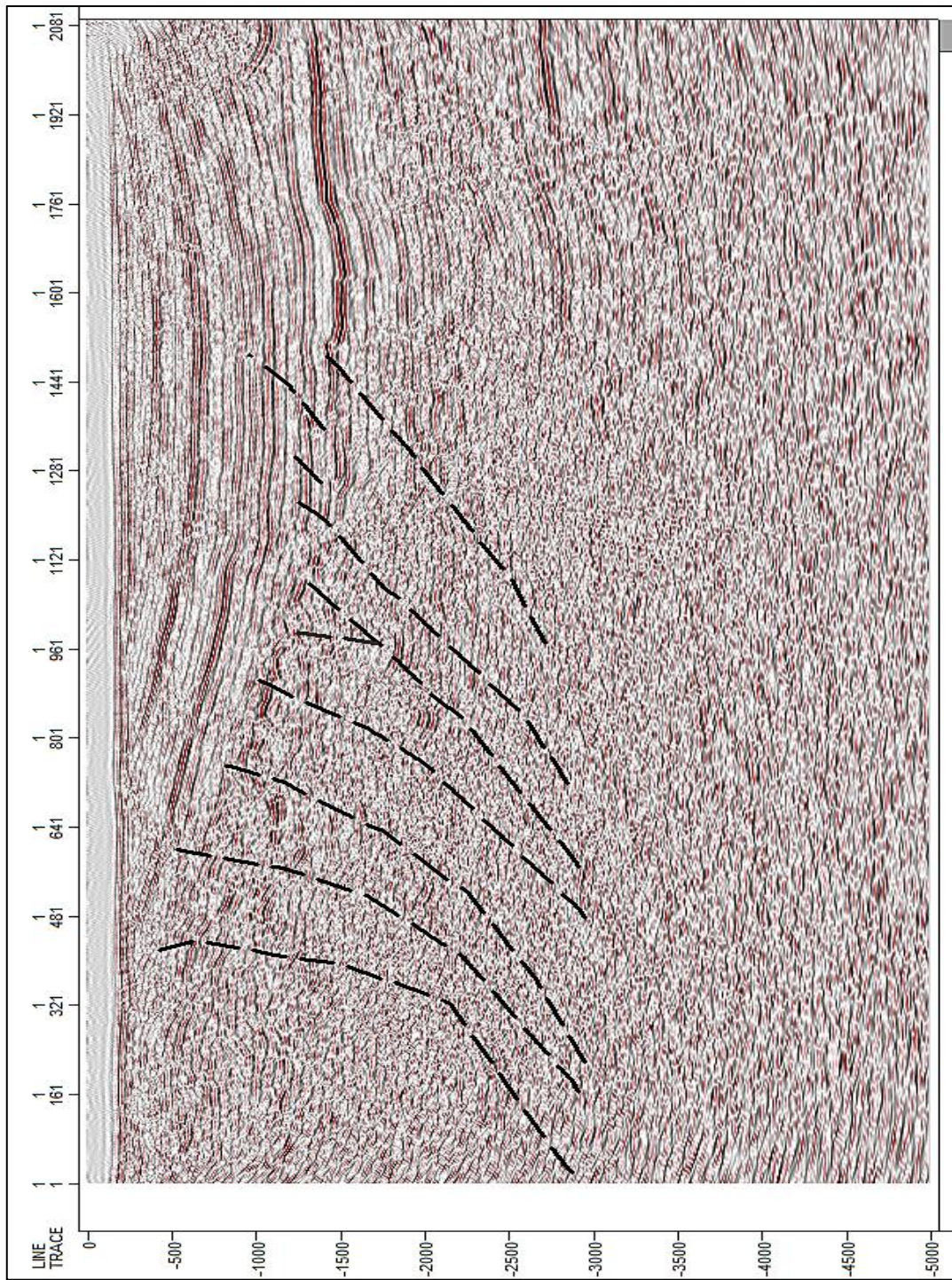




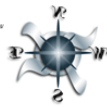


Seismic profile VM-07-9. Acquisition of this This survey was in 2007. Trace number versus TWT

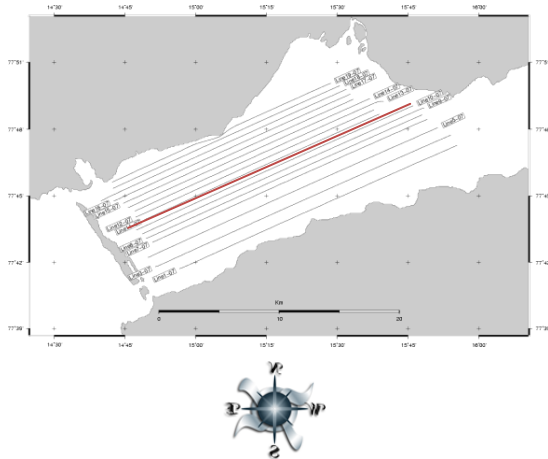
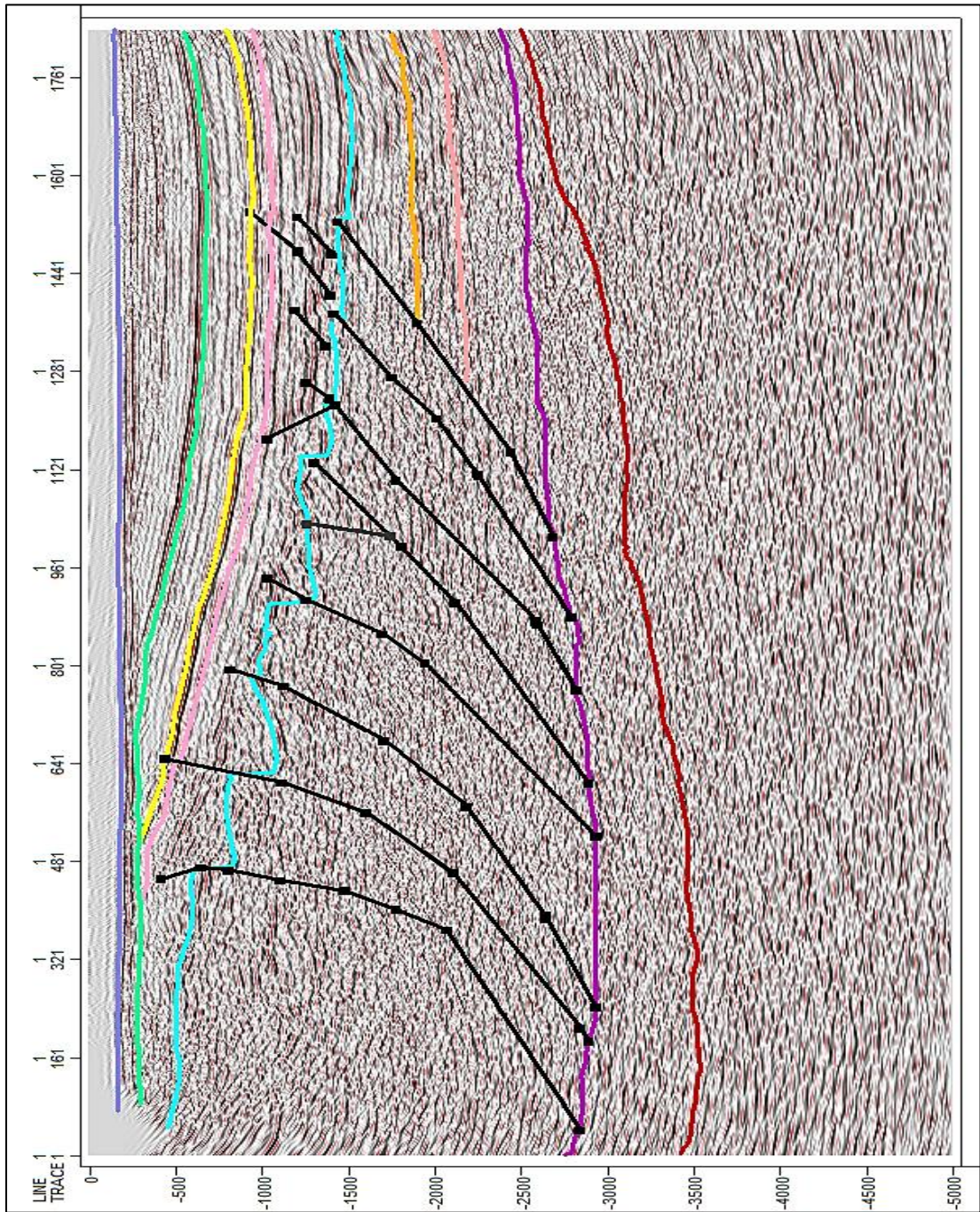




Seismic profile VM-07-10. Acquisition of this This survey was in 2007. Trace number versus TWT





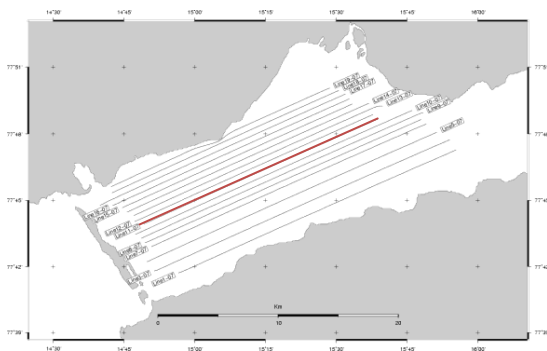
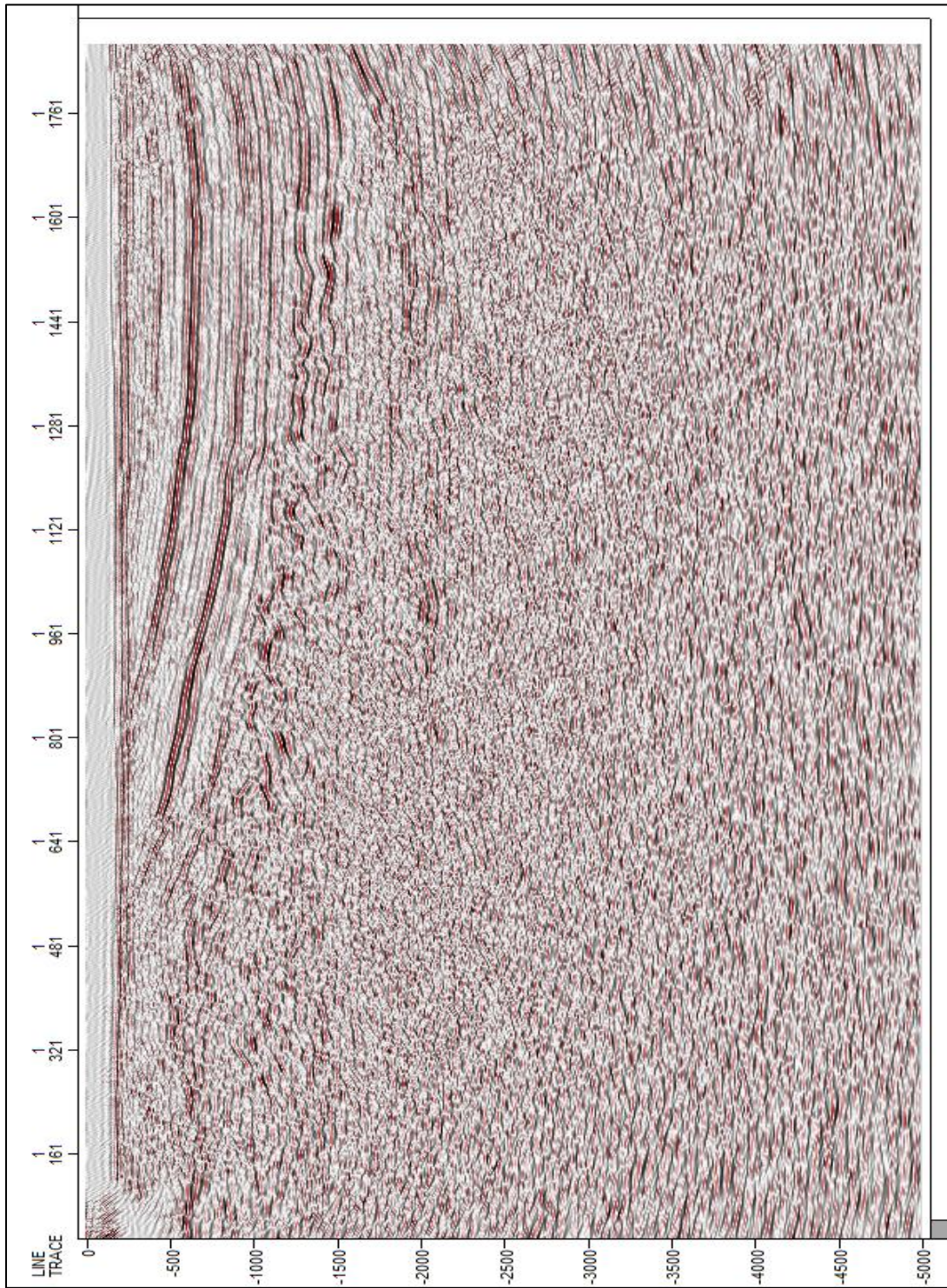


Seismic profile VM-07-11. Acquisition of this survey was in 2007. Trace number versus TWT

- Sea bed
- Lower Tertiary
- Lower Cretaceous
- Top Perm
- Lower Perm
- mid Tertiary,
- mid Cretaceous,
- Lower Jurassic
- mid Perm
- Basement.

F1-8 is reverse Faults in black colors

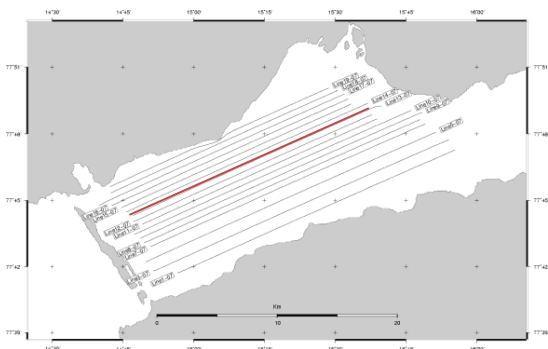
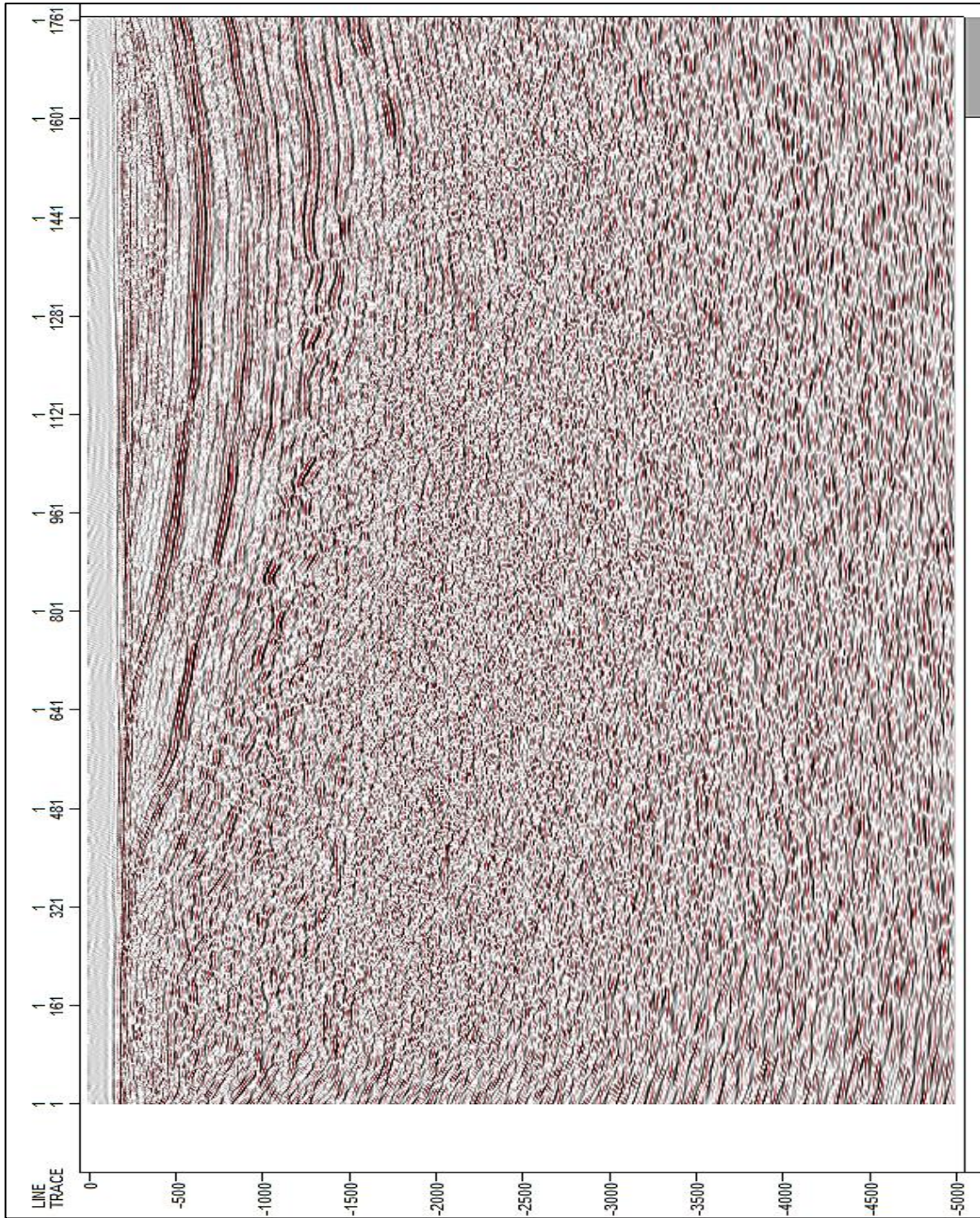




Seismic profile VM-07-12. Acquisition of this survey was in 2007. Trace number versus TWT



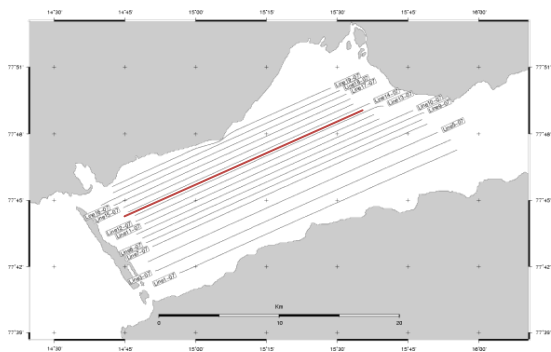
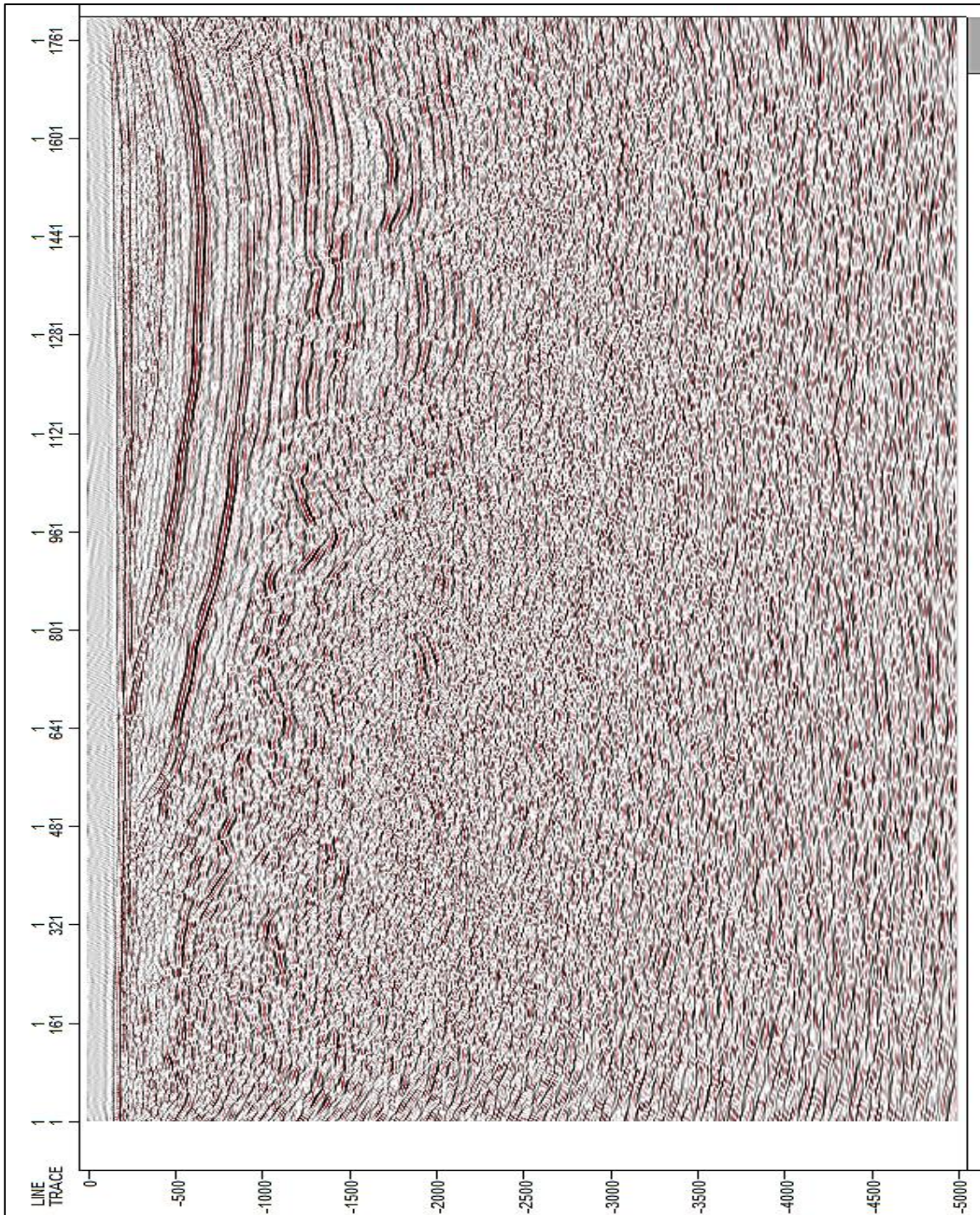




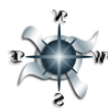
Seismic profile VM-07-13. Acquisition of this survey was in 2007. Trace number versus TWT



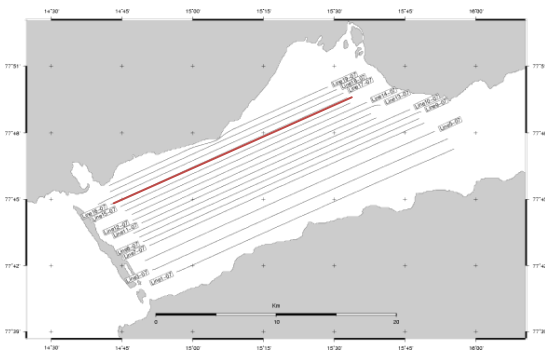
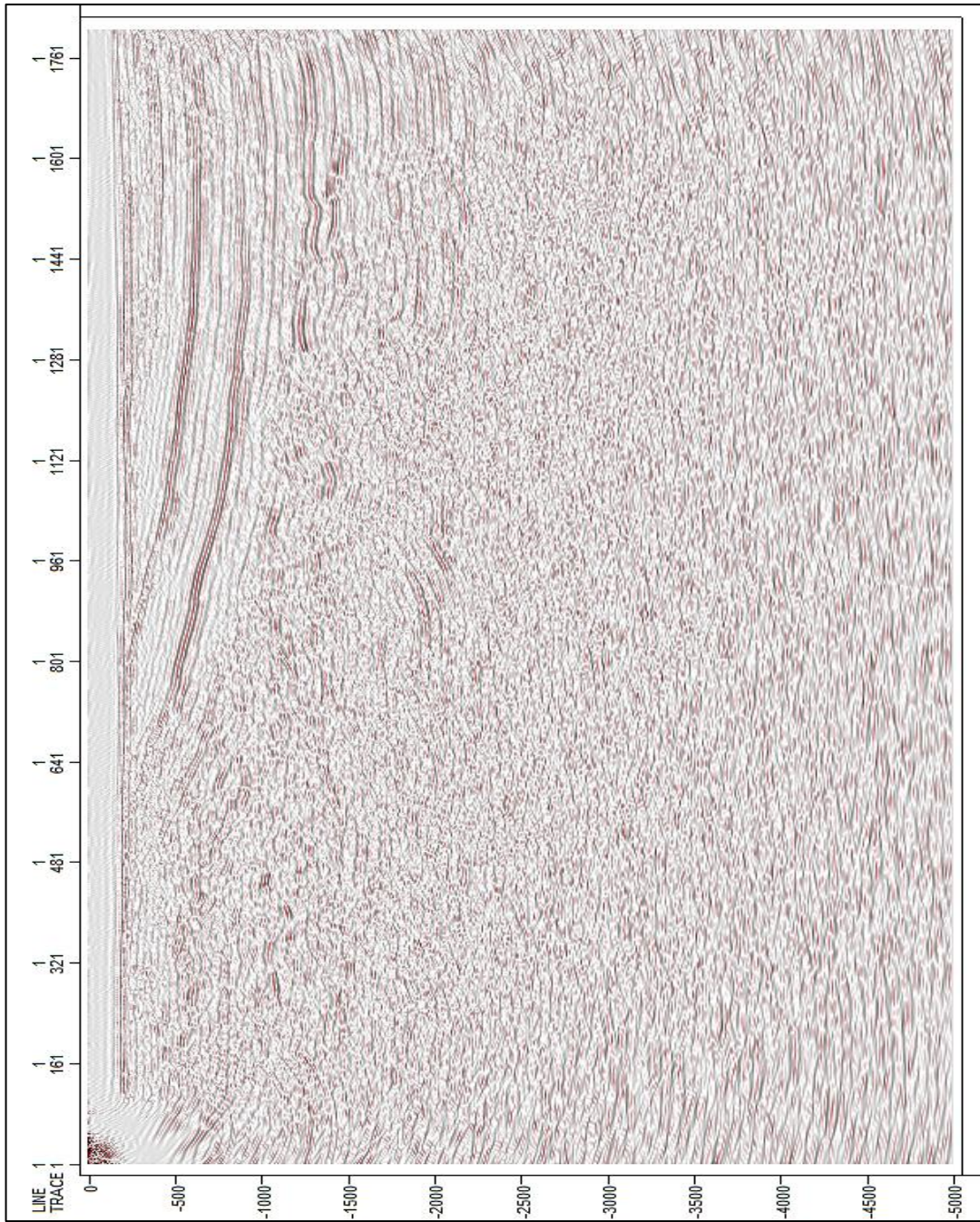




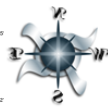
Seismic profile VM-07-14. Acquisition of this survey was in 2007. Trace number versus TWT



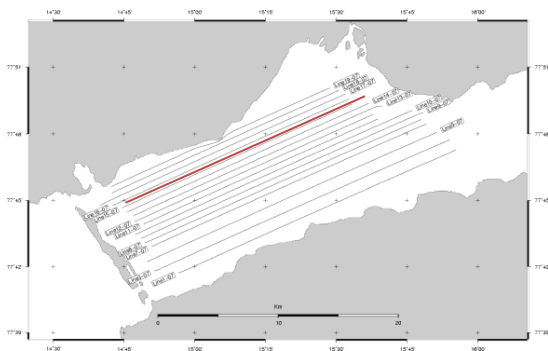
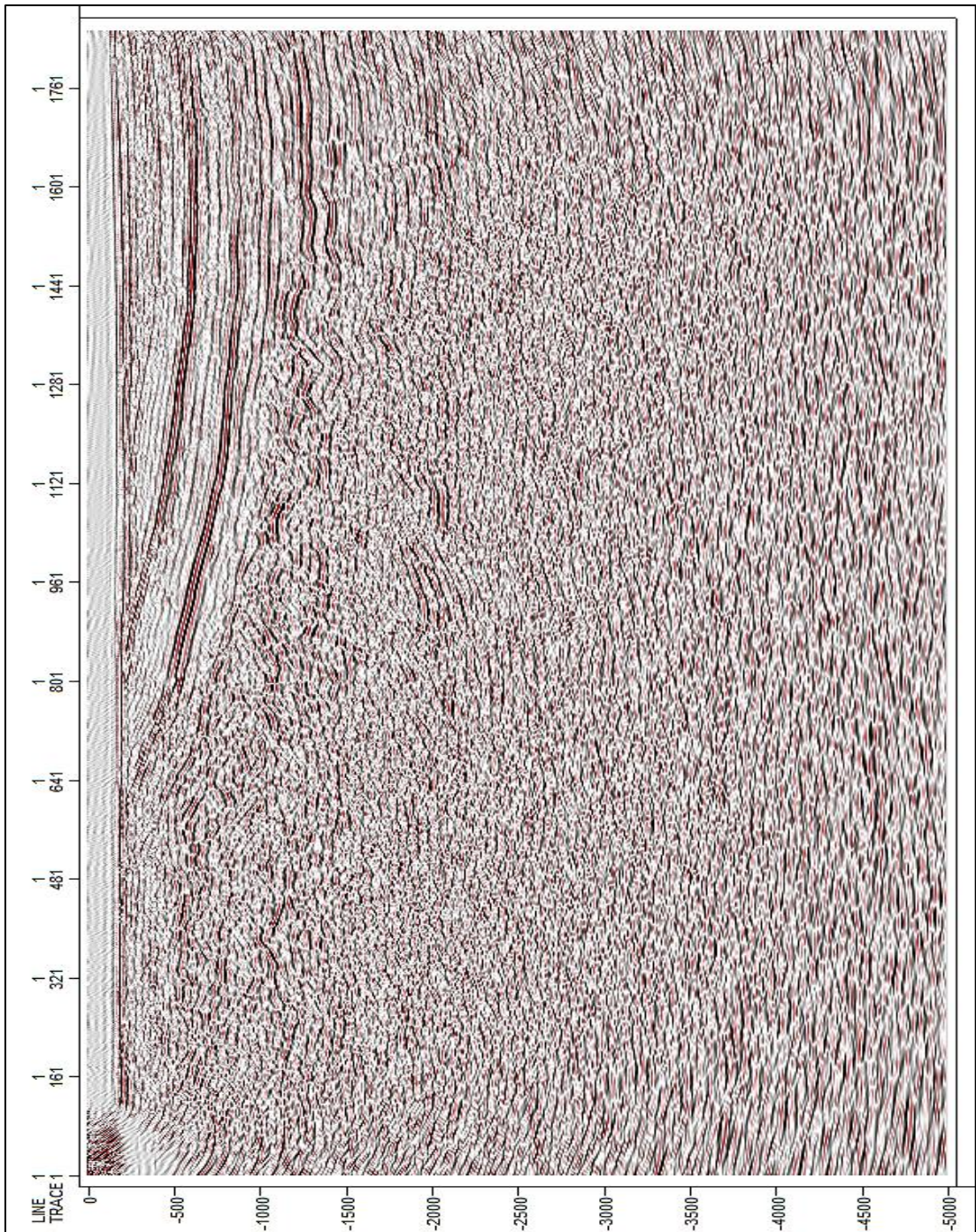




Seismic profile VM-07-15. Acquisition of this survey was in 2007. Trace number versus TWT

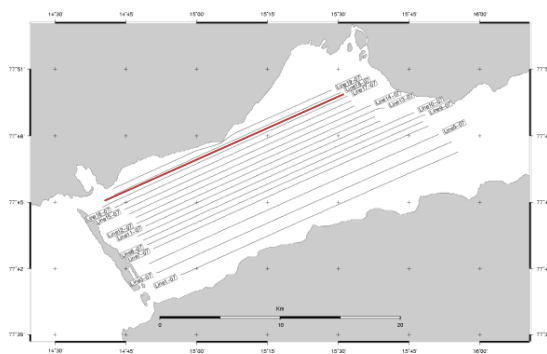
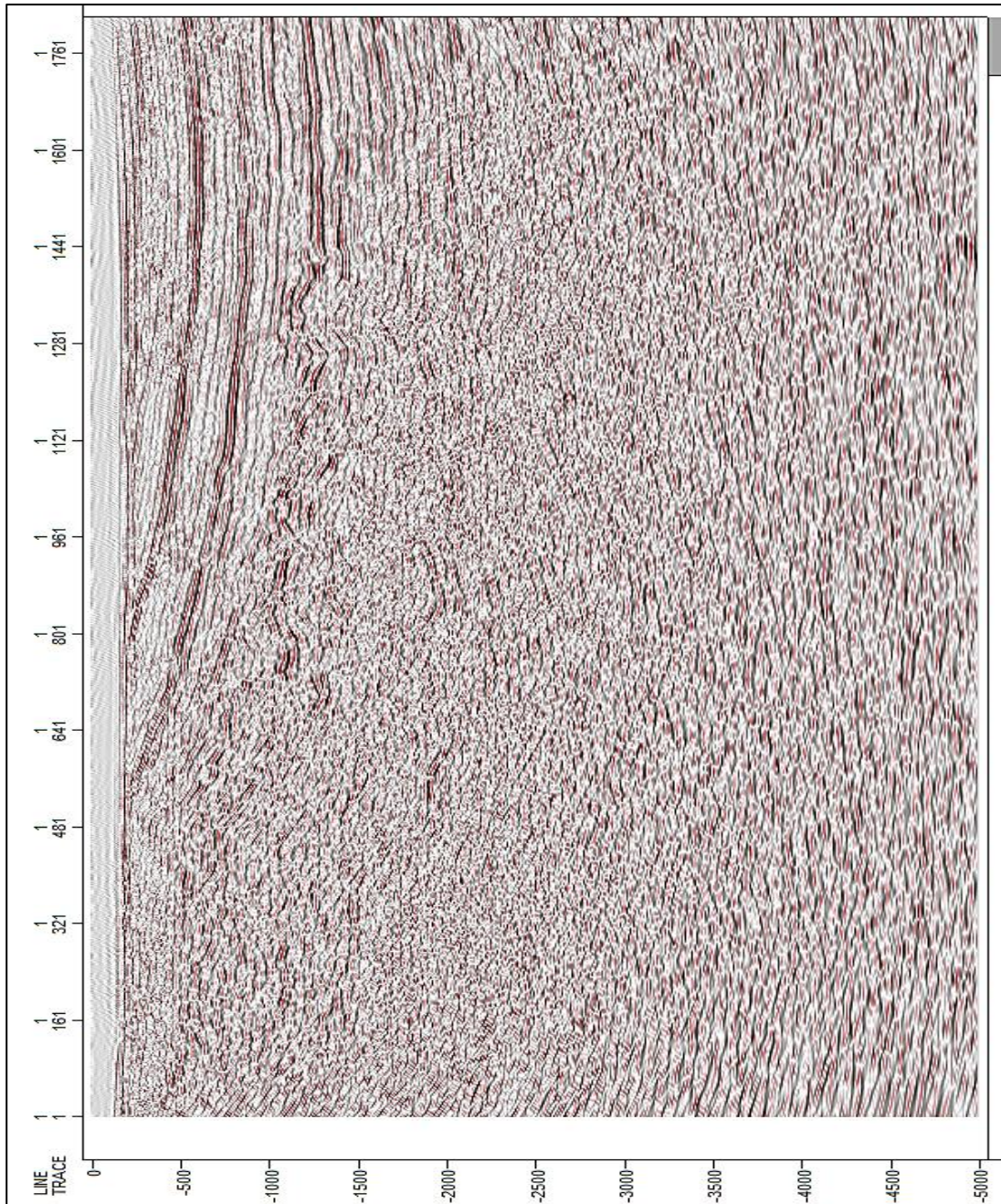






Seismic profile VM-07-16. Acquisition of this survey was in 2007. Trace number versus TWT

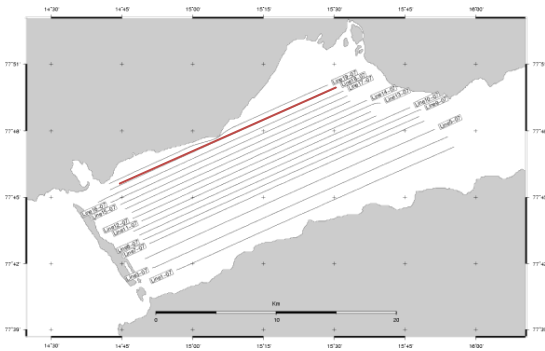
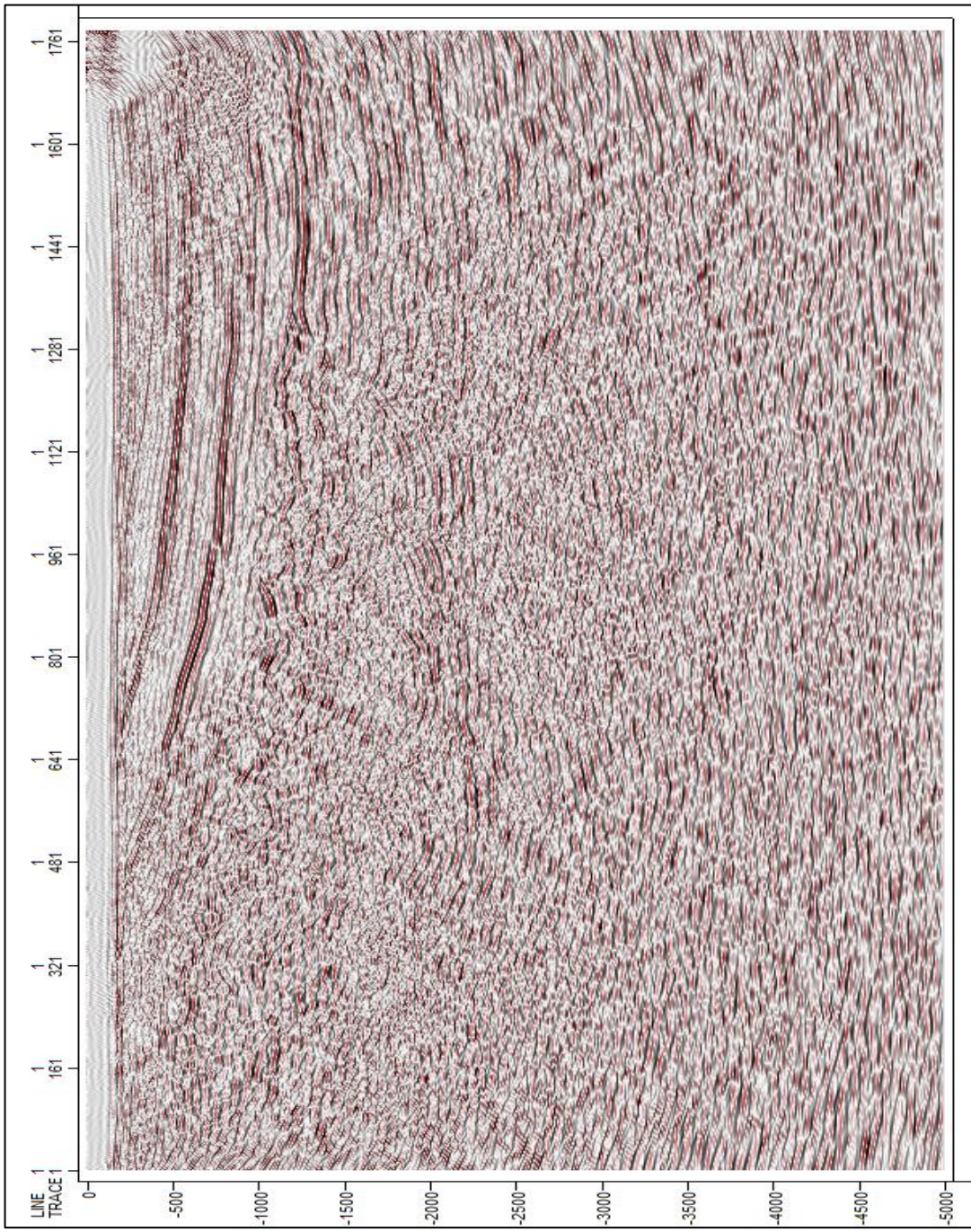




Seismic profile VM-07-17. Acquisition of this survey was in 2007. Trace number versus TWT



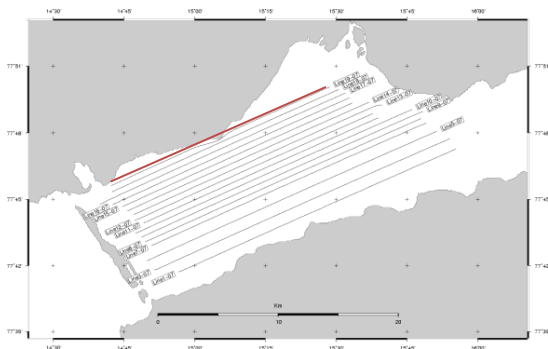
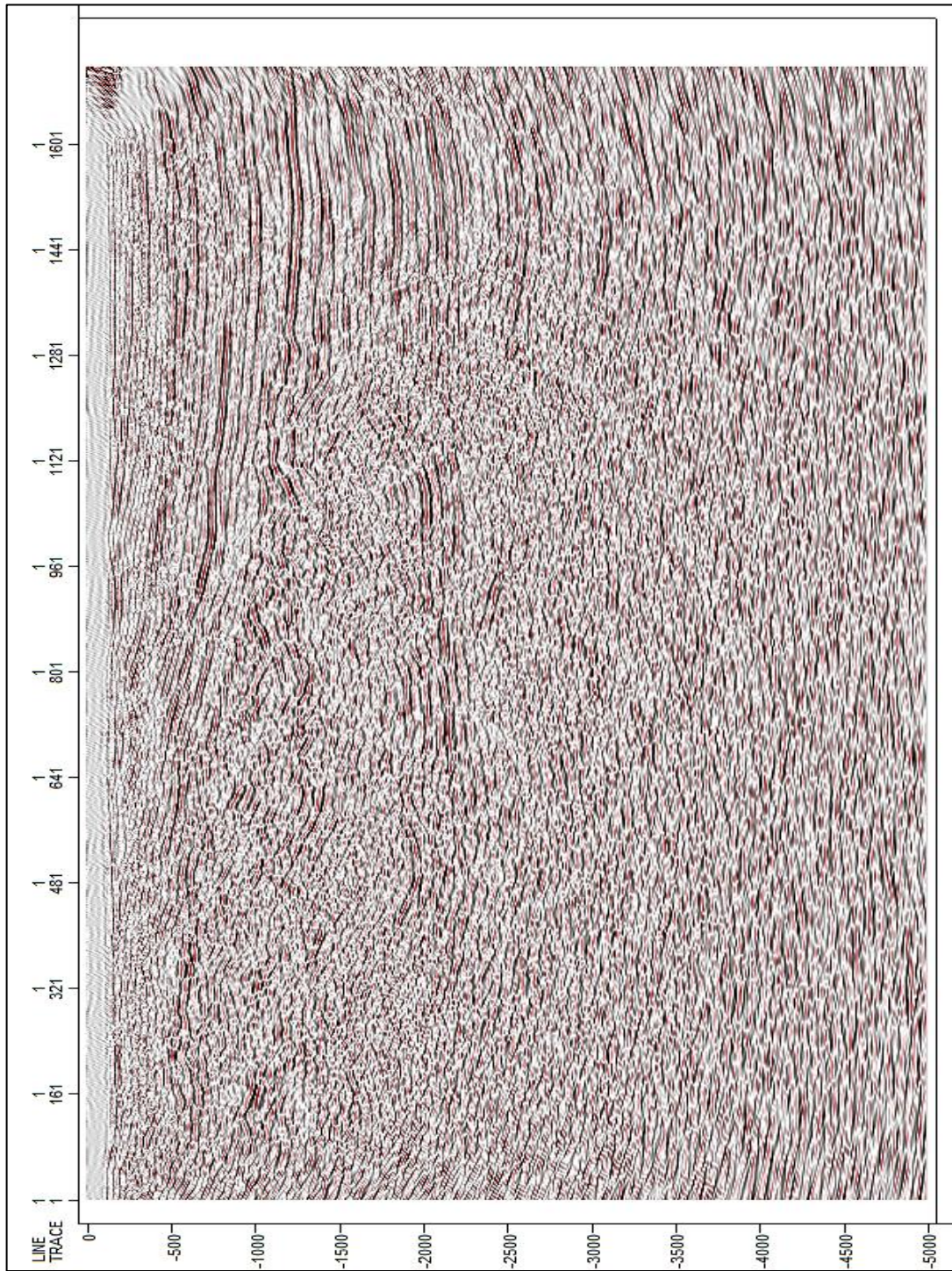




Seismic profile VM-07-18. Acquisition of this survey was in 2007. Trace number versus TWT







Seismic profile VM-07-19. Acquisition of this survey was in 2007. Trace number versus TWT

